

การสังเคราะห์และการศึกษาสารประกอบเชิงซ้อนรูทีเนียมไบพริดีนที่มีหมู่อะมิโด  
เพื่อใช้เป็นสีย้อมไวแสงสำหรับเซลล์สุริยะ

นางสาวผกาสุคนธ์ เมฆรัตน์ชัย

วิทยานิพนธ์นี้เป็นส่วนหนึ่งของการศึกษาตามหลักสูตรปริญญาวิทยาศาสตรมหาบัณฑิต

สาขาวิชาเคมี ภาควิชาเคมี

คณะวิทยาศาสตร์ จุฬาลงกรณ์มหาวิทยาลัย

ปีการศึกษา 2553

ลิขสิทธิ์ของจุฬาลงกรณ์มหาวิทยาลัย

SYNTHESIS AND STUDY OF BIPYRIDINE RUTHENIUM COMPLEXES  
CONTAINING AMIDO GROUPS AS PHOTSENSITIVE DYES  
FOR SOLAR CELLS

Miss Pagasukon Mekrattanachai

A Thesis Submitted in Partial Fulfillment of the Requirements  
for the Degree of Master of Science Program in Chemistry

Department of Chemistry

Faculty of Science

Chulalongkorn University

Academic Year 2010

Copyright of Chulalongkorn University

Thesis Title                   SYNTHESIS AND STUDY OF BIPYRIDINE  
RUTHENIUM COMPLEXES CONTAINING AMIDO  
GROUPS AS PHOTSENSITIVE DYES FOR SOLAR  
CELLS  
By                               Miss. Pagasukon Mekkattanachai  
Field of Study                Chemistry  
Thesis Advisor               Associate Professor Mongkol Sukwattanasinitt, Ph.D.  
Thesis Co-Advisor           Gamolwan Tumcharern, Ph.D.

---

Accepted by the Faculty of Science, Chulalongkorn University in Partial  
Fulfillment of the Requirements for the Master's Degree

..... Dean of the Faculty of Science  
(Professor Supot Hannongbua, Dr.rer.nat.)

#### THESIS COMMITTEE

..... Chairman  
(Professor Sophon Roengsumran, Ph.D.)

..... Thesis Advisor  
(Associate Professor Mongkol Sukwattanasinitt, Ph.D.)

..... Thesis Co-Advisor  
(Gamolwan Tumcharern, Ph.D.)

..... Examiner  
(Sumrit Wacharasindhu, Ph.D.)

..... External Examiner  
(Sirapat Pratontep, Ph.D.)

ผกาสุคนธ์ เมฆรัตนชัย: การสังเคราะห์และการศึกษาสารประกอบเชิงซ้อนรูทีเนียมไบไพรีดีนที่มีหมู่อะมิโดเพื่อใช้เป็นสีย้อมไวแสงสำหรับสำหรับเซลล์สุริยะ. (SYNTHESIS AND STUDY OF BIPYRIDINE RUTHENIUM COMPLEXES CONTAINING AMIDO GROUPS AS PHOTSENSITIVE DYES FOR SOLAR CELLS) อ. ที่ปรึกษาวิทยานิพนธ์หลัก: รองศาสตราจารย์ ดร. มงคล สุขวัฒน์สินินท์, อ. ที่ปรึกษาวิทยานิพนธ์ร่วม: ดร. กมลวรรณ ธรรมเจริญ, 74 หน้า

สารประกอบเชิงซ้อนรูทีเนียมชนิดใหม่ที่มีหมู่อะมิโด (Dye1, Dye2 และ Dye3) ได้ถูกสังเคราะห์และศึกษาในการเป็นสีย้อมไวแสงในเซลล์แสงอาทิตย์ชนิดสีย้อมโดยเปรียบเทียบกับสีย้อมมาตรฐาน N3 โดย Dye1 ประกอบด้วยไบไพรีดีนลิแกนด์ชนิดเดียวกันคือ 2,2'-bipyridine-4,4'-dicarboxamide และหมู่ไทโอไซยาเนตที่โคออดิเนตกับรูทีเนียมส่วน Dye2 และ Dye3 ประกอบด้วยไบไพรีดีนลิแกนด์ที่แตกต่างกันและหมู่ไทโอไซยาเนตที่โคออดิเนตกับรูทีเนียม ไบไพรีดีนลิแกนด์ของ Dye2 คือ *N,N'*-(2,2'-bipyridine-4,4'-diyl)diacetamide และ 4,4'-dicarboxy-2,2'-bipyridine ในขณะที่ไบไพรีดีนลิแกนด์ของ Dye3 คือ 2,2'-bipyridine-4,4'-dicarboxamide และ 4,4'-dicarboxy-2,2'-bipyridine โปรตรอนของไบไพรีดีนลิแกนด์ทั้งสองลิแกนด์ซึ่งถูกแสดงด้วย <sup>1</sup>H NMR สเปกตรัมนี้มีสภาพแวดล้อมที่ต่างกันแสดงว่าสีย้อมทั้งสี่ชนิดนั้นมีโครงสร้างแบบ *cis* คุณสมบัติทางกายภาพทางแสงและคุณสมบัติทางเคมีไฟฟ้าของ Dye1, Dye2 และ Dye3 คล้ายกับ N3 แต่ค่าสัมประสิทธิ์การดูดกลืนแสงมีค่าต่ำกว่า N3 เพียงเล็กน้อย ค่าระดับพลังงาน LUMO และ HOMO ของสีย้อมชนิดใหม่ทั้งสามที่คำนวณได้จากเทคนิคไซคลิกโวลแทมเมตรี และการวัดการดูดกลืนแสงนั้นมีค่าสูงกว่าระดับพลังงานนำไฟฟ้าของไทเทเนียมไดออกไซด์และอยู่ต่ำกว่าระดับพลังงาน HOMO ของ I<sub>3</sub><sup>-</sup> สีย้อม N3, Dye2 และ Dye3 แสดงค่าการดูดกลืนแสงบนขั้วไทเทเนียมไดออกไซด์ที่คล้ายกันในขณะที่ค่าการดูดกลืนแสงของ Dye1 มีค่า 30% ของ N3 เท่านั้น ค่าคุณสมบัติทางไฟฟ้าของเซลล์แสงอาทิตย์โดยใช้ Dye1, Dye2 และ Dye3 เป็นสีย้อมไวแสงนั้นแสดงค่าประสิทธิภาพการเปลี่ยนพลังงานแสงเป็นพลังงานไฟฟ้า 0.48, 1.21, 1.03 % ตามลำดับ ซึ่งมีค่าต่ำกว่าค่าของ N3 ซึ่งมีค่า 3.47% เนื่องจากค่าความหนาแน่นกระแสไฟฟ้ามีค่าต่ำ และค่าประสิทธิภาพของ Dye1 มีค่าต่ำที่สุดเนื่องจากไม่มีหมู่คาร์บอกซิลิกซึ่งเป็นหมู่ที่จำเป็นสำหรับยึดเกาะกับไทเทเนียมไดออกไซด์อีกทั้งค่าสัมประสิทธิ์การดูดกลืนแสงมีค่าต่ำที่สุด

ภาควิชา.....เคมี.....	ลายมือชื่อนิสิต.....
สาขาวิชา.....เคมี.....	ลายมือชื่ออ.ที่ปรึกษาวิทยานิพนธ์หลัก.....
ปีการศึกษา.....2553.....	ลายมือชื่ออ.ที่ปรึกษาวิทยานิพนธ์ร่วม.....

## 5072367623 : MAJOR CHEMISTRY

KEYWORDS : DYE SENSITIZED SOLAR CELLS / PHOTOVOLTAIC CELLS/  
LIGHT HARVESTING

PAGASUKON MEKRATTANACHAI: SYNTHESIS AND STUDY  
OF BIPYRIDINE RUTHENIUM COMPLEXES CONTAINING  
AMIDO GROUPS AS PHOTOSENSITIVE DYES FOR SOLAR  
CELLS. THESIS ADVISOR: ASSOC. PROF. MONGKOL  
SUKWATTANASINITT, Ph. D., THESIS CO-ADVISOR:  
GAMOLWAN TUMCHARERN, Ph. D., 74 pp.

The new ruthenium complexes containing amido groups (Dye1, Dye2 and Dye3) are synthesized and studied as sensitizing dyes in dye-sensitized solar cells (DSSC) by comparing to N3 reference dye (*cis*-dithiocyanato-bis(2,2'-bipyridyl-4,4'-dicarboxylate)ruthenium(II)) . Dye1 is a Ru complex consisting of two identical bipyridine ligands, 2,2'-bipyridine-4,4'-dicarboxamide, and two thiocyanate groups. Dye2 and Dye3 consist of two different bipyridine ligands and two thiocyanate groups coordinating to Ru center. The bipyridine ligands of Dye2 are *N,N'*-(2,2'-bipyridine-4,4'-diyl)diacetamide and 4,4'-dicarboxy-2,2'-bipyridine while those of Dye 3 are 2,2'-bipyridine-4,4'-dicarboxamide and 4,4'-dicarboxy-2,2'-bipyridine. Two pyridine rings in each bipyridine ligand, as revealed by the <sup>1</sup>H NMR spectra, are magnetically inequivalent indicating that all dyes are obtained as the *cis* geometrical isomer. The photophysical and electrochemical properties of Dye1, Dye2 and Dye3 are similar to N3 dye with slightly lower extinction coefficient. The LUMO and HOMO levels of all three dyes, determined from cyclic voltammetry and UV-vis absorption spectroscopy, are higher than the conduction band of TiO<sub>2</sub> and lower than the HOMO of I<sub>3</sub><sup>-</sup>, respectively. N3, Dye 2 and Dye3 show similar adsorptivity on TiO<sub>2</sub> electrode while the adsorptivity of Dye 1 is only 30%of that of N3. The photovoltaic performance of the cells using Dye1, Dye2 and Dye3 as the sensitizers exhibit overall conversion efficiencies of 0.48, 1.21, 1.03% respectively, lower than the value 3.47% obtained from the cell fabricated from N3, mainly due to the lower photocurrent density. The lowest efficiency of Dye1 sensitized cell is due to the lack of the carboxylic group necessary for anchoring on nanocrystalline TiO<sub>2</sub> as well as its lowest molar extinction coefficient.

Department : .....	Chemistry	Student's Signature : .....
Field of Study : .....	Chemistry	Advisor's Signature : .....
Academic Year : .....	2010	Co-Advisor's Signature : .....

## ACKNOWLEDGEMENTS

I am heartily thankful to my advisor, Associate Professor Dr. Mongkol Sukwattanasinitt for invaluable guidance, excellent supervision, the encouragement and support from the initial to the final stage enabling me to develop an understanding of my thesis. This research is impossible to succeed without his advice. And I also would like to show my gratitude to my Co-Advisor Dr. Gamolwan Tumcharean from National Nanotechnology Center (NANOTEC) for her useful advices and training on instruments.

I would like to show gratitude to Professor Dr. Professor Sophon Roengsumran, chairman of thesis defense committee for his attention and recommendation. I am grateful to Dr. Sumrit Wacharasindhu and Dr. Siraphat Protonethap, thesis committees, for their kind attention and valuable suggestion. I owe my deepest gratitude to Dr. Nattaporn Tonanon to allow me for using the materials and doing my experiment about dye sensitized solar cells fabrication in her laboratory. I also would like to thank Assistant Professor Dr. Paitoon Rashatasakorn for his suggestion during our group meeting. It is an honor for me to thank Professor Shuzi Hayase at Kyushu Institute of Technology (KIT), Japan, for giving me the scholarship and very good opportunity to visit KIT. I also thank Professor Shuzi Hayase's members for training me on solar cell fabrication, photovoltaic performance measurement and their hospitality during my stay at KIT.

Moreover, it is my pleasure to thank my colleagues, Yamonporn Yodta, Chaiwat Pollook-in, Thanakrit Chandra for their eternal friendships, suggestions, and caring support. I also would like to thank everyone in MS group for their help in everything and good wish.

My appreciation is also given to National Nanotechnology Center (NANOTEC), National Science and Technology Development Agency (NSTDA), Thailand (Project NN-B-22-FN9-10-52-06), the 90<sup>th</sup> Anniversary of Chulalongkorn University Fund (Ratchadaphiseksomphot Endowment Fund), Center for Petroleum, Petrochemicals and Advanced Materials, Chulalongkorn University.

Finally, I would like to dedicate this thesis to my family who constantly present their understandings and encouragement to me during both of my pleasant and hard time. This thesis would not have been possible without their supports.

# CONTENTS

	<b>Page</b>
<b>ABSTRACT(THAI)</b> .....	<b>iv</b>
<b>ABSTRACT (ENGLISH)</b> .....	<b>v</b>
<b>ACKNOWLEDGEMENTS</b> .....	<b>vi</b>
<b>LIST OF TABLE</b> .....	<b>x</b>
<b>LIST OF FIGURES</b> .....	<b>xi</b>
<b>LIST OF SCHEMES</b> .....	<b>xiv</b>
<b>LIST OF ABBREVIATIONS AND SIGNS</b> .....	<b>xiii</b>
<b>CHAPTER I INTRODUCTION</b> .....	<b>1</b>
1.1 Dye Sensitized Solar Cell.....	2
1.2 Key components of the dye sensitized solar cells.....	3
1.2.1 Dye sensitizer.....	3
1.2.2 Molecular engineering of photosensitizers.....	4
1.3 Measurements on solar cell performance.....	5
1.4 Photovoltaic performance stability.....	6
1.5 The electronic processes in the dye sensitized solar cells.....	7
1.5.1 The optical absorption.....	7
1.5.2 The electron migration.....	7
1.5.3 The electron recombination.....	8
1.6 Polydiacetylene.....	8
1.7 Cyclic voltammetry.....	9
1.8 Literature reviews.....	10
1.9 Objectives and scope of the thesis.....	23
<b>CHAPTER II EXPERIMENTAL</b> .....	<b>24</b>
Materials.....	24
Characterization.....	24
2.1 Synthesis.....	25
2.1.1 Synthesis of 2,2'-bipyridine- <i>N,N'</i> -dioxide.....	25
2.1.2 Synthesis of 4,4'-dinitro-2,2'-bipyridine- <i>N,N'</i> -dioxide.....	25
2.1.3 Synthesis of 4,4'-diamino-2,2'-bipyridine.....	26

	<b>Page</b>
2.1.4 Synthesis of <i>N,N'</i> -(2,2'-bipyridine-4,4'-diyl)- diacetamide (L1).....	26
2.1.5 Synthesis of 4,4'-dicarboxy-2,2'-bipyridine.....	27
2.1.6 Synthesis of diethyl 2,2'-bipyridine-4,4'- dicarboxylate.....	27
2.1.7 Synthesis of 2,2'-bipyridine-4,4'- dicarboxamide (L2).....	28
2.1.8 Synthesis of N3.....	28
2.1.9 Synthesis of [Ru(II)LL <sup>1</sup> (NCS) <sub>2</sub> ] (Where L= 4,4'-Dicarboxy- 2,2'-bipyridine and L <sup>1</sup> = <i>N,N'</i> -(2,2'-bipyridine-4,4'-diyl)diacetamide) (Dye1).....	29
2.1.10 Synthesis of [Ru(II)LL <sup>2</sup> (NCS) <sub>2</sub> ] (Where L= 4,4'-Dicarboxy-2,2'-bipyridine and L <sup>2</sup> = 2,2'-bipyridine-4,4'-dicarboxamide (Dye2) .....	30
2.1.11 Synthesis of [Ru(II)(L <sup>1</sup> ) <sub>2</sub> (NCS) <sub>2</sub> ] (Where L <sup>1</sup> = 2,2'- bipyridine-4,4'-dicarboxamide (Dye3).....	31
2.1.12 Synthesis of 4,4'-Diiido-2,2'- bipyridine.....	31
2.1.13 Synthesis of 4,4'-diethynyl-2,2'- bipyridine.....	32
2.1.14 Synthesis of methyl hexynoate.....	33
2.2.15 Synthesis of iodo methyl hexynoate.....	33
2.2. Fabrication of dye-sensitized solar cells.....	34
2.3 The preparation of polydiacetylene vesicle from 10,12 pentacosadiynoic acid (PCDA monomer).....	34
2.4 Preparation of dye sensitized photovoltaic cells by using polydiacetylene.....	34
2.5. Cyclic voltametry measurements.....	35
2.6 Photocurrent-voltage measurement.....	35
<b>CHAPTER III RESULTS AND DISCUSSION.....</b>	<b>36</b>
3.1 Synthesis of bipyridine ligands.....	36



	<b>Page</b>
3.1.1 Synthesis of N,N'-(2,2'-bipyridine-4,4'-diyl)- diacetamide.....	36
3.1.2 Synthesis of 2,2'-bipyridine-4,4'-dicarboxamide.....	38
3.2 Synthesis of Ruthenium complexes.....	40
3.3 ATR-FTIR Spectral data.....	46
3.4 Synthesis of bipyridine ligands containing diacetylene.....	48
3.4.1 Synthesis of bipyridine ligands containing diacetylene by Cadiot-Chodkiewicz coupling.....	48
3.4.2 Synthesis of bipyridine ligands containing diacetylene by using activating agent.....	49
3.5 Absorption and emission properties of N3, Dye1, Dye2 and Dye3.....	50
3.6 Electrochemical data.....	53
3.7 Preparation of dye sensitized photovoltaic cells.....	55
3.8 Photovoltaic performance.....	57
3.9 Preparation of dye sensitized photovoltaic cells by using polydiacetylene.....	58
<b>CHAPTER IV CONCLUSION.....</b>	<b>60</b>
4.1 Conclusion.....	60
4.2 Suggestion for the future work.....	61
<b>REFERENCES.....</b>	<b>62</b>
<b>APPENDICES.....</b>	<b>70</b>
<b>VITAE.....</b>	<b>74</b>

## LIST OF TABLES

	Page
<b>Table 1.1</b> Photovoltaic performance of reference dyes.....	3
<b>Table 1.2</b> The photovoltaic performance of protonated and nonprotonated form of dye sensitizer.....	10
<b>Table 1.3</b> The photovoltaic data of complexes 5-8.....	12
<b>Table 1.4</b> The photovoltaic data of C1, C6, C9, C13 and C18 dye.....	14
<b>Table 1.5</b> The photovoltaic data of D5 and D6 dyes.....	16
<b>Table 1.6</b> The photovoltaic data of D20-D23 dyes.....	17
<b>Table 1.7</b> Photovoltaic parameters of dye sensitized solar cells with Z907, C101 and C106 dyes.....	19
<b>Table 1.8</b> Photovoltaic parameters of dye sensitized solar cells with Z907 and C105 dye.....	20
<b>Table 1.9</b> Photovoltaic parameters of dye sensitized solar cells with T18 and N719 dye.....	22
<b>Table 3.1</b> Absorption and emission properties of N3, Dye1, Dye2 and Dye3 0.05 mM in methanol solution.....	52
<b>Table 3.2</b> Absorption properties of N3, Dye1, Dye2 and Dye3 coated on 19 $\mu\text{m}$ $\text{TiO}_2$ thickness.....	52
<b>Table 3.3</b> Electrochemical parameters of Ruthenium complex sensitizer..	55
<b>Table 3.4</b> Comparison of Photocurrent density ( $J_{sc}$ ), Open circuit voltage ( $V_{oc}$ ), Fill factor, and the Efficiency ( $\eta$ ) obtained using N3, Dye1, Dye2 and Dye3 on 19 $\mu\text{m}$ thick $\text{TiO}_2$ electrodes under AM 1.5 Sun.....	58
<b>Table 3.5</b> Comparison of Photocurrent density ( $J_{sc}$ ), Open circuit voltage ( $V_{oc}$ ), Fill factor, and the Efficiency ( $\eta$ ) obtained using N3, Dye2 with polydiacetylene.....	59

## LIST OF FIGURES

	Page
<b>Figure 1.1</b> Schematic presentation of reactions taking place in a dye sensitized solar cell.....	2
<b>Figure 1.2</b> Structure of common reference dyes.....	3
<b>Figure 1.3</b> Schematic presentation of the ways of anchoring of dye sensitizer on nanocrystalline TiO <sub>2</sub> surface.....	5
<b>Figure 1.4</b> Photocurrent-photovoltage curve of the dye sensitized solar cell.....	6
<b>Figure 1.5</b> The topological polymerization of diacetylene monomer.....	9
<b>Figure 1.6</b> Cyclic voltammograms of three different analytes.....	10
<b>Figure 1.7</b> Structures of N3, N719 and N712.....	11
<b>Figure 1.8</b> Structure of Z910.....	11
<b>Figure 1.9</b> Structures of complexes 5-8.....	13
<b>Figure 1.10</b> The structure of Z955.....	14
<b>Figure 1.11</b> Structure of C1, C6, C9, C13 and C18 dyes.....	15
<b>Figure 1.12</b> The structure of K8.....	15
<b>Figure 1.132</b> The structure of D5 and D6.....	16
<b>Figure 1.14</b> The structure of D20-D23.....	17
<b>Figure 1.15</b> The structure of N945.....	18
<b>Figure 1.16</b> The structure of K77.....	19
<b>Figure 1.17</b> Structures of Z907, C101 and C106.....	20
<b>Figure 1.18</b> Structure of C105.....	21
<b>Figure 1.19</b> Structure of Ru(2,2'-bipyridine-4,4'-dicarboxylic acid) (4,4'-bis(11-dodecenyl)2,2'-bipyridine)(NCS) <sub>2</sub> .....	21
<b>Figure 1.20</b> Structure of T18.....	22
<b>Figure 1.21</b> Scheme depicting the adsorption of two N719 carboxylic groups onto TiO <sub>2</sub> .....	22

<b>Figure 3.1</b>	$^1\text{H}$ NMR spectra of 2,2'-bipyridine- <i>N,N'</i> -dioxide in $\text{D}_2\text{O}$ , 4,4'-dinitro-2,2'-bipyridine- <i>N,N'</i> -dioxide in $\text{DMSO-d}_6$ , 4,4'-diamino-2,2'-bipyridine in $\text{DMSO-d}_6$ and <i>N,N'</i> -(2,2'-bipyridine-4,4'-diyl)diacetamide in $\text{DMSO-d}_6$ .....	38
<b>Figure 3.2</b>	$^1\text{H}$ NMR spectra of 4,4'-dicarboxyl-2,2'-bipyridine, diethyl 2,2'-bipyridine-4,4'-dicarboxylate and 2,2'-bipyridine-4,4'-dicarboxamide in $\text{D}_2\text{O}$ , $\text{CDCl}_3$ and $\text{DMSO-d}_6$ respectively.....	40
<b>Figure 3.3</b>	$^1\text{H}$ NMR spectra of N3, Dye1, Dye2 and Dye3 in methanol- $\text{d}_4$ .....	43
<b>Figure 3.4</b>	High resolution mass spectrometer of N3, Dye1, Dye2 and Dye3.....	46
<b>Figure 3.5</b>	IR spectra of N3 Dye1 Dye2 and Dye3.....	47
<b>Figure 3.7</b>	The absorption spectra of (a) N3, dye1, Dye2 and dye3 at 50 $\mu\text{M}$ in MeOH (b) N3, dye1, Dye2 and dye3 anchored on 19 $\mu\text{m}$ nanocrystalline $\text{TiO}_2$ .....	51
<b>Figure 3.8</b>	The normalized absorption and emission spectra of N3, dye1, Dye2 and dye3 at 50 $\mu\text{M}$ in MeOH.....	53
<b>Figure 3.9</b>	Cyclic voltammograms of three different analytes.....	54
<b>Figure 3.9</b>	Cyclic voltammograms of (a)N3, (b) Dye2 and (c) Dye3.....	54
<b>Figure 3.10</b>	Energy level diagram of N3, Dye2 and Dye3 compare to $\text{TiO}_2$ .....	56
<b>Figure 3.11</b>	The process of dye sensitized solar cell fabrication.....	56
<b>Figure 3.12</b>	I-V curve of N3, Dye1, Dye2 and Dye3.....	57
<b>Figure 3.13</b>	Dye sensitized solar cells using a) N3 and Dye2 as sensitizers and b) using N3, Dye2 and P(PCDA) vesicle as sensitizers.....	59
<b>Figure 3.14</b>	I-V curve of N3/P(PCDA) and Dye2/P(PCDA).....	59
<b>Figure A1</b>	$^1\text{H}$ NMR spectrum of 4,4'-diiodo-2,2'-bipyridine.....	71
<b>Figure A2</b>	$^1\text{H}$ NMR spectrum of 4,4'-bis((trimethylsilyl)ethynyl)- 2,2'-bipyridine.....	71
<b>Figure A3</b>	$^1\text{H}$ NMR spectrum of 4,4'-diethynyl-2,2'-bipyridine.....	72
<b>Figure A4</b>	$^1\text{H}$ NMR spectrum of methyl hexynoate.....	72
<b>Figure A5</b>	$^1\text{H}$ NMR spectrum of iodo methyl hexynoate.....	73

**LIST OF SCHEMES**

	<b>Page</b>
<b>Scheme 3.1</b> The synthesis of <i>N,N'</i> -(2,2'-bipyridine-4,4'-diyl)diacetamide.....	37
<b>Scheme 3.2</b> The synthesis of 2,2'-bipyridine-4,4'-dicarboxamide.....	39
<b>Scheme 3.3</b> The synthesis of N3, Dye1, Dye2 and Dye3.....	41
<b>Scheme 3.4</b> Synthesis of bipyridine ligand containing diacetylene.....	45
<b>Scheme 3.5</b> Synthesis of bipyridine ligand containing diacetylene by using activating agent.....	49

**LIST OF ABBREVIATIONS AND SIGNS**

$^{13}\text{C}$ NMR	carbon-13 nuclear magnetic resonance
$\text{CDCl}_3$	deuterated chloroform
$\text{CD}_3\text{OD}$	deuterated methanol
DMSO- $d_6$	deuterated dimethyl sulfoxide
DMSO	dimethylsulfoxide
$\text{D}_2\text{O}$	deuterium oxide
DMF	<i>N,N</i> -dimethylformamide
d	doublet (NMR)
dd	doublet of doublet (NMR)
m	multiplet (NMR)
t	triplet
s	singlet (NMR)
FT-IR	fourier transform infrared spectroscopy
g	gram (s)
$^1\text{H}$ NMR	proton nuclear magnetic resonance
Hz	hertz
HRESIMS	high resolution electrospray ionization mass spectrum
hr	hour (s)
IR	infrared
<i>J</i>	coupling constant
mg	milligram (s)
mL	milliliter (s)
mmol	millimole (s)
<i>m/z</i>	mass per charge
M	molar
bpy	bipyridine
rt	room temperature
TLC	thin layer chromatography
UV	ultraviolet
$\delta$	chemical shift
$^\circ\text{C}$	degree Celsius

$\mu\text{L}$	microliter (s)
$\mu\text{M}$	micromolar
% yield	percentage yield
DSSC	dye sensitized solar cell
TBA	tetrabutyl ammoniumhydroxide
$J_{\text{sc}}$	Photocurrent Density
$V_{\text{oc}}$	open circuit voltage
$ff$	fill factor
$\eta$	efficiency
IPCE	Incident photon to current conversion efficiency
$I_{\text{s}}$	incident light
AM	air mass
mA	milliampere
AgCl	silverchloride
LiI	lithium iodide
$\text{I}_2$	iodine
TBP	tetrabutyl pyridine
MeEtImDCA	ethylmethylimidazolium dicyanamide
DCC	dicyclohexyl carbodiimide
HOBt	hydroxyl benzotriazole
HBTU	benzotriazole $-N, N, N', N'$ -tetramethyl uranium hexafluoro phosphate
NHS	<i>N</i> -hydroxy succinamide
DMT-MM	(4-(4,6-dimethoxyl-1,3,5-triazin-2-yl)-4-methylmorphodinium chloride

## CHAPTER I

### INTRODUCTION

With both population and economic growth, increased energy demand has become one of the top research problems. The energy consumption is made up of about 88% fossil fuels, 6% hydroelectricity, 6% nuclear power and tiny fraction from biomass and solar energy sources. Fossil fuels are causing environment pollution. Nuclear energy from nuclear fission is considered very dangerous by most population and limited due to lack of safety confidence. Therefore, renewable energy has become an important topic for scientist and solar energy is one of the most popular choices.

The sun has shined huge amount of energy on earth and direct sunlight is available from sunrise until sunset. Solar collectors and modules are designed to capture the sun's energy and change it into more usable forms such as heat or electricity. Sunlight can be converted directly to electricity by a state of the art technology called a photovoltaic cell or solar cell. Most photovoltaic cells are made from silicon or heavy metals such as Cadmium, Gallium and Indium but there are several disadvantages in using these inorganic materials. The big problem is cost, solar cell that made from silicon is very expensive and heavy metals are toxic and environmentally hazardous. Thus, the other kind of solar cell called dye sensitized solar cells (DSSC) are attracting widespread interest for the conversion of sunlight into electricity because of their low cost and high efficiency. These cells were invented by Michael Gratzel and Brian O'regan in 1991 [1] and are also known as Gratzel cells. Dye sensitized solar cells presenting conversion efficiencies as high as 10-12% [1] it is however still lower than the efficiency of solar cells that made from silicon, therefore great efforts have been taken to improve the performance of the DSSC.

The development of these new types of solar cells is promoted by increasing public awareness that the oil reserves may run out during this century. As the energy needs of the planet are likely to double within the next 50 years, solar cell is set for an alternative energy reserve.<sup>2</sup> Fortunately, the supply of energy from the sun to the earth is gigantic:  $3 \times 10^{24}$  joules a year, or about 10,000 times more than the global population annual consumption. In the other word, converting 0.1% of the sunlight



energy with solar cells with an efficiency of 10% would satisfy the needs. But to tap sunlight energy into this huge energy reservoir remains an enormous challenge.

### 1.1 Dye sensitized solar cells

A dye sensitized solar cell (DSSC) can be considered as a hybrid version of photogalvanic cells and solar cells based on semiconductor electrodes. The cell consists of a dye-coated semiconductor electrode and a counter electrode arranged in a sandwich configuration and the inter-electrode space is filled with an electrolyte containing a redox mediator [3,4]. In several researches the researchers used a polypyridine complex of Ru as the dye sensitizer, nanocrystalline  $\text{TiO}_2$  as the semiconductor and the  $\text{I}_2/\text{I}_3^-$  solution as the redox mediator [5-7]. The reactions occur in a dye sensitized solar cell are shown schematically in Fig.1.1 Optical excitation of the dye with visible light leads to excitation of the dye to an excited state that undergoes electron transfer, injecting electrons into the conduction band of the semiconductor. The oxidized dye is subsequently reduced back to the ground state by the electron donor present in the electrolyte. The electrons in the conduction band collect at the electrode and subsequently pass through the external circuit to arrive at the counter electrode where they effect the reverse reaction of the redox mediator [3,4].

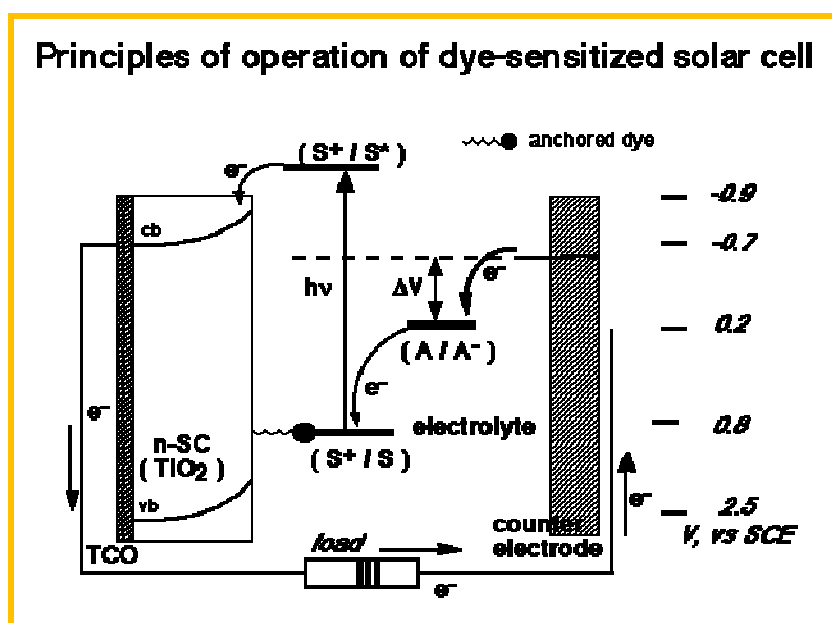
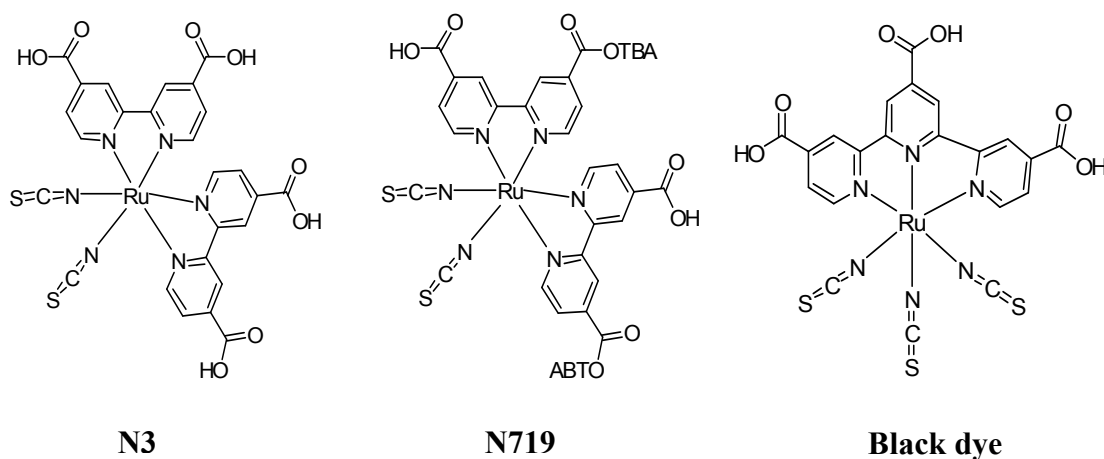


**Figure 1.1** Schematic presentation of reactions taking place in a dye sensitized solar cell.

## 1.2 Key components of the dye sensitized solar cells.

### 1.2.1 Dye sensitizer

The ideal sensitizer for a photovoltaic cell converting sunlight to electricity should absorb all light from the sun. Many dyes have been investigated as the sensitizer in DSSC. New dyes were synthesized and investigated photovoltaic performance by comparing to the reference dye. At present, there are three dyes, N3, N719 and black dye, commonly used as the reference (Figure 1.2) [3-5]. These dyes gave high efficiency as shown in Table 1.1. Although exhibiting high efficiency, the drawbacks of N3 are the lack of absorption in the red region of the visible spectrum and also relatively low molar extinction coefficient [8,9]. Therefore, searching for new dyes to improve the efficiency and increase molar extinction coefficient is an ardent research topic.



TBA = tetrabutylammoniumhydroxide

**Figure 1.2** Structure of common reference dyes.

**Table 1.1** Photovoltaic performance of reference dyes.

Complex	$J_{sc}$ (mA/cm <sup>2</sup> )	$V_{oc}$ (mV)	$ff$	Efficiency ( $\eta$ )
N3	19.0	600	0.65	7.4
N719	16.0	730	0.70	8.2
Black dye	20.5	720	0.74	10.4

### 1.2.2 Molecular engineering of photosensitizers [3,4, 9-13]

1.2.3 There are several key criteria that are preferably for the dyes to demonstrate as efficient photosensitizers in solar cells .

a) Spectral properties to ensure maximal visible light absorption.

The dye should absorb all of the visible and near IR photons of the sunlight incident on earth. Many Ru complexes of three ligand systems exhibited strong absorption bands in the spectral region of interest. Electronic transitions contributing to molar absorbance are metal to ligand charge transfer (MLCT) and  $\pi-\pi^*$  transition.

b) Redox properties in ground and excited state.

Efficient charge injection from the excited state of the dye into the conduction band of  $\text{TiO}_2$  depends on the redox potential of the dye in the excited state. The energy level of the excited state should be higher than conduction band of the  $\text{TiO}_2$  to minimize energetic losses during the electron transfer reaction. In addition, its reduction potential should be sufficiently positive that it can be regenerated via electron donation from the redox electrolyte.

c) The anchoring group

Dye sensitizer must carry attachment groups such as carboxylate or phosphonate to firmly graft it on the semiconductor oxide surface. Figure 1.3 showed different ways of anchoring of the dye via carboxylate onto the  $\text{TiO}_2$  surface.

d) The counterions and degree of protonation (overall charge).

Counterions and degree of protonation are selected to ensure sufficient solubility in organic solvents and control of proton and water content in the pores during the loading of the dye.

e) Nanocrystalline titaniumdioxide

It was mentioned earlier that one component in dye sensitized solar cell is oxide semiconductor such as titanium dioxide ( $\text{TiO}_2$ ). It's a white pigment and the most commonly used. It is a wide bandgap semiconductor with  $E_{bg}$  being ca. 3.2 eV. The films are made of a network of nanocrystalline should produce a junction of huge contact area to allow for efficient light harvesting by the adsorbed monolayer of the dye sensitizer [3,15].

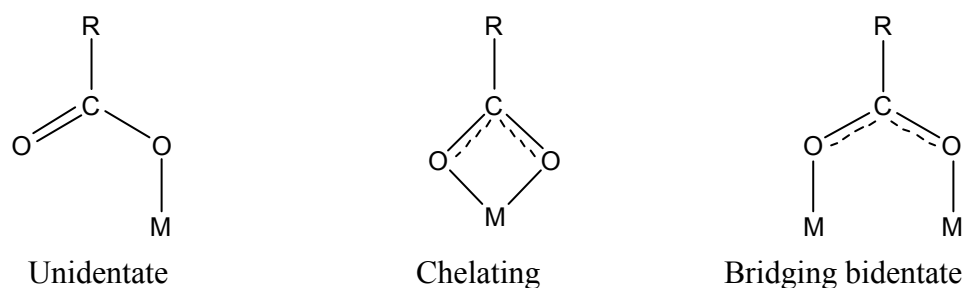


**Figure 1.3** Schematic presentation of the ways of anchoring of dye sensitizer on nanocrystalline  $\text{TiO}_2$  surface [3,15].

### 1.3 Measurements on solar cell performance

The solar cell performance is given by two key parameters, the first is the incident photon to current conversion efficiency (IPCE) for monochromatic radiation and the other is overall white light-to-electrical conversion efficiency ( $\eta$ ). The IPCE value is the ratio of the observed photocurrent divided by the incident photon flux, uncorrected for reflective losses during optical excitation through the conducting glass electrode.

$$\text{IPCE} = \frac{\text{no. of electron flowing through the external circuit}}{\text{no. of photons incident}}$$

The IPCE value can be considered as the effective quantum yield of the device. It is the product of three factors: (a) light harvesting efficiency (depend on the spectral and photophysical properties of the dye), (b) the charge injection (depend on the excited state redox potential and the exciton lifetime), and (c) the charge collection efficiency (depend on the structure and morphology of the  $\text{TiO}_2$  layer). The overall efficiency of the photovoltaic cell can be obtained as a product of the short circuit photocurrent density ( $J_{sc}$ ), the open circuit voltage ( $V_{oc}$ ), the fill factor ( $ff$ ) and the intensity of the incident light ( $I_s$ ) according to the following equation.

$$\eta = (J_{sc} V_{oc} ff) / I_s$$

$J_{sc}$  and  $V_{oc}$  are determined from the photocurrent-photovoltage curve of the cell (Fig 1.4). The fill factor was calculated according to equation 1,

$$ff = IV / J_{sc} V_{oc} \quad (1)$$

where  $I$  and  $V$  were determined from the point of the curve that the product of  $I$  and  $V$  is maximum.

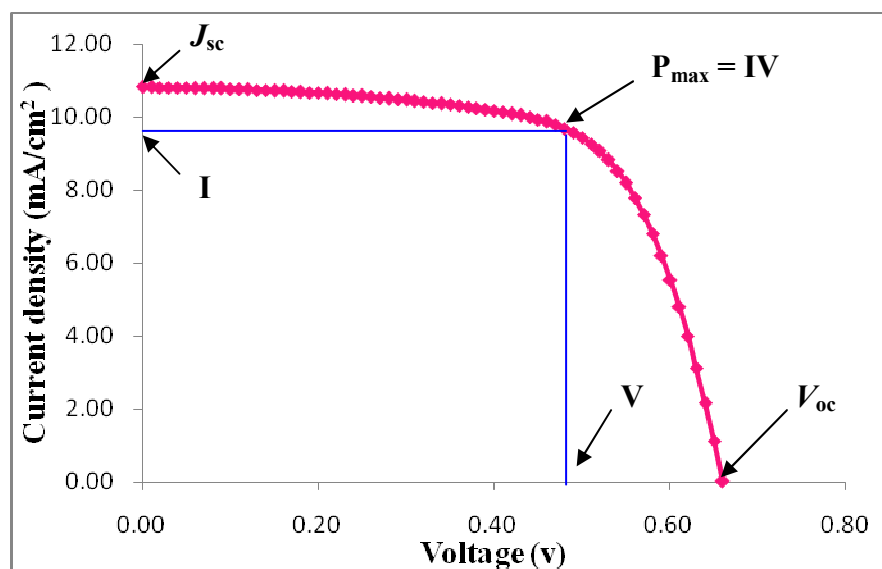


**Figure 1.4** Photocurrent-photovoltage curve of the dye sensitized solar cell.

#### 1.4 Photovoltaic performance stability

A photovoltaic device should remain serviceable for 20 years without significant loss of performance. So, the stability of all the constituents of the nanocrystalline oxide, the TiO<sub>2</sub> film, the conducting glass, the sensitizer, the electrolyte, the counter electrode and the sealant are important.

For a pure dye sensitizer such as N3 dye, it should sustain  $10^8$  redox cycles without loss of performance corresponding to 20 years of continuous operation in natural sunlight.<sup>6</sup> Regeneration of N3 in photovoltaic cell should occur rapidly, i.e. within nanosecond or microseconds to avoid the electron-hole recombination reaction.

In addition, other components of the device, such as electrolyte or sealing may leak under long-term illumination. These were therefore replaced by a highly polar nonvolatile solvent electrolyte which does not exhibit the undesirable property. Using nonvolatile solvent electrolyte conjunction with dye, it gave 1000 hr. stability test at 80°C in a dye sensitized solar cell [14,16-18]. Room temperature molten salts based on imidazolium iodides have revealed very attractive stability features. It can improve the overall efficiency exceeding 6% because the diffusion coefficient of the triiodide

ions in the melt is increased [16,17]. Long-term light soaking tests on sealed cells have also extensively studied over the last few years. These tests are very important, as the redox electrolyte or the sealing, may fail under long-term illumination. A recent stability test of a 12,000 h continuous full intensity light exposure has confirmed that this system does not exhibit an inherent instability[17,18].

## **1.5 The electronic processes in the dye sensitized solar cells.**

After the excitation by the sunlight, the electron from the chromophore or the dye sensitizer is injected to the semiconductor surface, typically on an ultrafast time scale. The electron movement in the dye-semiconductor system are involved in many processes, and the important processes which will be discussed here are the optical absorption, the electron migration, and the electron recombination. These processes can influence on the photovoltaic performances of solar cells. Therefore, these factors will be explained to understand the electronic processes in the solar cells.

### **1.5.1 The optical absorption.**

The dye sensitizers are usually designed to consist of the conjugation unit in the structure because they can displayed absorption bands that are intense and broad due to the wave function overlap between the electronic ground state and the lowest excited state and the geometry relaxations that occur in the excited state. The high extinction coefficients of the organic dye over a wide wavelength range can exhibit an efficient light harvesting to maximize electron excitation and lead to a high efficiency. The dye with the long conjugated system show strong electron-vibration coupling, when the electron was promoted to an electronic excited state, there might be the relaxation down to the lowest excited state. From this process, there is an energy loss in the system [19-21].

### **1.5.2 The electron migration.**

The dyes that are used in the dye sensitized  $\text{TiO}_2$  photovoltaic cell harvest visible light and are selected to match the  $\text{TiO}_2$  semiconductor energy levels and to be photochemically and thermally stable. To generate charge carrier, the electron need to migrate to the heterojunction between  $\text{TiO}_2$  and dye sensitizer before decay back to the ground state. [19-21].

The  $\text{TiO}_2$  surface state that accepts the injected electron is localized within the first surface layers. In some case, a single Ti atom can constitute 20% of the acceptor

state density. It indicates that the electron leaves the surface region and moves into the semiconductor bulk on a 100 fs time scale. Generally, the delocalization process is not uniform in space but rather exhibits preferential directions, which depends on the symmetry of the photoexcited state [19-22].

### 1.5.3 The electron recombination.

Due to the high surface area of dye-sensitized TiO<sub>2</sub>, an electron delocalized in bulk TiO<sub>2</sub> has a high probability of finding a surface. At the surface the electron can interact with the dye that still positively charge after the electron injection and with the electrolyte that has attached the surface. As the result, the open-circuit voltage ( $V_{oc}$ ) will be decrease and also the efficiency. In this case, Schmidt-Mende and coworkers improved the cell performance by attaching hydrophobic chains to the pyridine rings and used as ligand for ruthenium complex (Figure 1.10) [33,34]. The hydrophobic chains act more effectively as a spacer and blocking layer between TiO<sub>2</sub> and the hole conductor to avoid recombination processes. Therefore the dyes with longer hydrocarbon chains gave higher efficiency values when used as a sensitizer in solid-state dye-sensitized solar cells. With increasing chain length, the short currents density ( $J_{sc}$ ) and open-circuit voltages ( $V_{oc}$ ) is increased (Table 1.4) [19-23].

## 1.6 Polydiacetylene

Poly(diacetylene) (PDA) is one of polymers that has been extensively investigated since 1969 due to its excellent optical, electrical, and sensing properties. One of the important property of PDA arises from its mode of polymerization, topological photopolymerization [24,25]. Upon UV irradiation at 254 nm, well-aligned diacetylene (DA) can undergo 1,4-photopolymerization to form conjugate polymer with alternating ene-yne backbone structure. The topological polymerization is a polymerization of diacetylene monomers which were aligned within a suitable position [26] (Figure 1.5). The resulting polymer is intensely colored, typically a deep blue. PDAs show different phases such as well-known blue ( $\lambda_{max}$ : ~640 nm) and red ( $\lambda_{max}$ : ~530 nm) phases. Moreover, the blue phase can change to the red phase upon external stimuli, such as pH, temperature, solvent, mechanical stress and ligand-receptor interaction [27].

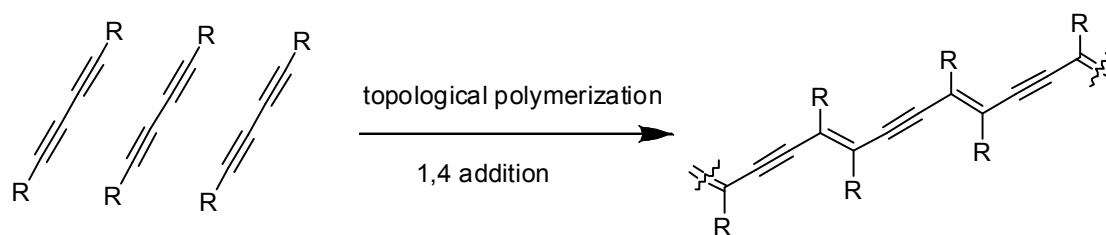


**Figure 1.5** The topological polymerization of diacetylene monomer.

### 1.7 Cyclic voltammetry

This technique is widely used for acquiring qualitative information about electrochemical reactions. In voltammetry, a potential was applied to an electrode immersed in an electrolyte solution, and the current is measured. Voltammetry is generally performed with a three-electrode cell, working electrode, reference electrode and counter electrode. An analyte is measured in a solution which contains the supporting electrolyte to maintain good electrical contact between the electrodes and the analyte in the solution. When the voltage is applied, the current is observed due to the reduction or oxidation of analyte solution. Figure 1.6 shows typical cyclic voltammograms for three reducible analytes [28]. The solid curve is for a reversible reaction. Point *A* is a cathodic peak, when the potential is first reversed (point *B*), the current remains positive and is largely due to the diffusion controlled reduction of the analyte. The potential *C* is reached at which the analyte is no longer reduced, the current here is zero. With further positive changes in potential, oxidation of the previously reduced species begins and proceeds until its concentration reaches zero (the anodic peak *D*). The curve labeled quasireversible is the voltammogram for a system which the electron transfer process is not instantaneous. The difference in potential between the cathodic and anodic peaks provides a measure of the relative rates of the reduction and oxidation reactions. The third curve is a voltammogram for an irreversible electrode process, only a cathodic peak is observed because the analyte is not reoxidized at a significant rate.



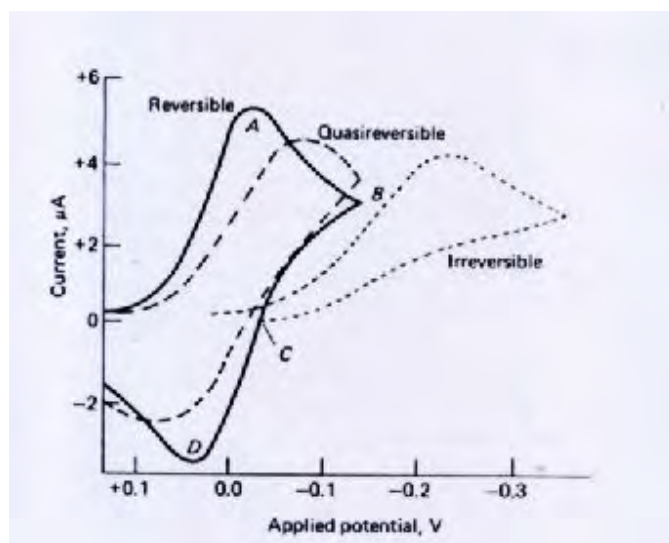


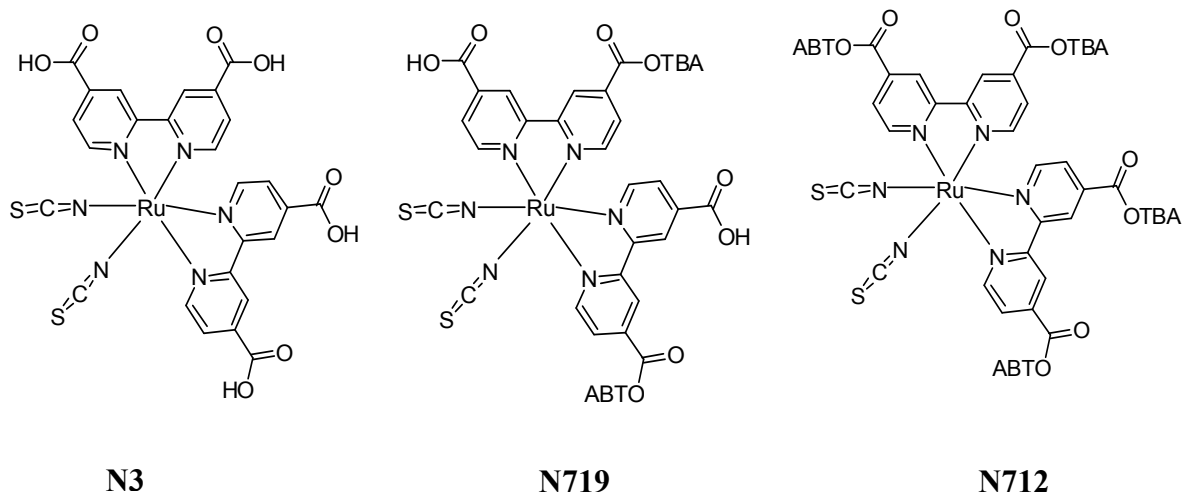
**Figure 1.6** Cyclic voltammograms of three different analytes.

### 1.8 Literature reviews

In 2003, Nazeeruddin *et.al* investigated the interaction between N3, N719 and N712 sensitizers (Figure 1.7) with nanocrystalline TiO<sub>2</sub> film by ATR-FTIR spectroscopy [29]. The results showed that these complexes anchored onto TiO<sub>2</sub> surface in the bridging coordination mode using two of their four carboxylic acid groups, which are *trans* to the NCS ligand. Moreover, the effect of protons on both the short circuit photocurrent and the open circuit photovoltage of a dye sensitized solar cells was investigated. As the results, the monoprotonated form of N3 dye exhibited the highest conversion efficiency under AM 1.5 sun compared to the four, three, two, and zero proton sensitizers, the datas were recorded in Table 1.2

**Table 1.2** The photovoltaic performance of protonated and nonprotonated form of dye sensitizer.

Complex	No. of protons	$J_{sc}$ (mA/cm <sup>2</sup> )	$V_{oc}$ (mV)	$ff$	Efficiency ( $\eta$ )(%)
N3	4	19.0	600	0.65	7.4
N719	2	17.0	730	0.68	8.4
N712	0	13.0	900	0.70	8.2
N3[TBA] <sub>3</sub>	1	16.8	770	0.72	9.3
N3[TBA]	3	17.0	700	0.65	7.7



TBA = tetrabutylammoniumhydroxide

**Figure 1.7** Structures of N3, N719 and N712

In 2004, Wang and coworkers synthesized a new heteroleptic polypyridyl ruthenium complex with a high molar extinction coefficient (Z910) [30]. A new dye demonstrated as a highly efficient and stable sensitizer for dye sensitized solar cells. The short-circuit photocurrent density ( $J_{sc}$ ), open circuit voltage ( $V_{oc}$ ), fill factor ( $ff$ ) and overall conversion efficiency ( $\eta$ ) of the photovoltaic device with Z910 dye are  $17.2 \text{ mA/cm}^2$ ,  $777 \text{ mV}$ ,  $0.764$  and  $10.2\%$ , respectively. For the stability test, a 3-methoxypropionitrile-base electrolyte was used for the test under moderate thermal stress and visible-light soaking at  $100 \text{ mW/cm}^2$ ,  $55 \text{ }^\circ\text{C}$ . All the parameters of the device ( $J_{sc}$ ,  $V_{oc}$ ,  $ff$ ,  $\eta$ ) are stable during 1000 hr. accelerating test.

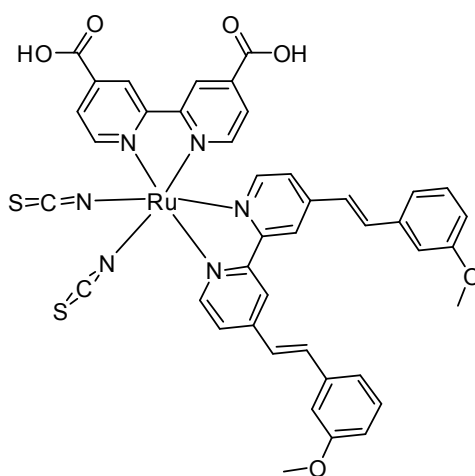


**Figure 1.8** Structure of Z910

In 2004, Klein *et al.* synthesized amphiphilic ligand [31,32] 4,4'-bis(1-adamantyl-aminocarbonyl)-2,2'-bipyridine (**L1**), 4,4'-bis{5- $\{N$ -[2-(3 $\beta$ -cholest-5-en-3-ylcarbamate- $N$ -yl) ethyl] aminocarbonyl}}-2,2'-bipyridine (**L2**), 4,4'-bis{5- $\{N$ -[2-(3 $\beta$ -cholest-5-en-3-ylcarbamate- $N$ -yl)- propyl]aminocarbonyl}}-2,2'-bipyridine (**L3**), and 4,4'-bis(dodecan-12-ol)-2,2'-bipyridine (**L4**) and their heteroleptic ruthenium(II) complexes of the type [Ru(II)LL1(NCS)2] (**5**), [Ru(II)LL2(NCS)2] (**6**), [Ru(II)LL3(NCS)2] (**7**), and [Ru(II)-LL4(NCS)2] (**8**) (where L) 4,4'-bis(carboxylic acid)-2,2'-bipyridine). The photovoltaic performance of complexes 5-8 as photosensitizer in 12+4  $\mu$ m thick nanocrystalline TiO<sub>2</sub>-based solar cells was studied using an electrolyte having a composition of 0.6 M *N*-methyl-*N*-butyl imidazolium iodide, 0.05 M iodine, 0.05 M LiI, and 0.5 M *tert*-butylpyridine in a 50:50 (v/v) mixture of valeronitrile and acetonitrile (Table 1.3).

**Table 1.3** The photovoltaic data of complex 5-8

Complex	$J_{sc}$ (mA/cm <sup>2</sup> )	$V_{oc}$ (mV)	$ff$	Efficiency ( $\eta$ )
5	15.3	695	0.66	7.01
6	15.47	676	0.71	7.42
7	16.11	676	0.7	7.62
8	17.5	700	0.72	8.86

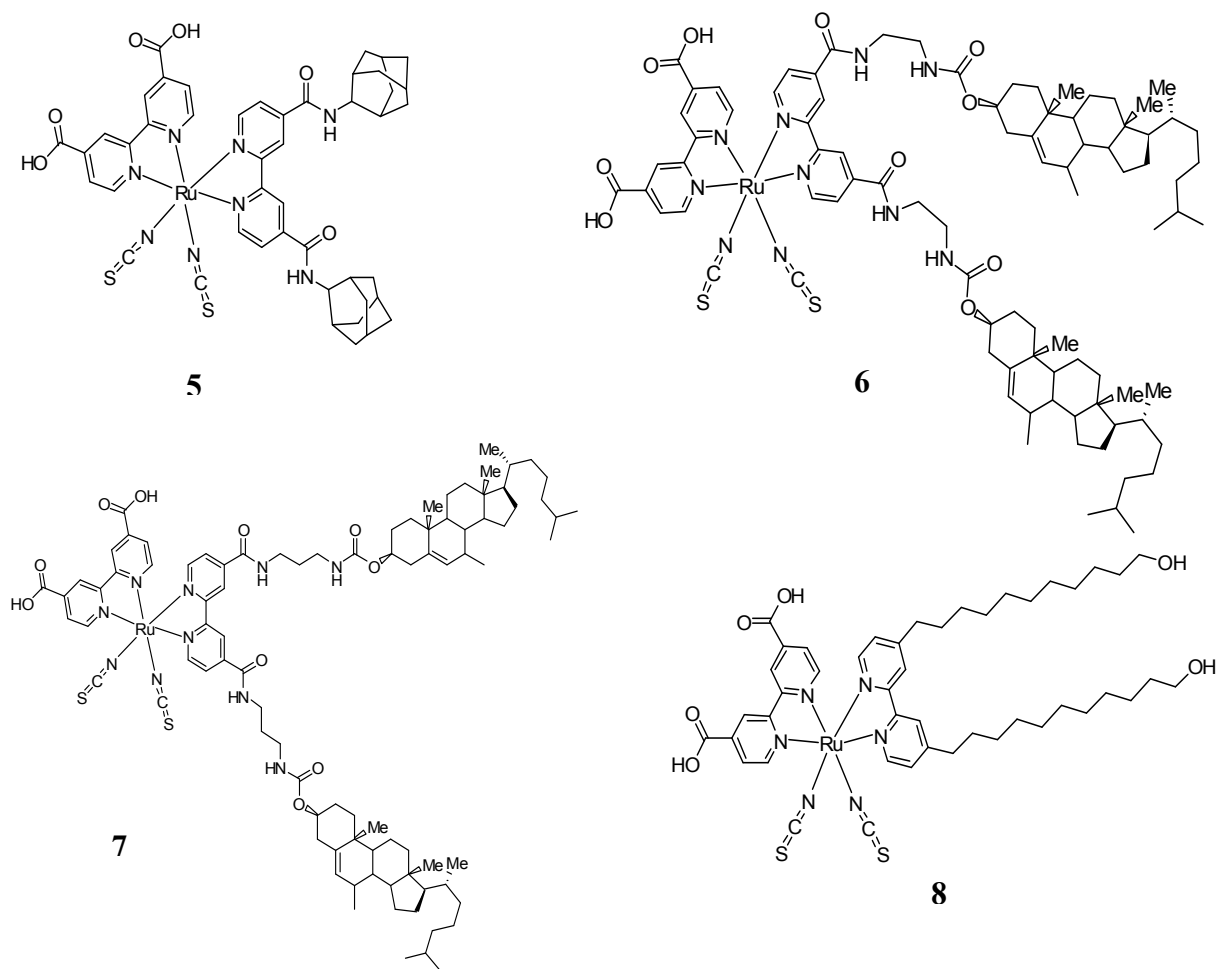


**Figure 1.9** Structures of complexes 5-8.

In 2004, Wang and coworkers reported a new amphiphilic polypyridyl ruthenium complex (Z955) [33]. The new dye consists of 4,4'-diphosphonic acid-2,2'-bipyridine as the anchoring group instead of 4,4'-dicarboxyl-2,2'-bipyridine. The device with Z955 dye exhibited the short-circuit photocurrent density ( $J_{sc}$ ), open circuit voltage ( $V_{oc}$ ), fill factor ( $ff$ ) and overall conversion efficiency ( $\eta$ ) 16.37 mA/cm<sup>2</sup>, 707 mV, 0.693 and 8.0%, respectively. Additionally, the device showed excellent stability under light soaking at 55-60 °C during 1000 hr.

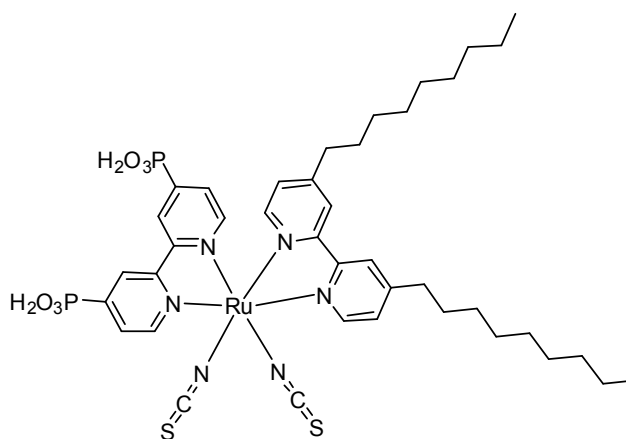


**Figure 1.10** The structure of Z955

In 2005, Schmidt-Mende and coworkers studied the influence of the hydrocarbon chain length of amphiphilic ruthenium complexes on the device performance in solid state dye sensitized solar cells [34,35]. They concluded that the dye containing longer hydrocarbon chains gave higher efficiency due to higher current density and open circuit voltage. The results were recorded in Table 1.4 and the structures of dyes were shown in Figure 1.11.

**Table 1.4** The photovoltaic data of C1, C6, C9, C13 and C18 dye.

Complex	$J_{sc}$ (mA/cm <sup>2</sup> )	$V_{oc}$ (mV)	$ff$ (%)	Efficiency (η)(%)
C1	5.4	714	59.7	2.3
C6	5.8	712	60.5	2.5
C9	6.3	738	61.3	2.8
C13	6.3	744	66.0	3.1
C18	5.8	718	55.2	2.3

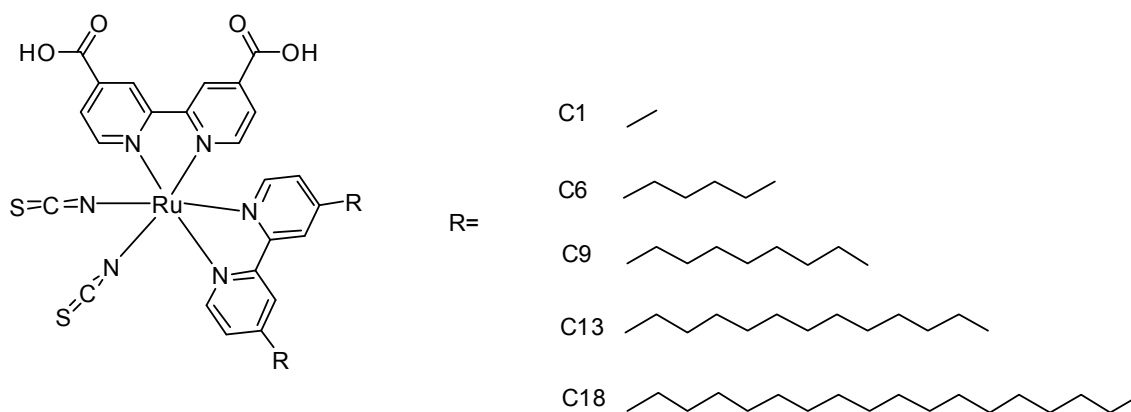


**Figure 1.11** Structure of C1, C6, C9, C13 and C18 dyes.

In 2005, a novel ligand 4,4'-bis(carboxyvinyl)-2,2'-bipyridine (L) and its ruthenium (II) complex  $[\text{Ru}(\text{II})\text{L}_2(\text{NCS})_2]$  (K8) was synthesized and used as dye sensitizer by Klein *et al.* [36]. The metal to ligand charge transfer band of K8 is red shifted 20 nm and the molar extinction coefficient increased by 30% when compared to N3 dye. For device fabrication, the cell gave current density of  $18.0 \text{ mA/cm}^2$ , 640 mV open circuit voltage, 0.75 fill factor and yielding 8.64% conversion efficiency. It gave the excellent efficiency results from its strong optical light absorbance the visible spectrum and the ligand containing extended conjugation.

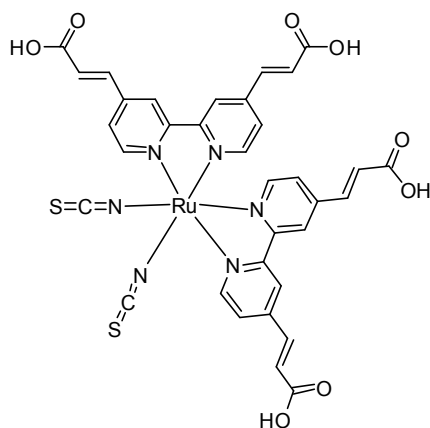
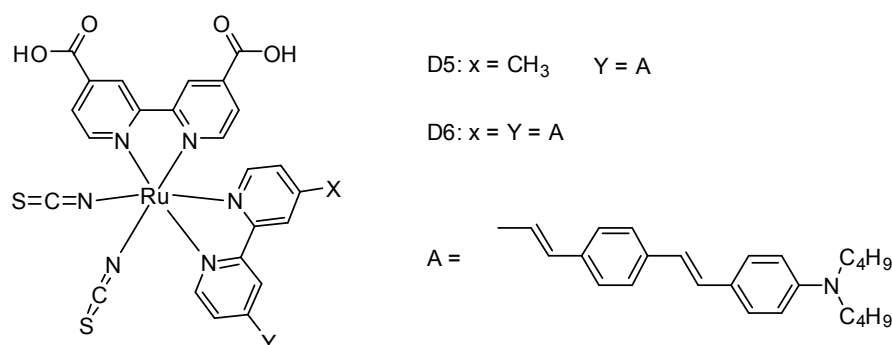


**Figure 1.12** The structure of K8.

In 2006, Jang and coworkers synthesized new oligophenylenevinylene functionalized Ru(II)bipyridine sensitizers (D5 and D6) for using in dye sensitized TiO<sub>2</sub> solar cells (DSSC) [37]. D5 and D6 enabled about 12% and 17% enhancement in solar-to-electricity conversion efficiency, respectively, compared to N3 (Table 1.5). The enhancement are correlated with higher molar absorption coefficients of these sensitizers which containing oligophenylenevinylene  $\pi$ -conjugated backbones with one *N,N'*-dibutylamino moiety.

**Table 1.5** The photovoltaic data of D5 and D6 dyes.

Complex	$J_{sc}$ (mA/cm <sup>2</sup> )	$V_{oc}$ (mV)	$ff$ (%)	Efficiency ( $\eta$ )(%)
N3	9.80	0.63	0.66	4.1
D5	10.8	0.63	0.68	4.6
D6	11.7	0.63	0.66	4.8

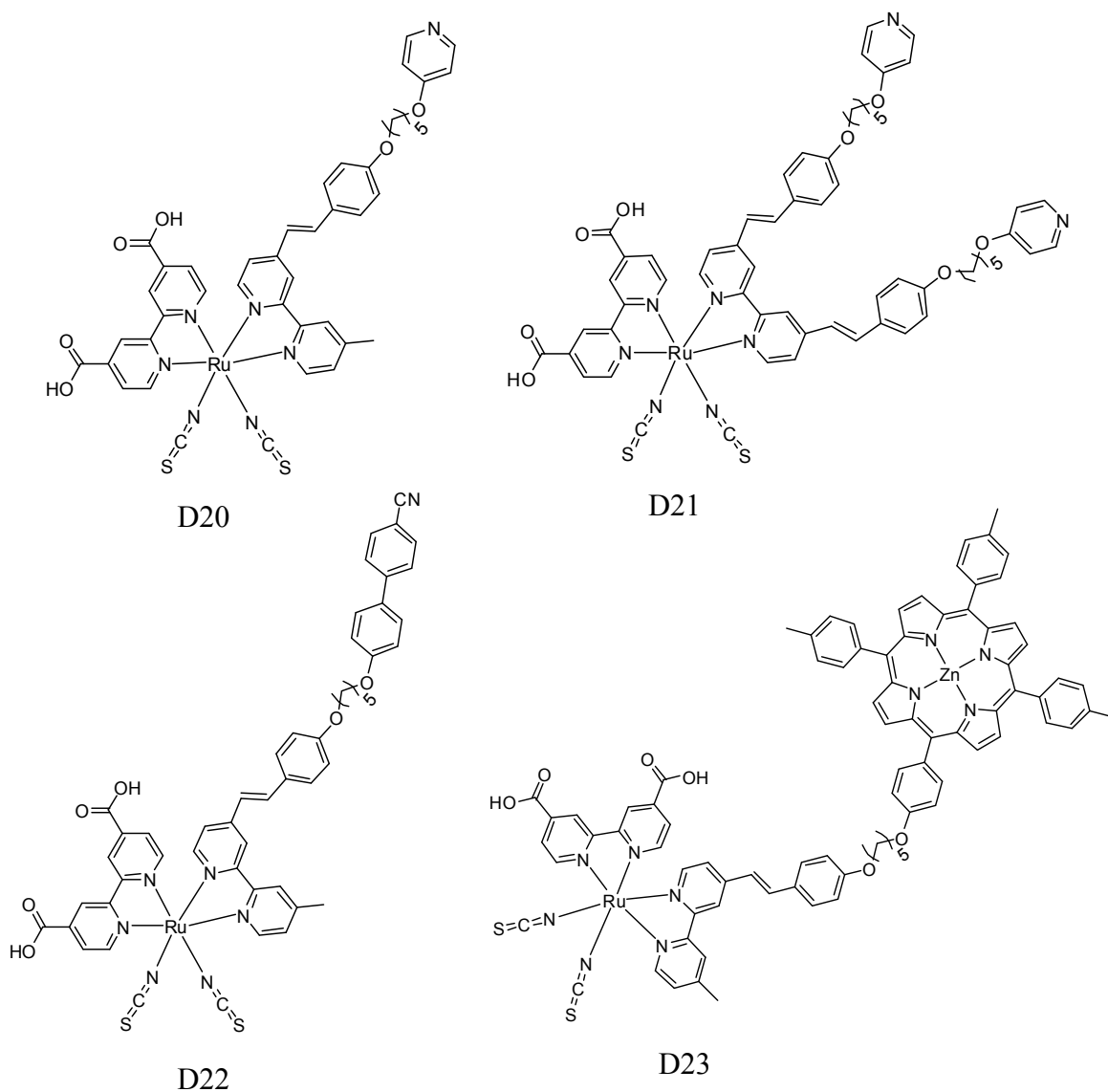


**Figure 1.13** The structure of D5 and D6.

In 2007, Jung *et.al.* synthesized new ruthenium sensitizers containing styryl substituted bipyridine and antenna fragment (D20-D23) for increase the extinction coefficient of sensitizer and stability of device performance [38]. All complexes exhibit a broad metal to ligand charge transfer band around 520-530 nm in DMF solution. The photovoltaic data were collected in Table1.6, from the results the efficiency of D23 is the lowest due to the decrease amount of dye molecule on TiO<sub>2</sub> film.

**Table 1.6** The photovoltaic data of D20-D23 dyes.

Complex	$J_{sc}$ (mA/cm <sup>2</sup> )	$V_{oc}$ (mV)	$ff$ (%)	Efficiency ( $\eta$ )(%)
N3	13.13	0.73	0.66	6.32
D20	13.31	0.64	0.68	5.81
D21	9.32	0.65	0.73	4.40
D22	6.45	0.63	0.73	2.98
D23	6.45	0.63	0.73	2.98

**Figure 1.14** The structure of D20-D23.



In 2007, Nazeeruddin and coworkers synthesized tetrabutylammonium [Ru(4-carboxylic acid-4'-carboxylate-2,2'-bipyridine)(4,4'-di-(2-(3,6-dimethoxyphenyl) ethenyl) -2,2'-bipyridine)(NCS)<sub>2</sub>] (N945) [39]. The new sensitizer anchored TiO<sub>2</sub> films exhibit excellent power conversion efficiency, the complex show a short-circuit current density ( $J_{sc}$ ) of 18.84 mA/cm<sup>2</sup>, open-circuit voltage ( $V_{oc}$ ) 783 mV and fill factor ( $ff$ ) 0.73, resulting conversion efficiency ( $\eta$ ) 10.82%, under Air Mass (AM) 1.5 sunlight. The dye sensitizer show the high efficiency because it's extended  $\pi$ -system with electron donor group, which is expected to increase molar extinction coefficient and shows panchromatic response.

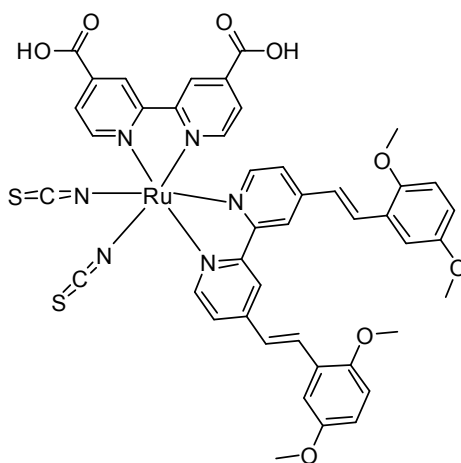


**Figure 1.15** The structure of N945.

In 2007, Kuang *et al.* synthesized the newly designed high molar extinction coefficient sensitizer (K77) [40]. The new dye gave the efficiency more than 10.5% with a volatile electrolyte and 9.5% with a nonvolatile electrolyte. In addition, DSSC using K77 as sensitizer exhibited long-term stability (1000 h) under both light soaking and thermal stressing with a new nonvolatile organic-solvent-based electrolyte.

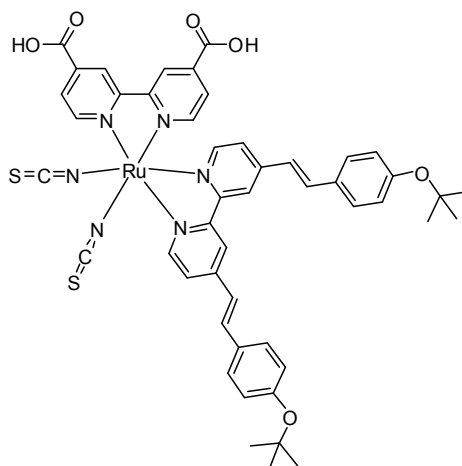


**Figure 1.16** The structure of K77.

In 2009, Cao and coworkers reported a new ruthenium sensitizer featuring a 2-(hexylthio)thiophene conjugated bipyridine ligand (C106) [41]. The new heteroleptic polypyridyl ruthenium complex exhibited a high molar extinction coefficient of  $1.87 \times 10^4 \text{ M}^{-1}\text{cm}^{-1}$  and the DSSC using this dye gave high efficiency of 10.57%. They fabricated photovoltaic device using C106 as dye sensitizer comparing to Z907 and C101. The photovoltaic performances are shown in Table 1.7.

**Table 1.7** Photovoltaic parameters of dye sensitized solar cells with Z907, C101 and C106 dyes.

Dye	$J_{sc}$ (mA/cm <sup>2</sup> )	$V_{oc}$ (mV)	$ff$	Efficiency ( $\eta$ ) (%)
Z907	17.13	730	0.724	9.05
C101	17.75	749	0.777	10.33
C106	18.28	749	0.772	10.57

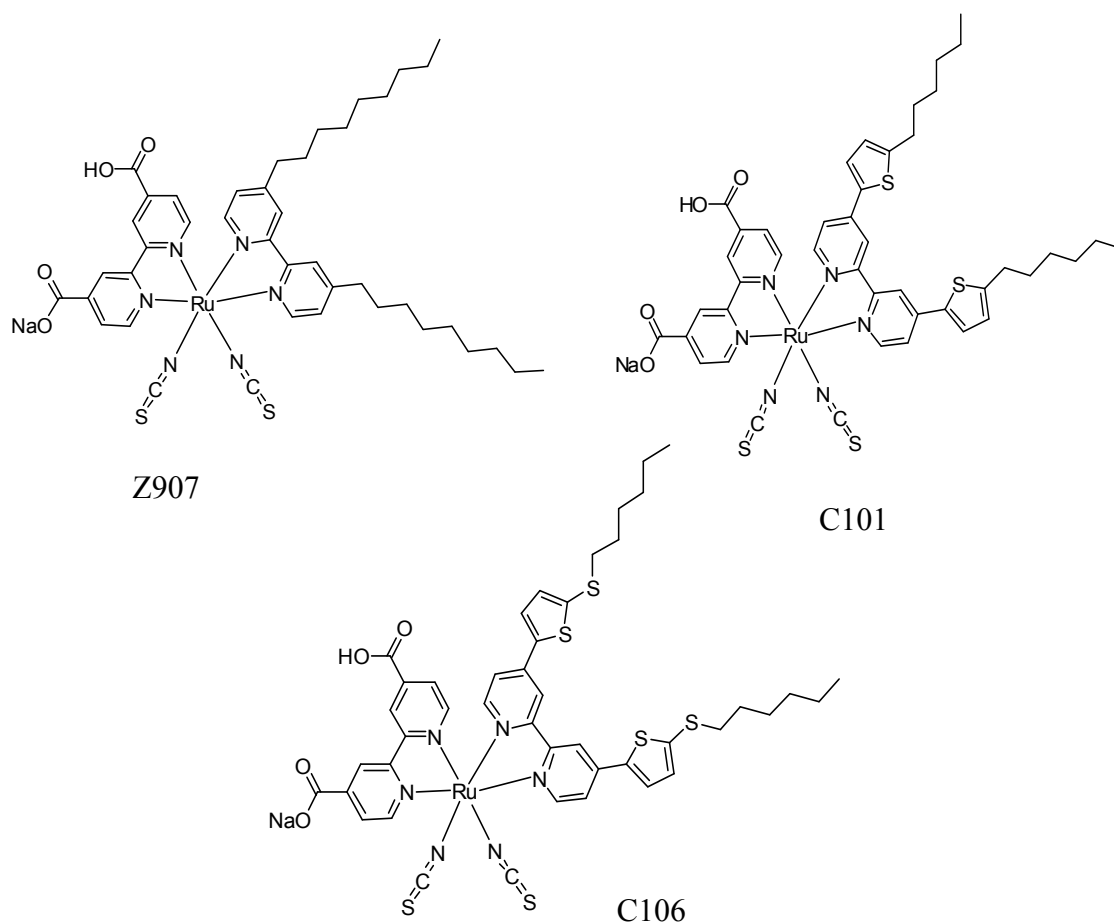


**Figure 1.17** Structures of Z907, C101 and C106

In 2009, Gao and coworkers synthesized ruthenium complex featuring electron-rich selenophene unit in its ancillary ligand (C105) [42]. The photovoltaic performances of this new sensitizer were compared with Z907 amphiphilic dye and the results are shown in Table 1.8. As the results, the device with C105 dye demonstrated higher efficiency than Z907 because the new dye improved the optical absorptivity of mesoporous titanium film.

**Table 1.8** Photovoltaic parameters of dye sensitized solar cells with Z907 and C105 dye.

Dye	$J_{sc}$ (mA/cm <sup>2</sup> )	$V_{oc}$ (mV)	$ff$	Efficiency ( $\eta$ ) (%)
Z907	16.37	767.2	0.717	9.00
C105	18.09	747.8	0.744	10.06

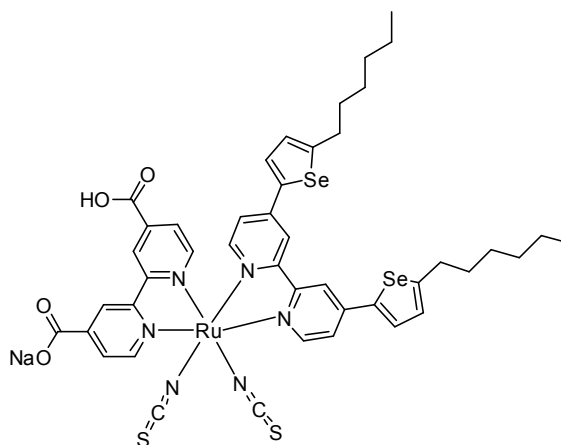


**Figure 1.18** Structure of C105.

In 2010, a new crosslinkable light sensitizer, Ru(2,2'-bipyridine-4,4'-dicarboxylic acid)(4,4'-bis(11-dodecenyl)2,2'-bipyridine)(NCS)<sub>2</sub> was synthesized by Liu and coworkers [43]. The DSSC fabricated from this dye with poly(methylacrylate)-gelled electrolyte system showed  $J_{sc}$ ,  $V_{oc}$ ,  $ff$  and  $\eta$  of 11.1 mA/cm<sup>2</sup>, 0.68 V, 0.67, 5.1%, respectively. Additionally, it also gave long life stability at AM 1.5 illumination (100 mW/cm<sup>2</sup>).

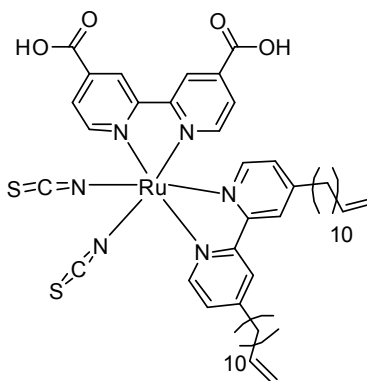


**Figure 1.19** Structure of Ru(2,2'-bipyridine-4,4'-dicarboxylic acid)(4,4'-bis(11-dodecenyl)2,2'-bipyridine)(NCS)<sub>2</sub>

In 2010, A new ruthenium sensitizer (T18) which consist of an electron rich ketene thioacetal modified bipyridyl group was synthesized by Kissarwan and coworkers [44]. The new sensitizer showed a red shift and larger metal to ligand charge transfer absorption when compared to N719. The photovoltaic performance og solar cell sensitized with T18 showed higher currents than N719 (Table 1.9).

**Table 1.9** Photovoltaic parameters of dye sensitized solar cells with T18 and N719 dye.

Dye	$J_{sc}$ (mA/cm <sup>2</sup> )	$V_{oc}$ (mV)	$ff$	Efficiency ( $\eta$ ) (%)
N719	16.2	0.60	0.67	6.5
T18	16.8	0.57	0.71	6.8

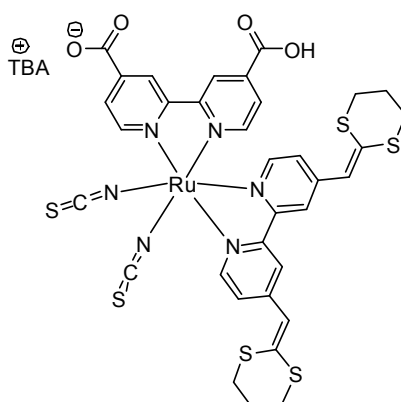


**Figure 1.20** Structure of T18.

In 2010, Lee K. E. *et al.* studied the adsorption mechanism of N719 dye on TiO<sub>2</sub> films by using ATR-FTIR and confocal Raman imaging [45]. ATR-FTIR spectroscopy of the high wavenumber region displayed Ti-OH/Ti-OH<sub>2</sub> bands before and after N719 dye adsorption, indicating the N719 molecules interact via both hydrogen bonding and covalent bidentate-bridging bonding. Additionally, the Raman imaging distribution of COO<sup>-</sup> on TiO<sub>2</sub> was used to show the covalent and hydrogen bonding of N719 dye-adsorbed TiO<sub>2</sub> films and the scheme depicting the adsorption of two N719 carboxylic groups onto TiO<sub>2</sub> is shown in Figure 1.21.

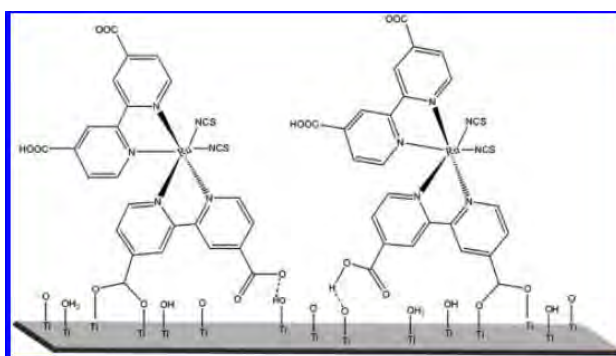


**Figure 1.21** Proposed two adsorption modes of N719 molecules onto TiO<sub>2</sub>

### **1.9 Objectives and scope of the thesis.**

According to all literature reviews, most of ruthenium complexes consist of the long conjugation or long alkyl chain at the *para* position of bipyridine ligand to improve the photophysical properties and conversion efficiency. And the study of electronic effect on the bipyridine ligand is not widespread. Therefore, the objectives of this work are to synthesize bipyridine ruthenium complexes containing amide groups to investigate the electronic effect on bipyridine ring on the photophysical properties, electrochemical properties and photovoltaic performance by comparing them to the reference dye (N3).

## CHAPTER II

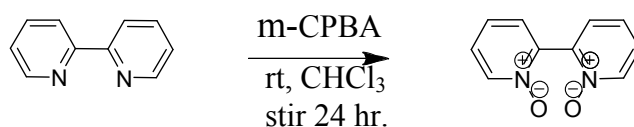
### Materials and Experimental Procedures

**Materials:** Reagent grade chemicals were purchased from Fluka (America) and Sigma-aldrich (Switzerland) and used as received without further purification. Commercial grade organic solvents were distilled prior to use. Column chromatography was performed using Merck silica gel 60 (70-230 mesh). Sephadex LH-20 was purchased from GE healthcare Bio Science. Thin layer chromatography (TLC) was performed on Merck silica gel 60 (70-230 mesh) using UV lamp or a potassium permanganate dipping solution, followed by heating on a hot plate to approximately 350 °C for visualization. Fluorine-doped tin oxide (FTO) coated glass slides were purchased from Pilkington (Canada). Nanocrystalline titaniumdioxide D/SP (casual size) and thin adhesive polymeric film were purchased from Solaronix (Switzerland).

**Characterization:** UV-Vis and photoluminescence spectra were measured in a 1 cm path length quartz cell using a Shimadzu CPS-240A UV-visible spectrophotometer and a Varian Cary Eclipse spectrofluorometer, respectively. <sup>1</sup>H NMR and <sup>13</sup>C NMR measurements were carried out on a Varian Mercury 400 MHz and Bruker 400 MHz NMR spectrometry as CDCl<sub>3</sub>, DMSO-d<sub>6</sub> and Methanol-d<sub>4</sub> solutions. The ATR-FTIR spectra were measured using Nicolet 6700 FT-IR spectrometer equipped with Germanium crystal for contacting the sample. The FT-IR spectrometer was equipped with Schwarzschild Cassegrain infrared beamsplitter and mercury cadmium-telluride (MCT) detector. High resolution mass spectra were recorded on an electrospray ionization mass spectrometer (MicroTOF, Bruker Daltomics).

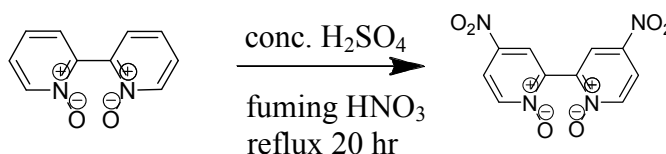
## 2.1 Synthesis

### 2.1.1. Synthesis of 2,2'-bipyridine-*N,N'*-dioxide [46].



A solution of 2,2'-bipyridine (1.00 g, 6.41 mmol) in chloroform (40 mL) was cooled to 0 °C in an ice bath and a solution of *m*-CPBA (4.81 g, 28.0 mmol) in chloroform (40 mL) was carefully added. The mixture was stirred at room temperature for 24 hr. and then extracted with deionized water (30 × 3 mL). The aqueous phase was collected and then evaporated to give 2,2'-bipyridine-*N,N'*-dioxide as a white solid (0.85 g, 71% yield). <sup>1</sup>H NMR (400 MHz, D<sub>2</sub>O) δ (ppm): 8.31 (2H, d, *J* = 6.4 Hz, H6, H6'), 7.69 (2H, t, *J* = 7.3 Hz, H3, H3'), 7.65-7.55 (4H, m, H4, H4', H5, H5') (>170 °C decompose).

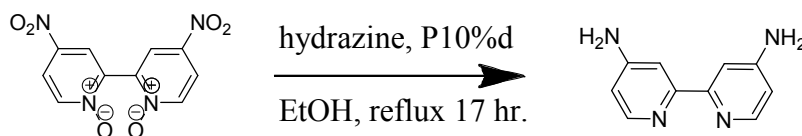
### 2.1.2. Synthesis of 4,4'-dinitro-2,2'-bipyridine-*N,N'*-dioxide [47].



Concentrated sulfuric acid (3 mL, 56.3 mmol) was added to 2,2'-bipyridine-*N,N'*-dioxide (0.50 g, 2.66 mmol). The mixture was first cooled in an ice bath and cautiously added with fuming nitric acid (2 mL, 47.0 mmol). The resulting solution was stirred at reflux (95–100 °C) for 20 hr before cooling to room temperature. The acidic mixture was then poured onto ice. Initially, the solution became green with liberation of N<sub>2</sub>O<sub>4</sub> brown fume. After continued stirring, a bright yellow precipitate formed. The slurry was subsequently filtered and the yellow precipitate was collected. The solid was washed successively with water (3 × 25 mL) and allowed to air dry to give the desired product as a yellow solid (0.27 g, 37% yield). <sup>1</sup>H NMR (400 MHz, DMSO-*d*<sub>6</sub>) δ (ppm):=8.69 (2H, d, *J* = 3.2 Hz, H3, H3'), 8.59 (2H, d, *J* = 7.2 Hz, H6, H6'), 8.37 (2H, dd, *J* = 3.2 and 7.2 Hz, H5, H5') (>200 °C decompose).

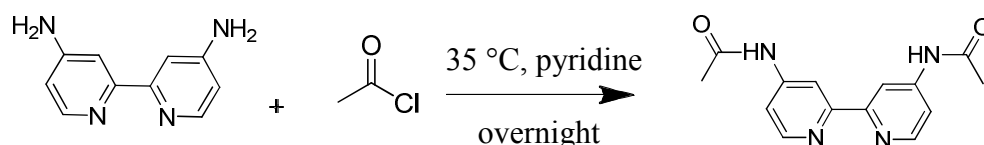


### 2.1.3 Synthesis of 4,4'-diamino-2,2'-bipyridine [48].



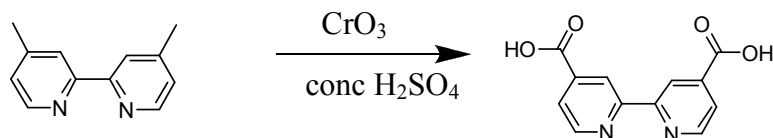
A suspension of 4,4'-dinitro-2,2'-bipyridine-*N,N'*-dioxide (1.11 g, 4.00 mmol) and Pd/C 10% (0.24 g, 0.23 mmol) in ethanol (120 mL) was purged with N<sub>2</sub> gas. The suspension was then heated to reflux under nitrogen and, after 4,4'-dinitro-2,2'-bipyridine-*N,N'*-dioxide was completely dissolved, hydrazine hydrate (8.6 mL, 0.276 mol) in ethanol (30 mL) was added dropwise over a period of 1 hr. The resulting solution was stirred at reflux for 15 hr. When completed, the mixture was immediately filtered hot through a bed of celite and the pad was washed with boiling ethanol (4 × 30 mL). After removal of the solvent, the yellow precipitate was dispersed in water (80 mL) and left in refrigerator overnight. The yellow solid that separated was vacuum filtered, washed with cold water and dried at ambient temperature to give the desired product as a yellow solid (0.52 g, 69% yield). <sup>1</sup>H NMR (400 MHz, DMSO-*d*<sub>6</sub>) δ (ppm): 8.02 (2H, d, *J* = 5.5 Hz, H6, H6'), 7.52 (2H, d, *J* = 2.2 Hz, H3, H3'), 6.44 (2H, dd, *J* = 2.2, 5.5 Hz, H5, H5'), 6.03 (4H, s, NH<sub>2</sub>) (>270 °C decompose).

### 2.1.4 Synthesis of *N,N'*-(2,2'-bipyridine-4,4'-diyl)diacetamide (L2) [49].



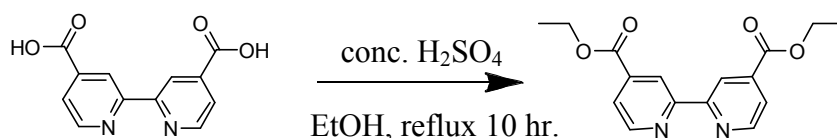
A solution of 4,4'-diamino-2,2'-bipyridine (0.103 g, 0.55 mmol) in pyridine (15 mL) was cooled in an ice bath and acetyl chloride (0.2 mL, 28.1 mmol) was added slowly. The resulting solution was stirred at 35 °C overnight. After cooling at room temperature, the precipitate was filtered, and the solid was washed with methanol and dried to obtain the desired product as a white solid (0.077g, 52% yield) <sup>1</sup>H NMR (400 MHz, DMSO-*d*<sub>6</sub>) δ (ppm): 10.46 (2H, s, NH), 8.55 (2H, s, H3, H3'), 8.50 (2H, d, *J* = 5.5 Hz, H6, H6'), 7.69 (2H, d, *J* = 7.4, H5, H5'), 2.11 (6H, s, CH<sub>3</sub>).

### 2.1.5 Synthesis of 4,4'-dicarboxy-2,2'-bipyridine [50].



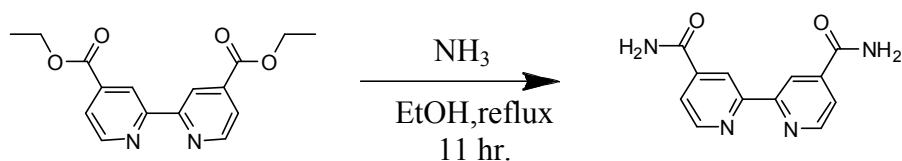
A solution of 4,4'-dimethyl-2,2'-bipyridine (1.00 g, 5.43 mmol) in concentrated  $\text{H}_2\text{SO}_4$  (45 mL) was cooled at 0 °C in an ice bath and  $\text{CrO}_3$  (3.12 g, 31 mmol) was added in small portions during 1 h. The mixture which turned blue-green was heated to 75 °C and stirred for 3 h. The reaction mixture was cooled to room temperature and stirred for 10 hours before being poured into a mixture of ice and water. The white precipitate was separated by centrifugation and washed several times with water. The powder was then suspended in water, and KOH was added under vigorous stirring until the solution was basic. The blue insoluble residual solid was filtered off. The aqueous filtrate was acidified with HCl to precipitate the diacid which was filtered, washed with water, methanol, and diethyl ether, and dried *in vacuo* to give the desired product as a white solid (0.95 g, 72% yield).  $^1\text{H}$  NMR (400 MHz,  $\text{D}_2\text{O}$ )  $\delta$  (ppm): 8.51 (2H, d,  $J = 4.91$ , H6, H6'), 8.12 (2H, s, H3, H3'), 7.60 (2H, d,  $J = 4.04$  Hz, H5, H5').

### 2.1.6 Synthesis of diethyl 2,2'-bipyridine-4,4'-dicarboxylate [51].



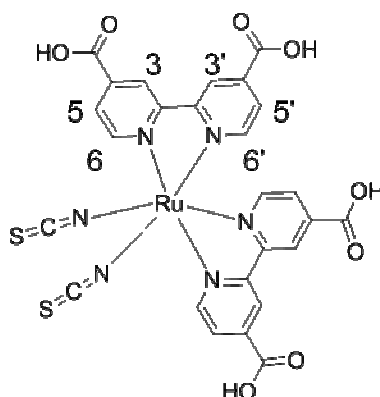
A solution of 2,2'-bipyridine-4,4'-dicarboxylic acid (2.02 g, 8.30 mmol) in a mixture of concentrated sulfuric acid (21 mL) and absolute ethanol (45 mL) was stirred at reflux for 10 hr and was then allowed to cool to room temperature before pouring on ice. Neutralization with 25% aqueous sodium hydroxide caused precipitation of a white solid. The solid was collected by filtration, washed with water and air dried. The solid was recrystallized in absolute ethanol to give the desired product as a white solid (1.05 g, 42% yield).  $^1\text{H}$  NMR (400 MHz,  $\text{CDCl}_3$ )  $\delta$  (ppm): 8.95 (2H, s, H3, H3'), 8.86 (2H, d,  $J = 5.0$  Hz, H6, H6'), 7.88 (2H, d,  $J = 5.0$  Hz, H5, H5'), 4.43 (4H, q,  $J = 7.1$ ,  $\text{CH}_2$ ), 1.42 (6H, t,  $J = 7.1$  Hz,  $\text{CH}_3$ ) (m.p. 160-162 °C).

### 2.1.7 Synthesis of 2,2'-bipyridine-4,4'-dicarboxamide (L1) [51].



A suspension of diethyl-2,2'-bipyridine-4,4'-dicarboxylate (0.051 g 0.17 mmol) in absolute ethanol (3 mL) saturated with anhydrous ammonia at 0 °C was heated in a sealed tube for 11 hr at 90 °C. After cooling, the content of the tube was filtered, and the solid thus obtained was washed with absolute ethanol and dried to afford a white solid. The product was recrystallized in ethylene glycol to afford the pure product as a white solid 0.028 g (67% yield). <sup>1</sup>H NMR (400 MHz, DMSO-d<sub>6</sub>) δ (ppm): 8.84 (2H, d, *J*=5.0 Hz, H6, H6'), 8.75 (2H, s, H3, H3'), 7.83 (2H, d, *J*=5.0 Hz, H5, H5').

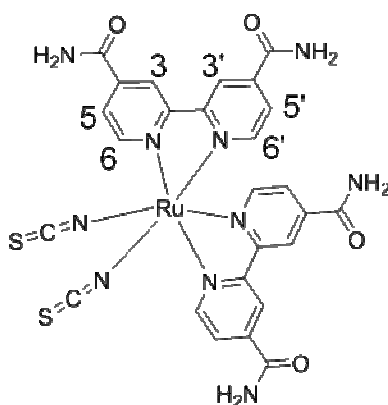
### 2.1.8 Synthesis of N3 [52].



A mixture of dichloro(*p*-cymene)ruthenium(II) dimer (0.101g, 0.17 mmol) and 4,4'-dicarboxylic acid-2,2'-bipyridine (0.161 g, 0.66 mmol) were dissolved in DMF (30 mL). The mixture was stirred at 140 °C for 4 hr under N<sub>2</sub> in the dark. Subsequently, an excess of NH<sub>4</sub>NCS (1.03 g, 13.5 mmol) was added into the flask and kept heating at 140 °C for additional 4 hr. The reaction mixture was then cooled down to room temperature and the solvent was removed in a rotary evaporator under vacuum. Water was added to cause precipitation. The pH was adjusted to 3 with HNO<sub>3</sub> (0.2 M) and the mixture was allowed to stand in the fridge overnight. The resulting purple solid was filtered, washed with water and Et<sub>2</sub>O. Purification on

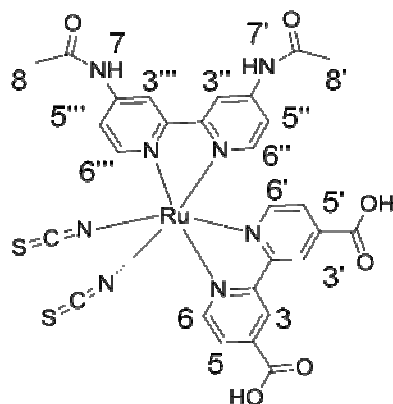
Sephadex LH20 using methanol as an eluent afforded the desired complex as a dark purple solid 0.181 g (100 % yield).  $^1\text{H}$  NMR (400 MHz, methanol- $d_4$ )  $\delta$  (ppm): 9.58 (2H, d,  $J = 5.8$  Hz, H6'), 9.03 (2H, s, H3'), 8.87 (2H, s, H3), 8.30 (2H, d,  $J = 5.8$  Hz, H5'), 7.79 (2H, d,  $J = 5.9$  Hz, H6), 7.61 (2H, d,  $J = 5.9$  Hz, H5).

**2.1.9 Synthesis of  $[\text{Ru}(\text{II})(\text{L}^1)_2(\text{NCS})_2]$  (Where  $\text{L}^1 = 2,2'$ -bipyridine-4,4'-dicarboxamide (Dye1) [52].**



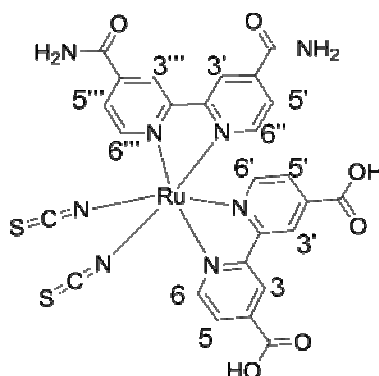
A mixture of dichloro(*p*-cymene)ruthenium(II) dimer (0.100g, 0.16 mmol) and 2,2'-bipyridine-4,4'-dicarboxamide (0.1600 g, 66  $\mu\text{mol}$ ) were dissolved in DMF (30 mL). The mixture was stirred at 140  $^\circ\text{C}$  for 4 hr under  $\text{N}_2$  in the dark. Subsequently, an excess of  $\text{NH}_4\text{NCS}$  (1.03 g, 13.5 mmol) was added into the flask and kept heating at 140  $^\circ\text{C}$  for additional 4 hr. The reaction mixture was then cooled down to room temperature and the solvent was removed in a rotary evaporator under vacuum. Water was added to cause precipitation and the mixture was allowed to stand in the fridge overnight. The resulting dark solid was filtered, washed with water. Purification on Sephadex LH20 using methanol as an eluent to remove the impurity. The precipitate on the top of sephadex column was collected and dissolved in methanol and small amount of DMF. Again, purification on Sephadex LH20 using methanol as an eluent afforded the desired complex as a dark solid 0.071 g (62 % yield).  $^1\text{H}$  NMR (400 MHz, DMSO- $d_6$ )  $\delta$  (ppm): 9.34 (2H, d,  $J = 6.0$  Hz, H6'), 9.18 (2H, s, H3'), 9.02 (2H, s, H3), 8.32 (2H, d,  $J = 6.0$  Hz, H5'), 7.77 (2H, d,  $J = 5.9$  Hz, H6), 7.56 (2H, d,  $J = 5.9$  Hz, H5).

**2.1.10 Synthesis of  $[\text{Ru}(\text{II})\text{LL}^2(\text{NCS})_2]$  (Where L= 4,4'-Dicarboxy-2,2'-bipyridine and  $\text{L}^2 = \text{N,N}'\text{-(2,2'-bipyridine-4,4'-diyl)diacetamide}$  (Dye2) [30].**



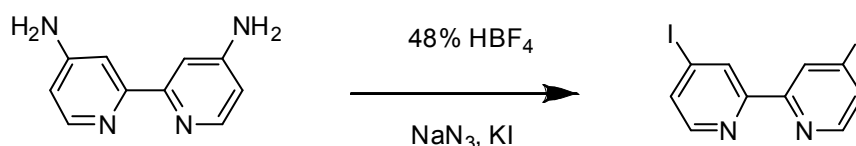
A mixture of dichloro(*p*-cymene)ruthenium(II) dimer (0.102g, 0.17 mmol) and *N,N'*-(2,2'-bipyridine-4,4'-diyl)diacetamide (0.090 g, 0.33 mmol) were dissolved in DMF (30 mL). The reaction mixture was stirred at 80 °C for 4 hr under  $\text{N}_2$  in the dark. Subsequently, 4,4'-dicarboxylic acid-2,2'-bipyridine (0.081 g, 0.33 mmol) was added into the flask and the mixture was heated to 140 °C and the stirring was continued for 4 hr. An excess of  $\text{NH}_4\text{NCS}$  (1.03 g, 14 mmol) was added to the resulting dark reaction mixture while the stirring was continued at 140 °C for 4 hr more. The reaction mixture was cooled down to room temperature and the solvent was removed by a rotary evaporator. Water was added to give dark precipitate. The solid was collected on a sintered glass crucible by suction filtration, washed with water and dried *in vacuo*. The crude complex was dissolved in MeOH and purified on a Sephadex LH-20 column using methanol as an eluent. The main band was collected and dried *in vacuo* to give the desired product as dark purple solid (0.192 g, 100% yield).  $^1\text{H}$  NMR (400 MHz, methanol- $\text{d}_4$ )  $\delta$  (ppm): 9.48 (1H, d,  $J = 5.7$  Hz, H6'), 9.21 (1H, d,  $J = 6.2$  Hz, H6''), 8.95 (1H, s, H3'), 8.81 (1H, s, H3), 8.78 (1H, s, H3'''), 8.62 (1H, s, H3''), 8.17 (1H, d,  $J = 5.7$  Hz, H5'), 7.91 (1H, d,  $J = 6.2$  Hz, H5''), 7.72 (1H, d,  $J = 5.9$  Hz, H6), 7.55 (1H, d,  $J = 5.9$  Hz, H5), 7.32 (1H, d,  $J = 6.4$  Hz, H6'''), 7.26 (1H, d,  $J = 6.4$  Hz, H5'''), 4.62 (2H, s, NH), 2.29 (3H, s, H8), 2.14 (3H, s, H8').

**2.1.11 Synthesis of  $[\text{Ru}(\text{II})\text{LL}^1(\text{NCS})_2]$  (Where  $\text{L} = 4,4'$ -Dicarboxy-2,2'-bipyridine and  $\text{L}^1 = 2,2'$ -bipyridine-4,4'-dicarboxamide (Dye3) [30].**



Dye3 was synthesized by a procedure similar to Dye2 except  $\text{L}^1$  (0.082 g, 0.33 mmol) was used in place of  $\text{L}^2$ . Yield = 0.11 g (96% yield).  $^1\text{H}$  NMR(400 MHz, Methanol- $\text{d}_4$ )  $\delta$  (ppm): 9.62 (1H, d,  $J = 5.9$  Hz,  $\text{H}_{6''}$ ), 9.45 (1H, d,  $J = 5.7$  Hz,  $\text{H}_{6''}$ ), 9.05 (H, s,  $\text{H}_{3''}$ ), 9.01 (1H, s,  $\text{H}_3$ ), 8.89 (1H, s,  $\text{H}_{3''''}$ ), 8.85 (1H, s,  $\text{H}_{3''}$ ), 8.22 (1H, d,  $J = 5.9$  Hz,  $\text{H}_{5''}$ ), 7.78 (2H, d,  $J = 5.9$  Hz,  $\text{H}_{5''}$ ), 7.63 (1H, d,  $J = 5.9$  Hz,  $\text{H}_6$ ), 7.56 (2H, t,  $J = 6.74$  Hz,  $\text{H}_5$ ).

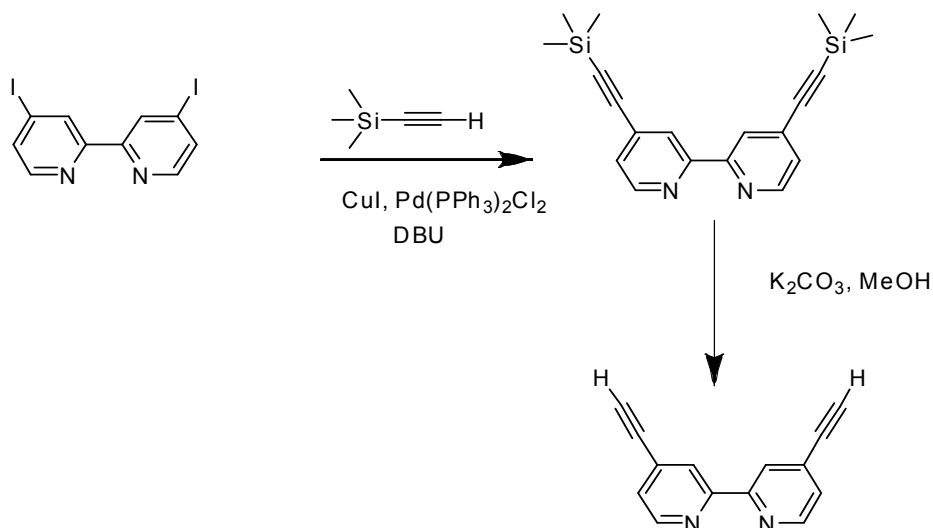
**2.1.12 Synthesis of 4,4'-diiodo-2,2'-bipyridine [53].**



4,4'-diamino-2,2'-bipyridine (0.506 g, 2.7 mmol) was suspended in 48% aqueous  $\text{HBF}_4$  (15 mL) and cooled to  $-10$  °C. Then, sodium nitrite (0.800 g, 12 mmol) was added portionwise over the course of about 1 hr. After an additional 15 min stirring, the precipitate of diazonium salt was isolated by suction filtration. This was then added to a cooled ( $-10$  °C) solution of potassium iodide (3.09 g, 19 mmol) in an acetone-water (2:3, 15 mL) portionwise over the course of about 30 min. The reaction mixture was stirred for 30 min. Then, it was neutralized by adding aqueous sodium carbonate and a saturated sodium thiosulphate solution (20 mL) was added to decolorized the solution. Extraction with dichloromethane ( $4 \times 25$  mL) gave a yellow solution, which was dried over anhydrous  $\text{MgSO}_4$  and treated with activated carbon. Following filtration through a bed of celite and the pad, the solvent was removed

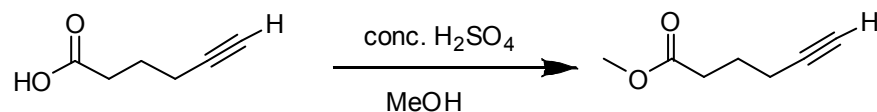
under vacuum to afford the white solid (0.376 g, 34%yield).  $^1\text{H}$  NMR (400 MHz,  $\text{CDCl}_3$ )  $\delta$  (ppm): 8.80 (2H, s, H3), 8.31 (2H, d,  $J = 5.1$  Hz, H6), 7.71 (2H, d,  $J = 5.1$  Hz, H5).

### 2.1.13 Synthesis of 4,4'-diethynyl-2,2'-bipyridine [54-57]



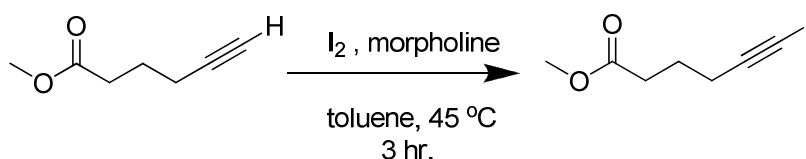
The mixture of 4,4'-Diiodo-2,2'-bipyridine (0.103 g, 0.25 mmol),  $\text{Pd}(\text{PPh}_3)_2\text{Cl}_2$  (0.009 g, 0.012 mmol) and  $\text{CuI}$  (0.004 g, 0.021 mmol) was put together in a round-bottomed flask, toluene (10 mL) was added and this then was purged with  $\text{N}_2$  gas 15 min. After that, 1,8-diazabicycloundec-7-ene (0.1 mL, 0.67 mmol) and ethynyltrimethylsilane (0.1 mL, 1.0 mmol) were added. The reaction mixture was stirred at room temperature overnight. Then, toluene was removed under vacuum and the crude product was purified by column chromatography using 5% ethylacetate in hexane as an eluent to get the product (0.023 g, 26%yield). Next step, methanol solvent (20 mL) was added in 4,4'-bis(trimethylsilyl)ethynyl-2,2'-bipyridine (0.066 g, 0.19 mmol), then  $\text{K}_2\text{CO}_3$  (0.001 g, 0.007 mmol) was added. The reaction mixture was stirred at room temperature 1 hr. After that, it was neutralized by adding 2 M  $\text{HCl}$  and water (20 mL) was added. Extraction with hexane ( $3 \times 20$  mL) which was dried over anhydrous  $\text{MgSO}_4$ . The organic phase was collected and evaporated under vacuum to afford the desired product (0.040 g, 100% yield).  $^1\text{H}$  NMR (400 MHz,  $\text{CDCl}_3$ )  $\delta$  (ppm): 8.65 (2H, d,  $J = 4.9$  Hz, H6), 8.48 (2H, s, H3), 7.38 (2H, d,  $J = 4.9$  Hz, H5), 3.32 (1H, s,  $-\text{C}\equiv\text{CH}$ ).

### 2.1.14 Synthesis of methyl hexynoate [51]



The methanol solvent (25 mL) and a few drops of conc.  $\text{H}_2\text{SO}_4$  were added in 5-hexynoic acid (1.048 g, 9.35mmol). The mixture was refluxed for 3 hr, then it was cooled to room temperature and the solvent was removed in a rotary evaporator under vacuum. It was then extracted with  $\text{Na}_2\text{CO}_3$  (1 M, 30 mL) and dichloromethane ( $3 \times 25$  mL), the organic phase was collected and dried over anhydrous  $\text{MgSO}_4$ . The solvent was removed under vacuum to get the ester product (1.43 g, 100%yield).  $^1\text{H}$  NMR (400 MHz,  $\text{CDCl}_3$ )  $\delta$  (ppm): 3.62 (3H, s,  $\text{OCH}_3$ ), 2.40 (2H, t,  $J = 7.2$  Hz,  $-\text{COCH}_2$ ), 2.21 (2H, t,  $J=6.9$ ,  $\text{C}\equiv\text{CCH}_2$ -), 1.9 (1H, s,  $-\text{C}\equiv\text{CH}$ ), 1.79 (2H, q,  $J = 7.2$ ,  $-\text{COCH}_2\text{CH}_2\text{CH}_2$ ).

### 2.1.15 Synthesis of iodo methyl hexynoate



A solution of morpholine (10 mL, 114mmol) in toluene (175 mL) was added with iodine (4.49 g, 18 mmol), shielded from light and stirred at 45 °C for 3 hr. A solution of methyl hexynoate (1.43g, 11.3 mmol) was gradually added and the reaction mixture was stirred at 45 °C for 3 hr. Then, the reaction mixture was cooled to room temperature and filtered to remove the by-product salt. The filtrate was poured over a mixture of diethylether (200 mL) and saturated aqueous solution of  $\text{Na}_2\text{S}_2\text{O}_3$  (50 mL) and shaken until the organic layer was colorless. The organic layer was separated, dried over anhydrous  $\text{MgSO}_4$ , filtered, concentrated and purified by column chromatography with hexane and ethylacetate (8:2 v/v) as an eluent to afford the desired product (1.84 g, 65%yield) The product was not stable that it should be kept in a refrigerator, shielded from light or used as fresh as a starting material for the



next synthetic step.  $^1\text{H}$  NMR (400 MHz,  $\text{CDCl}_3$ )  $\delta$  (ppm): 3.66 (3H, s,  $\text{OCH}_3$ ), 2.42 (4H, t,  $J = 7.9$  Hz,  $-\text{COCH}_2\text{CH}_2\text{CH}_2-$ ), 1.82 (2H, quint,  $J = 7.14$ ,  $-\text{COCH}_2\text{CH}_2\text{CH}_2-$ ).

## 2.2. Fabrication of dye-sensitized solar cells [58]

A transparent conducting fluorine-doped tin oxide (FTO) coated glass slides was screen printed with the nanocrystalline  $\text{TiO}_2$  and sintered at  $450\text{ }^\circ\text{C}$  for 60 min. Screen printing process of  $\text{TiO}_2$  particles were repeated to produce  $\text{TiO}_2$  layer of  $19\text{ }\mu\text{m}$  thick measured by Dektak 6 M Stylus Profiler. The  $\text{TiO}_2$  glass was dipped into a dye solution ( $3 \times 10^{-4}$  M in methanol) for 48 hr. The dye-coated electrode was rinsed with methanol and a platinum glass electrode was put on the dye-coated electrode separated by thin adhesive polymeric film sheets (Solaronix, Switzerland). The sandwiched electrodes were tightly held, and then heated around the thin film sheets to attach the two electrodes. The electrolyte, consisting of  $\text{LiI}$ ,  $\text{I}_2$ , TBP (tetrabutyl pyridine) and MeEtImDCA (ethylmethylimidazolium dicyanamide) was introduced into the inter-electrode space. Then, the cells were sealed with epoxy sealant to avoid leakage of the electrolyte solution.

## 2.3 The preparation of polydiacetylene vesicle from 10,12 pentacosadiynoic acid (PCDA monomer)

A known amount of PCDA was dissolved in chloroform and followed by evaporated by nitrogen gas to remove the solvent. A volume of Milli-Q water was added and the suspension was heated to  $75\text{-}80\text{ }^\circ\text{C}$  and sonicated in ultrasonic bath for 30 minutes. The solution was kept in refrigerature overnight. Then, the vesicle solution was UV irradiated at 254 nm and filtered through a filter paper no.1 to give a clear blue solution.

## 2.4 Preparation of dye sensitized photovoltaic cells by using polydiacetylene.

The fabrication of dye sensitized solar cell with an incorporation of polydiacetylene vesicle is similar to the procedure described above. Only one step was inserted in the procedure; after dipping  $\text{TiO}_2$  glass in the dye solution for 48 hr and dried by blowing with  $\text{N}_2$  gas. The dye adsorbed  $\text{TiO}_2$  was then immersed in 2 mM polydiacetylene vesicle for 48 hr.

## **2.5. Cyclic voltametry measurements**

The cyclic voltametry was performed using an AUTOLAB system ( $\mu$ 3Aut70834). All measurements were made at room temperature on sample solutions in freshly distilled methanol with 0.1 M tetra-n-butylammonium hexafluorophosphate as an electrolyte and the concentration of N3 and new dyes was 1.0 mM. The electrolyte solution was degassed by nitrogen bubbling. A glassy carbon working electrode, a platinum wire counter electrode, and a Ag/AgCl (Sat.) reference electrode were used in all cyclic voltametric experiments. And the samples were measured with scan rate 100 mV/sec.

## **2.6 Photocurrent-voltage measurement**

Photovoltaic performance data were measured using a 1000 W ozone free xenon light source that gives intensity at the cell surface of 100 mW/cm<sup>2</sup> equivalent to one sun at Air Mass (AM) 1.5

## CHAPTER III

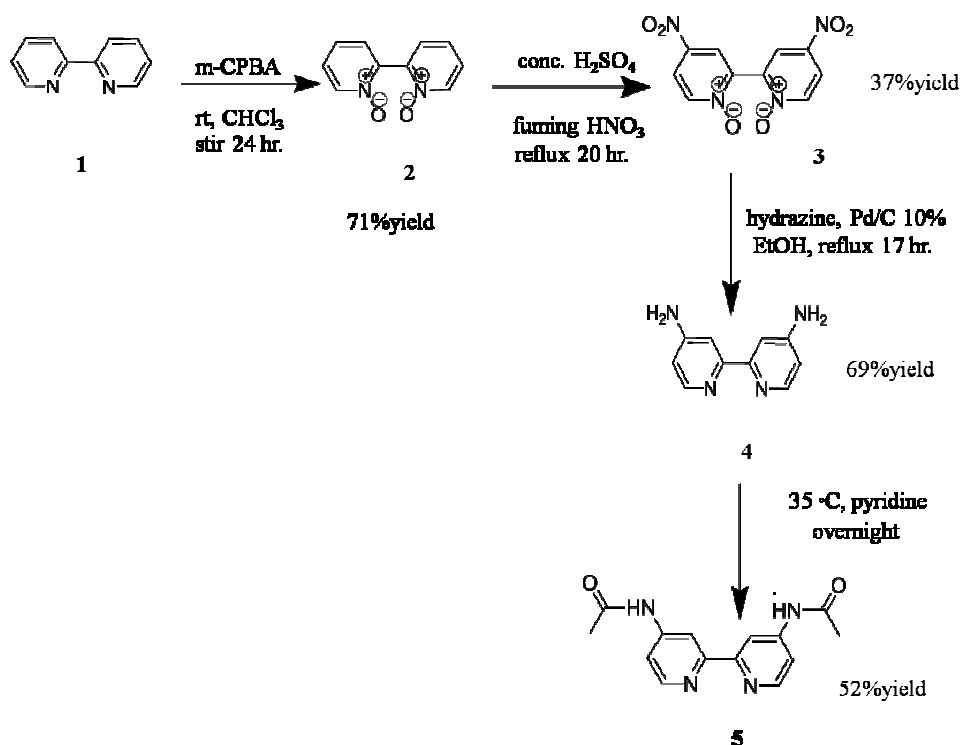
### RESULTS AND DISCUSSION

The outline of this chapter starts with the results and discussion of synthesis and characterization of the bipyridine ligands and their new ruthenium complexes followed by the electrochemical and photophysical properties of the new ruthenium complexes. The photovoltaic performances of the photovoltaic cells using the ruthenium complexes as photosensitizers are presented at the final part of this chapter.

#### 3.1 Synthesis of bipyridine ligands

##### 3.1.1 Synthesis of *N,N'*-(2,2'-bipyridine-4,4'-diyl)diacetamide **5**

The synthesis of *N,N'*-(2,2'-bipyridine-4,4'-diyl)diacetamide **5** started with the oxidation reaction of 2,2'-bipyridine **1** using meta chloroperbenzoic acid to afford 2,2'-bipyridine-*N,N'*-dioxide **2** as a white solid in 71% yield (Scheme 3.1) [46]. Next, nitration of **2** with a mixture of concentrated sulfuric acid and fuming nitric acid (H<sub>2</sub>SO<sub>4</sub>/HNO<sub>3</sub>) under reflux condition gave compound **3** in 37% yield [47]. The nitro groups of compound **3** were reduced by hydrazine and Pd/C as a catalyst to obtain 4,4'-diamino-2,2'-bipyridine **4** in 69% yield [48]. Finally, acetylation of the diaminobipyridine **4** with acetyl chloride gave the corresponding diacetamide compound **5**, (*N,N'*-(2,2'-bipyridine-4,4'-diyl)diacetamide), in 52% yield [49].



**Scheme 3.1** The synthesis of *N,N'*-(2,2'-bipyridine-4,4'-diyl)diacetamide (**5**)

The  $^1\text{H}$  NMR spectra of the bipyridine compounds synthesized are shown in Figure 3.1. All signals can be assigned to all protons presenting in the corresponding structures. The signals around 6.0-9.0 ppm correspond to aromatic protons of the bipyridine rings. The 2,2'-bipyridine-*N,N'*-dioxide **2** showed three signals of the aromatic protons. The doublet, triplet and multiplet signals at 8.3 ppm 7.7 ppm 7.6 ppm with an integral ratio of 1:1:2 correspond to  $\text{H}_6$ ,  $\text{H}_5$  and the combination of  $\text{H}_3$  and  $\text{H}_4$ , respectively. After the nitration, the three signals were shifted to appear within the range of 8.0-9.0 ppm as a singlet, doublet and doublet signals with an integral ratio of 1:1:1 corresponding to  $\text{H}_3$ ,  $\text{H}_6$  and  $\text{H}_5$ , respectively, agreeing well with the para substitution on the bipyridine rings of nitro compound **3**. When the nitro groups were reduced to amino groups, the three signals shifted significantly down field to appear within the range of 6.5-8.0 ppm and a new peak appeared at 6.0 ppm corresponding to the amino protons. Upon acetylation, the amino groups were converted to the acetamide groups which showed the proton signal at 10.5 ppm and the three aromatic signals shifted downfield to 7.7- 8.5 ppm range. In addition, a singlet signal of methyl group was observed at 2.1 ppm confirming the structure of **5**.

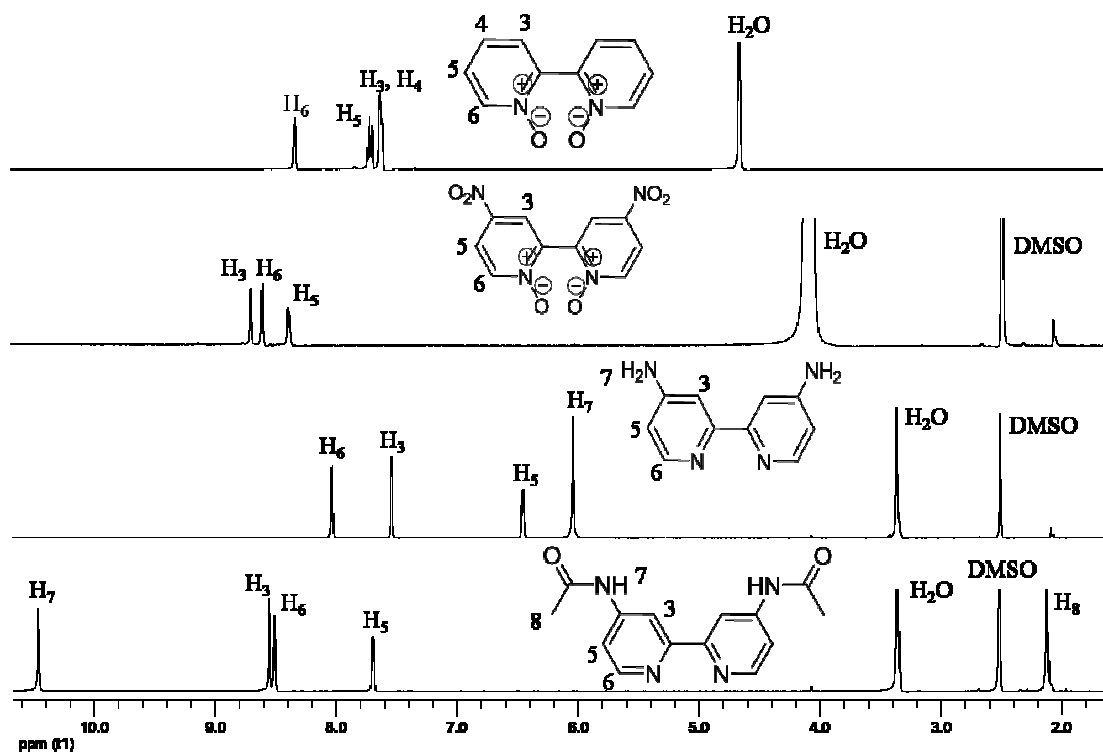
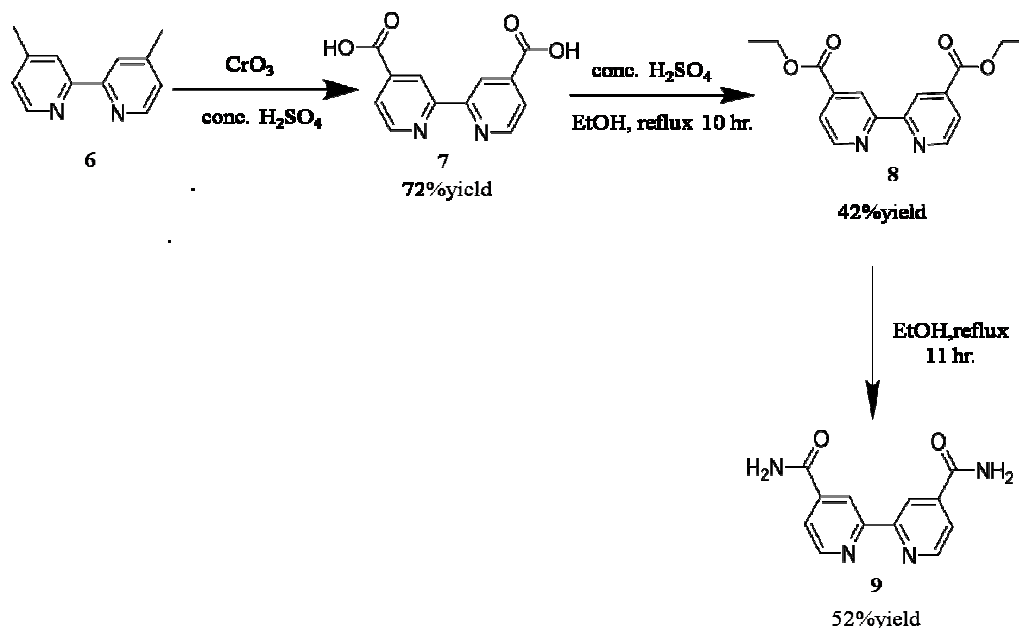


**Figure 3.1**  $^1\text{H}$  NMR spectra of 2,2'-bipyridine- $N,N'$ -dioxide in  $\text{D}_2\text{O}$ , 4,4'-dinitro-2,2'-bipyridine- $N,N'$ -dioxide in  $\text{DMSO-d}_6$ , 4,4'-diamino-2,2'-bipyridine in  $\text{DMSO-d}_6$  and  $N,N'$ -(2,2'-bipyridine-4,4'-diyl)diacetamide in  $\text{DMSO-d}_6$ .

### 3.1.2 Synthesis of 2,2'-bipyridine-4,4'-dicarboxamide **9**

The synthesis of 2,2'-bipyridine-4,4'-dicarboxamide **9** was achieved in three steps according to Scheme 3.2. Initially oxidation of 4,4'-dimethyl-2,2'-bipyridine with chromium(VI) oxide ( $\text{CrO}_3$ ) in the presence of concentrated sulfuric acid afforded 4,4'-dicarboxyl-2,2'-bipyridine [50]. The second step, carboxyl compound **7** was treated with a mixture of absolute ethanol and concentrated sulfuric acid to form diethyl 2,2'-bipyridine-4,4'-dicarboxylate **8** [51]. Finally, finished the synthesis of 2,2'-bipyridine-4,4'-dicarboxamide from condensation of the ester compound **8** and  $\text{NH}_3$  gas using ethanol as solvent [51].



**Scheme 3.2** The synthesis of 2,2'-bipyridine-4,4'-dicarboxamide (**9**)

The  $^1\text{H}$  NMR spectrum of bipyridine compounds synthesized are shown in Figure 3.2. The signals of dicarboxylic acid **7** showed signals of aromatic protons of bipyridine ring as a doublet at 8.5 ppm, a singlet at 8.1 ppm and a doublet at 7.6 ppm with an integral ratio of 1:1:1 corresponding to  $\text{H}_6$ ,  $\text{H}_3$  and  $\text{H}_5$ , respectively. Upon the conversion of **7** to diethyl ester **8**, the three aromatic signals were shifted up field to 7.9-9.0 ppm range. The singlet, doublet and doublet signals with an integral ratio of 1:1:1 correspond to  $\text{H}_3$ ,  $\text{H}_6$  and  $\text{H}_5$ , respectively. In addition, a quartet and triplet signals of ethyl group were observed at 4.4 and 1.4 ppm. After amidation of **8**, the signals of ethyl group disappeared and only the signal of  $\text{H}_3$  was significantly shifted from 9.0 to 8.8 ppm while the other two aromatic signals remained largely at the same positions.

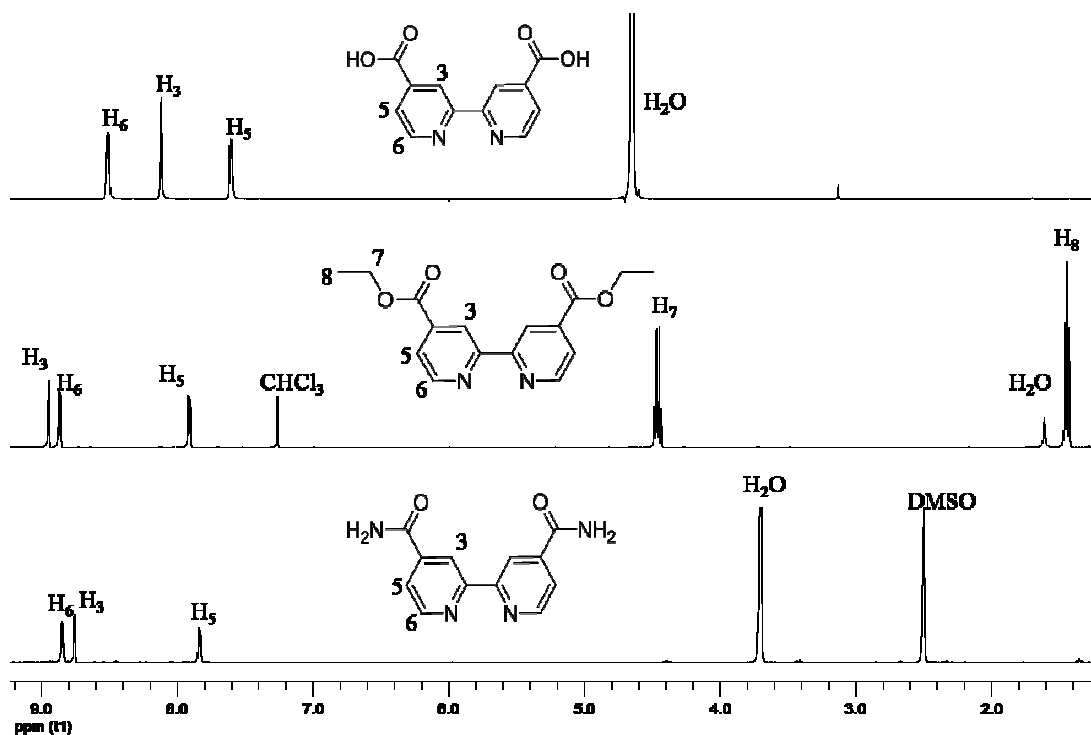
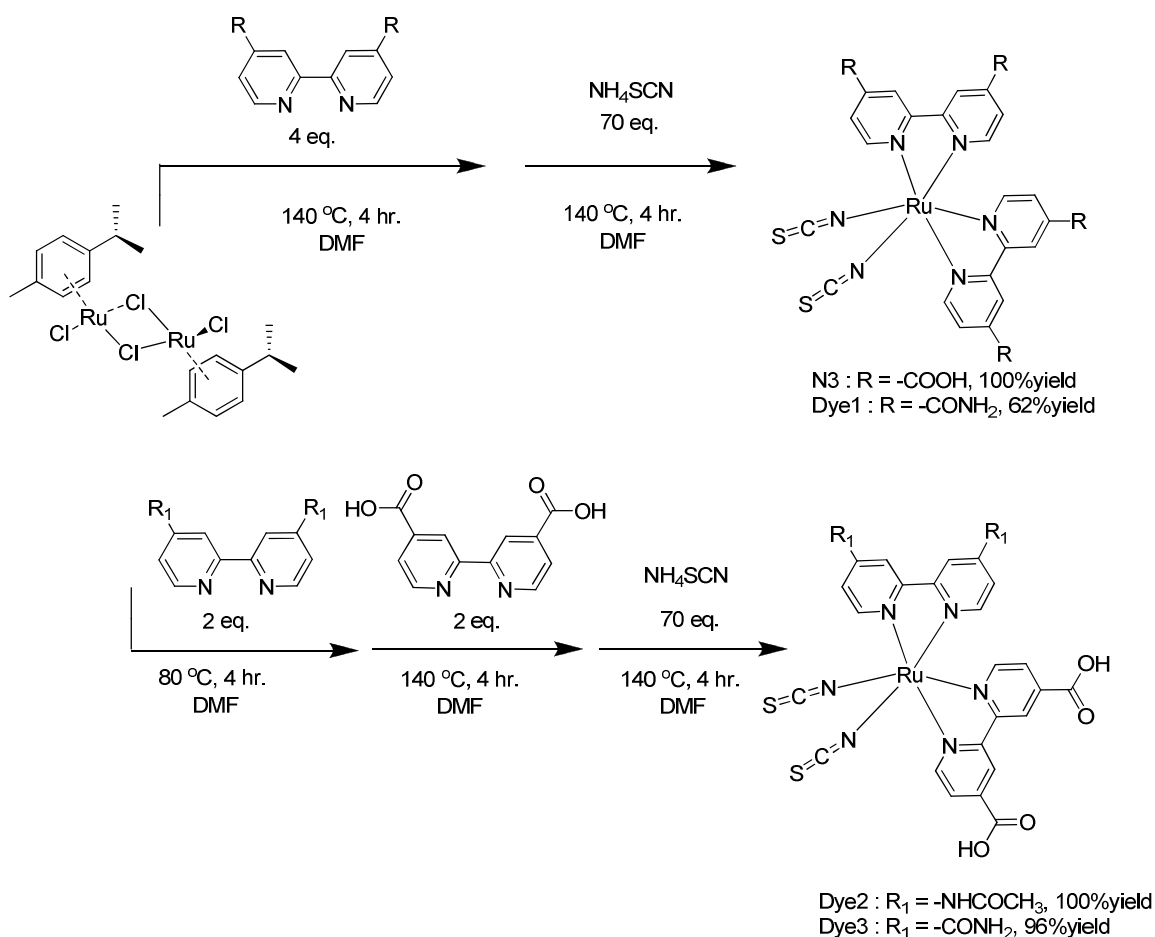


**Figure 3.2**  $^1\text{H}$  NMR spectra of 4,4'-dicarboxyl-2,2'-bipyridine, diethyl 2,2'-bipyridine-4,4'-dicarboxylate and 2,2'-bipyridine-4,4'-dicarboxamide in  $\text{D}_2\text{O}$ ,  $\text{CDCl}_3$  and  $\text{DMSO-d}_6$  respectively.

### 3.2 Synthesis of Ruthenium complexes

The bipyridine compounds **5**, **7**, and **9** were used as ligands for the synthesis of four ruthenium complexes, N3, Dye1, Dye2 and Dye3 (Scheme 3.3). N3 and Dye1 are the complexes consisting of the same bipyridine ligands. They were synthesized in two steps from  $[\text{RuCl}_2(p\text{-cymene})]_2$  [52]. The first step involved ligand displacement with 4,4'-dicarboxy-2,2'-bipyridine **7** for the synthesis of N3 and with 2,2'-bipyridine-4,4'-dicarboxamide **9** for the synthesis of Dye1. In the second step, the last two binding positions of the original ligand were displaced with two thiocyanate groups by heating with a large excess of ammonium thiocyanate. In the synthesis of Dye2 and Dye3 [30], different bipyridine ligands were reacted with  $[\text{RuCl}_2(p\text{-cymene})]_2$  in the synthesis sequence. The sequence of ligands **5** and **7** was used in the synthesis of Dye2 while the sequence of ligands **9** and **7** was used in the synthesis of Dye3. Again, two thiocyanate groups were incorporated in the last step. All the reactions were carried out under dark condition to avoid light induced *cis* to *trans* isomerisation.



**Scheme 3.3** Synthesis of N3, Dye1, Dye2 and Dye3.

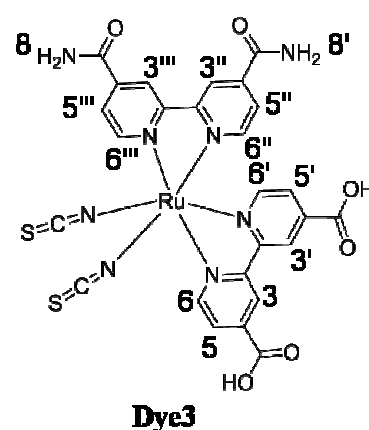
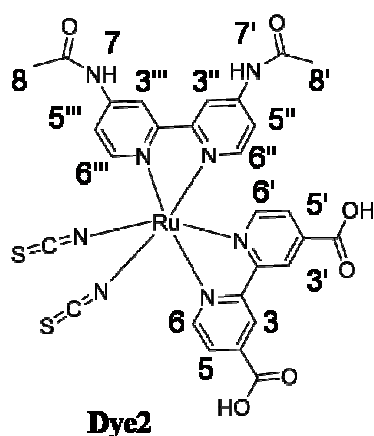
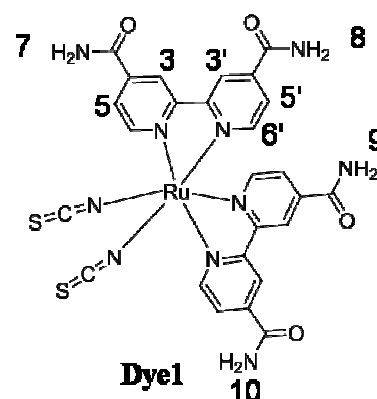
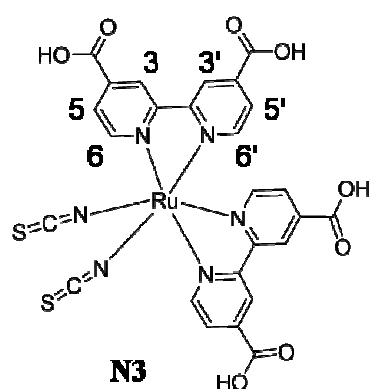
N3, Dye1, Dye2 and Dye3 were obtained from  $[\text{RuCl}_2(\text{p-cymene})\text{]}_2$  in 100, 62, 100 and 96% yield, respectively after purification on Sephadex LH20 column using methanol as an eluent. All the dyes were obtained as the dark purple solids which were characterized by  $^1\text{H}$  NMR, MS and ATR-IR. The  $^1\text{H}$  NMR spectra of N3 and new ruthenium complexes (Dye1-Dye3) are shown in Figure 3.3.

N3 and Dye1 contain two identical bipyridine ligands and two isocyanate groups. Their  $^1\text{H}$  NMR spectra showed six peaks of the bipyridine aromatic protons [59] indicating that the isocyanate groups were *cis* to each other, with  $\text{C}_2$  point group, as the more symmetrical *trans* isomer ( $\text{D}_{2d}$  point group) would have only three chemically inequivalent protons. There were four doublet signals corresponding to  $\text{H}_6$ ,  $\text{H}_6'$ ,  $\text{H}_5$  and  $\text{H}_5'$  and two singlet signals corresponding to  $\text{H}_3'$ ,  $\text{H}_3'$ . All the signals were observed in the range of 7.0-10.0 ppm. In addition, the  $^1\text{H}$  NMR spectrum of Dye1 showed more four singlet peaks ( $\text{H}_7$ ,  $\text{H}_8$ ,  $\text{H}_9$  and  $\text{H}_{10}$ ) in the range of 7.8-8.8 ppm

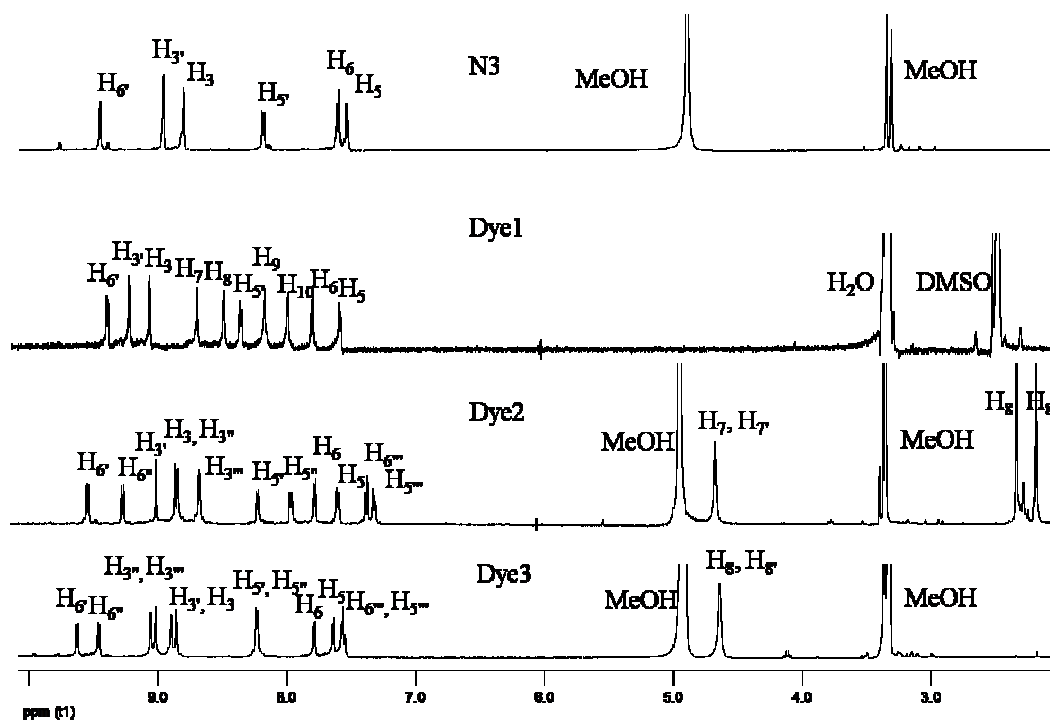


corresponding to the N-H proton which will be exchanged when D<sub>2</sub>O was added into the DMSO-d<sub>6</sub> solution of Dye1, therefore the four singlet signals disappeared (Figure 3.3b) and only six peaks of aromatic protons remained in the spectrum.

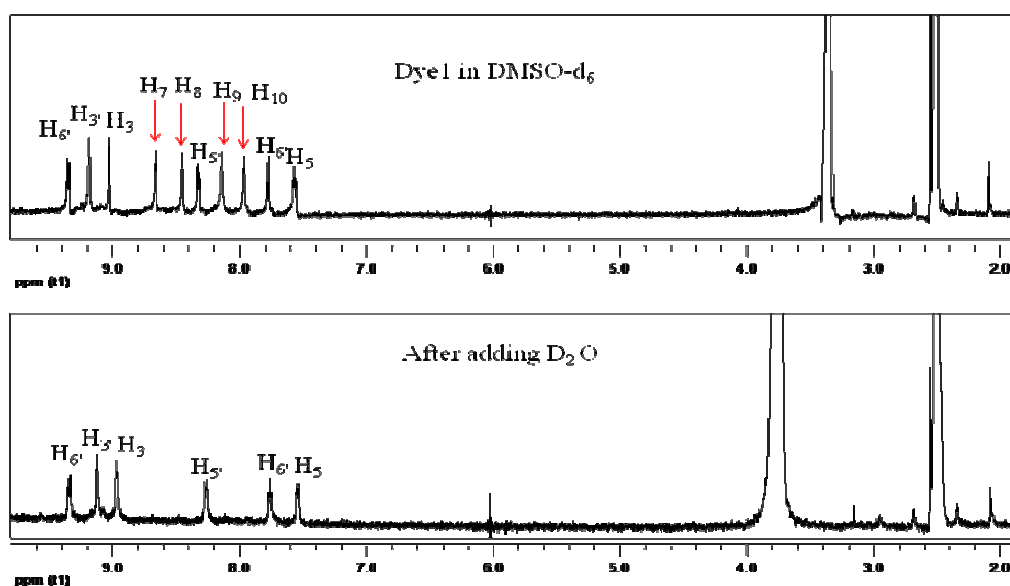
Dye2 and Dye3 possessed two different bipyridine ligands and two thiocyanate groups coordinating to Ru center. Their <sup>1</sup>H NMR spectra showed twelve and eight signals, respectively, suggesting that these complexes were also obtained as a *cis* isomer. The *cis* isomer belongs to C<sub>1</sub> point group possessing twelve chemically inequivalent aromatic protons while the *trans* isomer belongs to C<sub>2v</sub> symmetry possessing only six chemically inequivalent aromatic protons. In the spectrum of Dye2, there were eight doublet signals corresponding to H<sub>6</sub>, H<sub>6'</sub>, H<sub>5</sub>, H<sub>5'</sub> of carboxyl bipyridine ring and H<sub>6''</sub>, H<sub>6'''</sub>, H<sub>5''</sub>, H<sub>5'''</sub> of *N,N'*-(2,2'-bipyridine-4,4'-diyl)diacetamide. The other four singlet signals were assigned to H<sub>3</sub>, H<sub>3'</sub>, H<sub>3''</sub>, H<sub>3'''</sub>. Moreover, the signals of methyl group from 4,4'-diacetamido-2,2'-bipyridine ligand were also observed at 2.1 and 2.0 ppm. For Dye3, there were eight signals in aromatic region, four singlet signals corresponding to H<sub>3</sub>, H<sub>3'</sub>, H<sub>3''</sub>, H<sub>3'''</sub> and the other four doublet signals with an integral ratio of 2:2:2:2 corresponding to H<sub>6</sub>, H<sub>6'</sub>, H<sub>5</sub>, H<sub>5'</sub>, H<sub>6''</sub>, H<sub>6'''</sub>, H<sub>5''</sub>, H<sub>5'''</sub>. In addition, the amido N-H protons of Dye2 and Dye3 were also observed at 4.5 and 4.6 ppm, respectively.



(a)

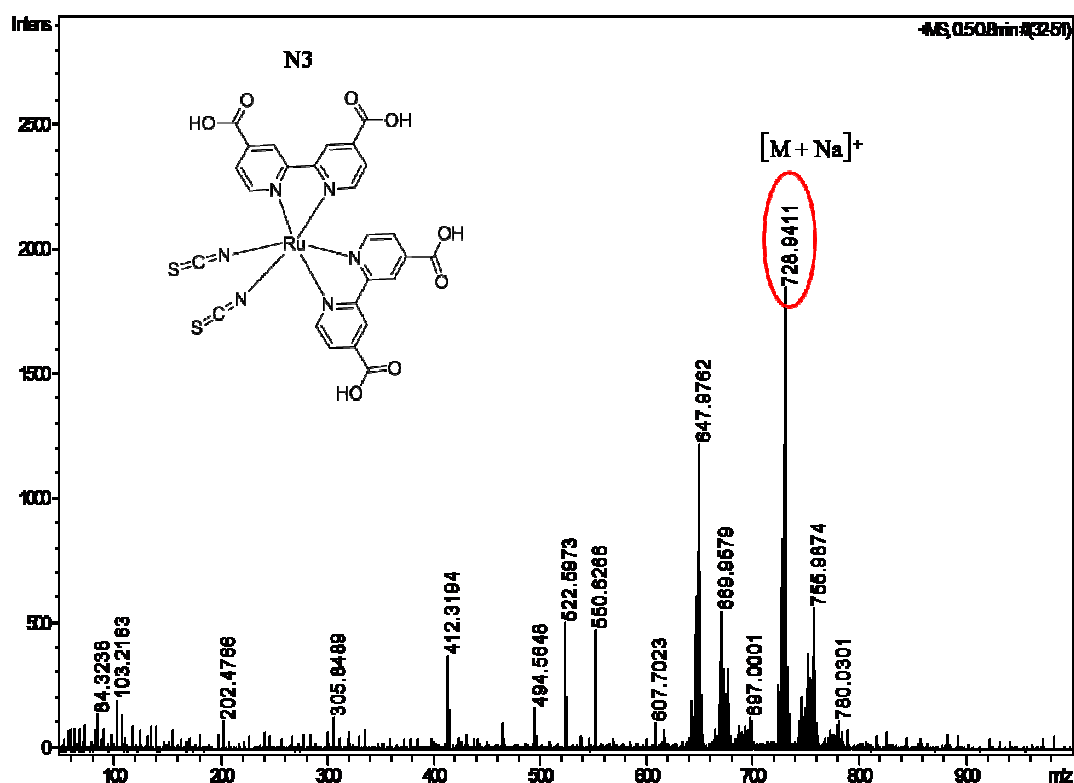


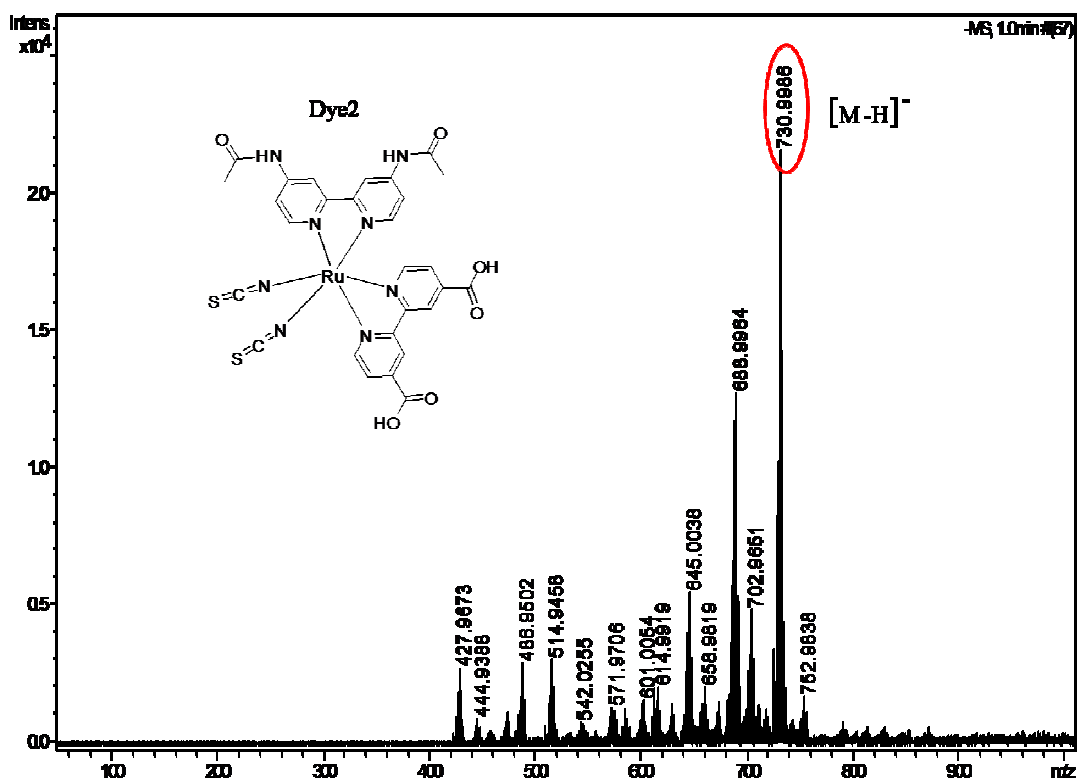
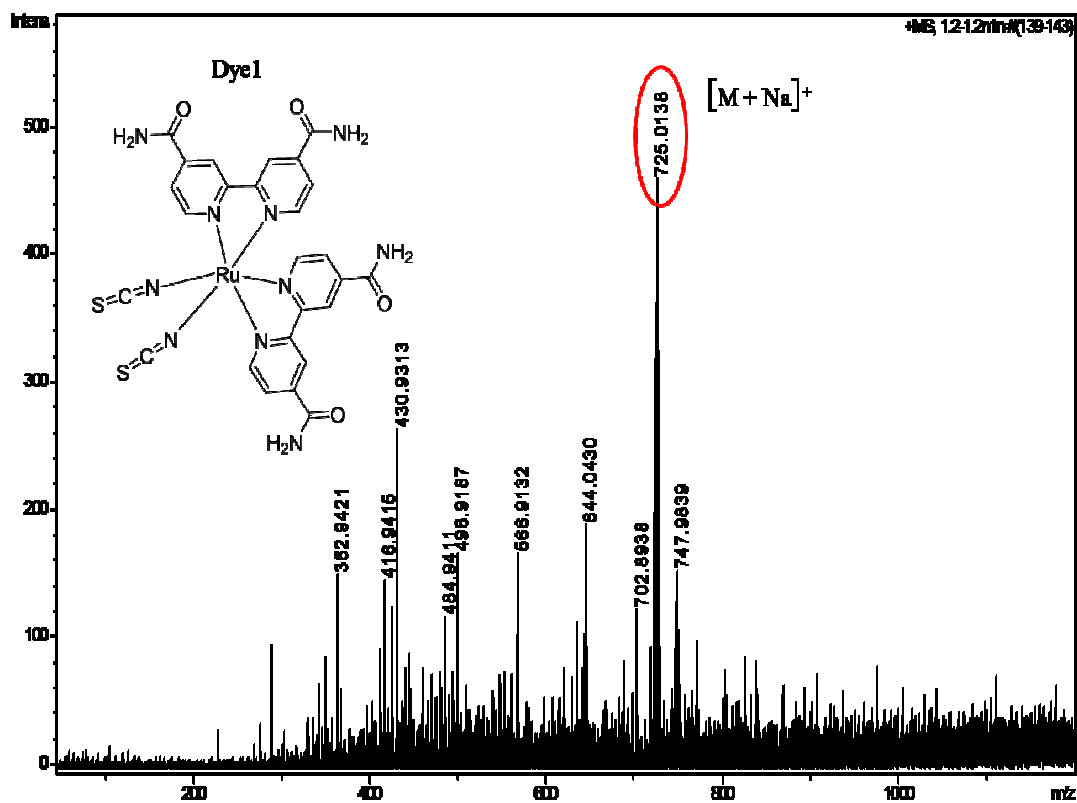
(b)



**Figure 3.3**  $^1\text{H}$  NMR spectra of a) N3, Dye1, Dye2 and Dye3 in DMSO- $d_6$  for Dye1 and methanol- $d_4$  for N3, Dye2 and Dye3 and b) After adding  $\text{D}_2\text{O}$  into Dye1 in DMSO- $d_6$

The high resolution mass spectrometry of N3, Dye1, Dye2 and Dye3 are shown in Figure 3.4 to provide further characterization for the ruthenium complexes. In positive ion mode of ESI-MS, N3 gave a molecular ion peak corresponding to  $[M+Na]^+$  at  $m/z = 728.9411$  (calculated mass for  $C_{26}H_{16}N_6NaO_8RuS_2 = 728.9412$ ) and Dye1 showed the molecular ion peak  $[M+Na]^+$  at  $m/z = 725.0138$  (calculated mass for  $C_{26}H_{20}N_{10}NaO_4RuS_2 = 725.0052$ ) Dye3 showed the molecular ion peak corresponding to  $[M-2H+3Na]^+$  at  $m/z = 770.9327$  (calculated mass for  $C_{26}H_{16}N_8Na_3O_6RuS_2 = 770.9371$ ) [60]. For Dye2, the molecular ion peak  $[M-H]^-$  was observed in the negative ion mode at  $m/z = 730.9986$  (calculated mass for  $C_{28}H_{21}N_8O_6RuS_2 = 731.0069$ ).





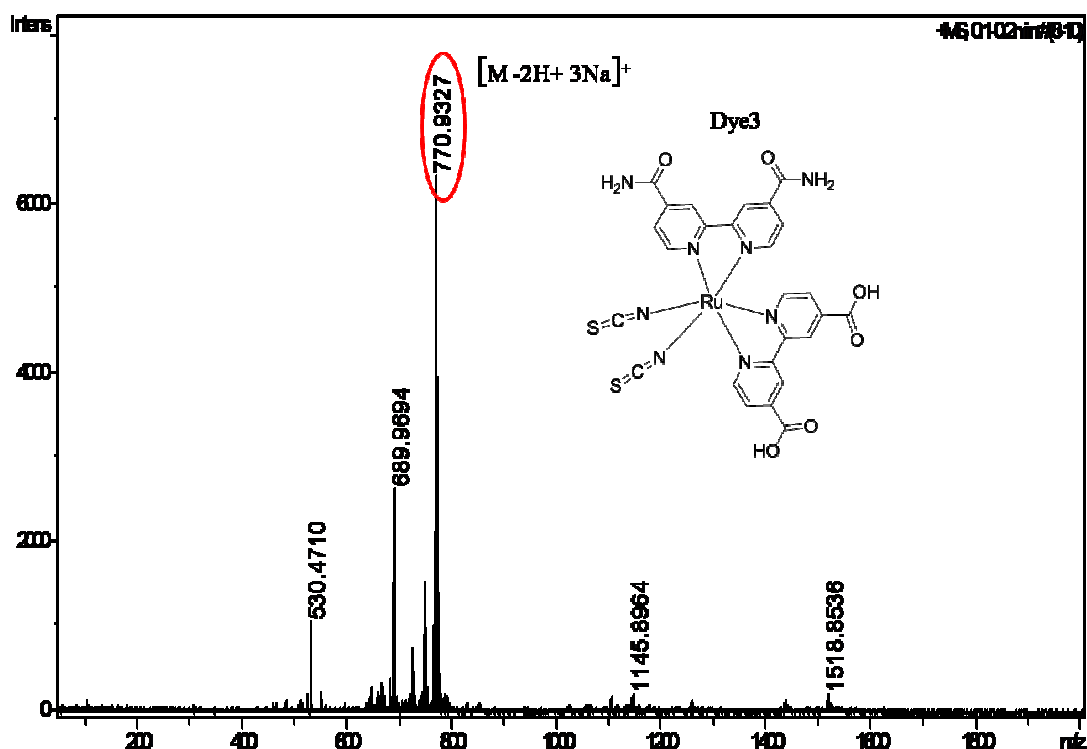
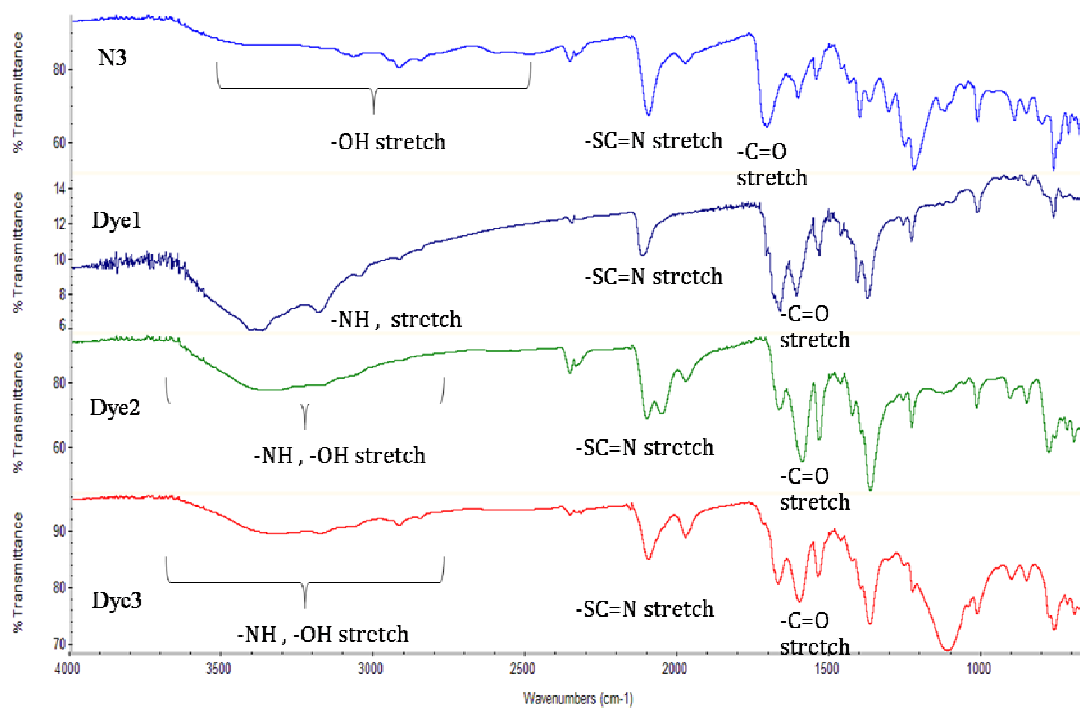


Figure 3.4 High resolution mass spectrometry of N3, Dye1, Dye2 and Dye3.

### 3.3 ATR-FTIR Spectral data

The IR spectra of N3, Dye1, Dye2 and Dye3 acquired by ATR-FTIR technique from powder samples are shown in Figure 3.5. The carboxylic O-H and amido N-H stretching signals for appeared as broad absorption bands within the same range of 2500-3700  $\text{cm}^{-1}$ . The  $-\text{C}=\text{N}$  stretching signals of the thiocyanate groups were found near 2100  $\text{cm}^{-1}$ . The  $\text{C}=\text{O}$  stretching signals of the carboxylic acid and amide groups in the 1600-1700  $\text{cm}^{-1}$ . The peak near 1200  $\text{cm}^{-1}$  is due to the C-O stretching. The signals observed for these complexes were similar to those previously reported for the similar complexes by C. Klein and coworkers [30,31].

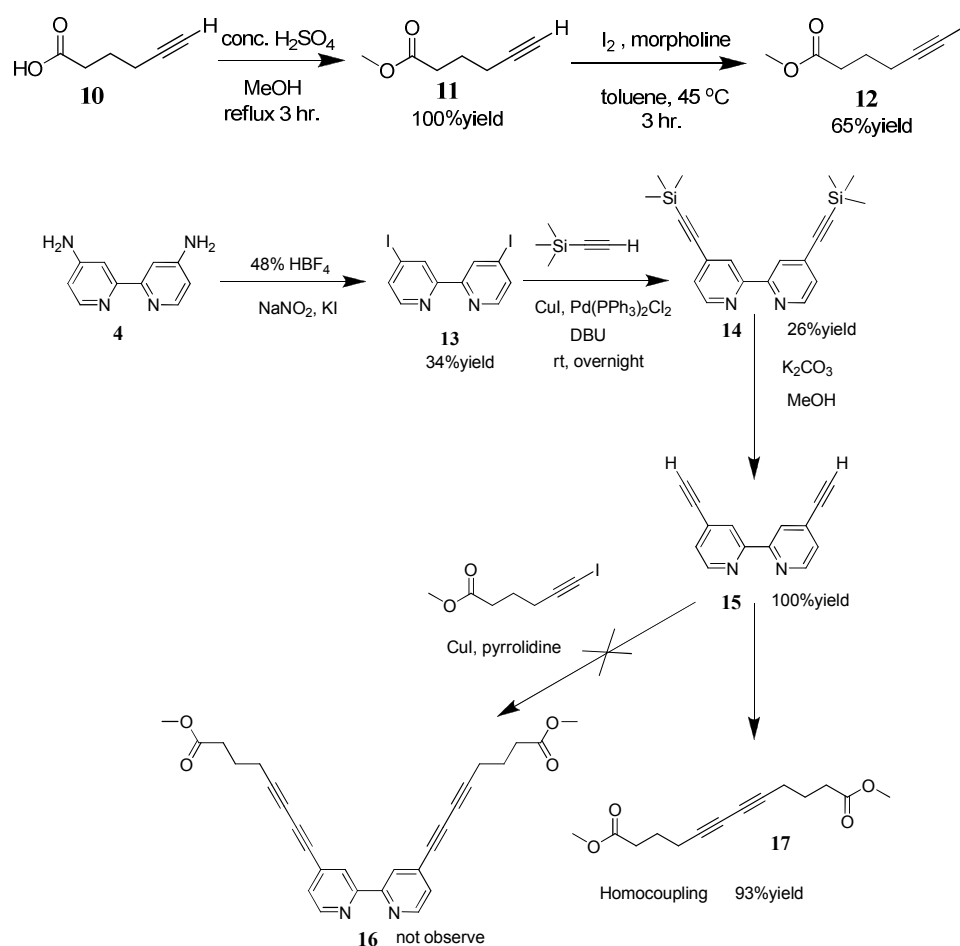


**Figure 3.5** IR spectra of N3 Dye1 Dye2 and Dye3

### 3.4 Synthesis of bipyridine ligands containing diacetylene.

#### 3.4.1 Synthesis of bipyridine ligands containing diacetylene by Cadiot-Chodkiewicz coupling

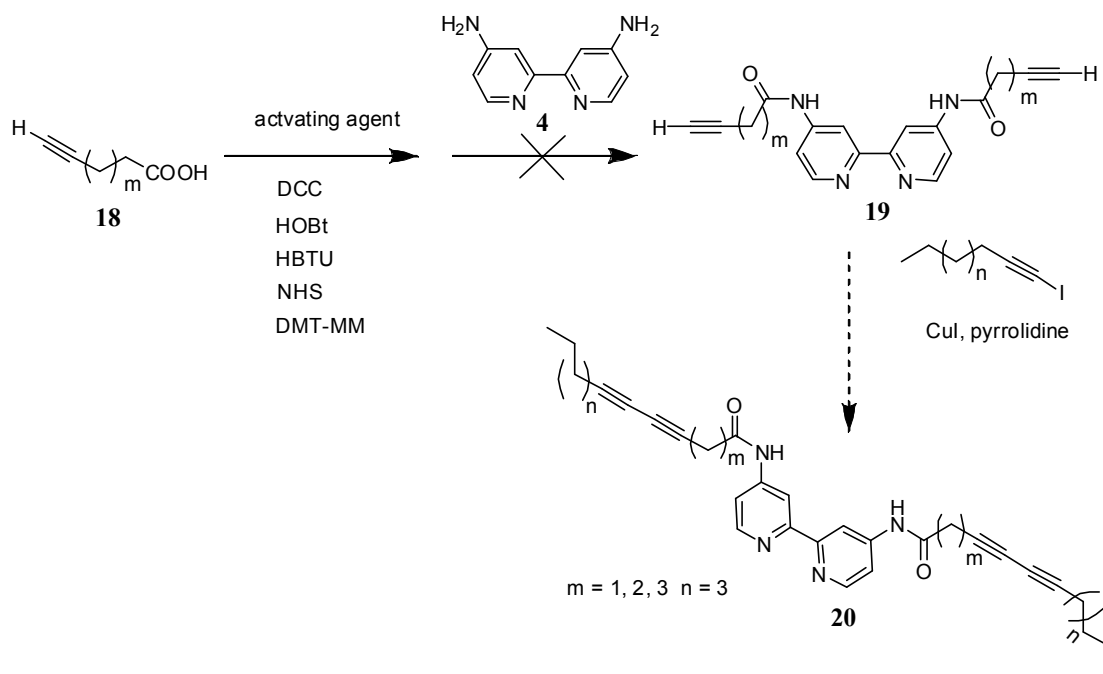
The synthetic route of bipyridine containing diacetylene was proposed in Scheme 3.4. The key step is Cadiot-Chodkiewicz coupling between methyl 6-iodo-5-hexynoate **12** and ethynyl bipyridine **15**. The ester **12** was prepared from compound **11** by treating with I<sub>2</sub> in the present of morpholine and toluene. Ethynyl bipyridine **15** was synthesized by iodination of the diazonium salt generated from 4,4'-diamino-2,2'-bipyridine **4** with KI, NaN<sub>3</sub> and hydrofluoroboric acid [53] followed by Sonogashira coupling with ethynyltrimethylsilane [54-57] and desilylation. Unfortunately, attempts on Cadiot-Chodkiewicz coupling [61] between diethynylbipyridine **15** with iodomethylhexynoate **12** did not give diacetylene **16** but only the homocoupling product of **12**, diacetylene compound **17**, was obtained.



**Scheme 3.4** Synthesis of bipyridine ligand containing diacetylene.

### 3.4.2 Synthesis of bipyridine ligands containing diacetylene by various amide coupling agent.

Another pathway proposed for incorporating diacetylene units into the bipyridine ligand is the condensation between diacetylene carboxylic and diaminobipyridine **4** in which the attempts with various activating agents [62-65] (Scheme 3.6) were all fruitless. Only the starting diamino bipyridine was recovered indicating extremely poor nucleophilicity of the amino groups presumably due to the electronwithdrawing effect from the bipyridine ring. Steric hindrance of the activated carboxyl group might also another important factor attributing to this unsuccessful condensation.



**Scheme 3.5** Synthesis of bipyridine ligand containing diacetylene by using activating agent



### 3.5 Absorption and emission properties of N3, Dye1, Dye2 and Dye3.

Figure 3.5a showed absorption spectra of N3, Dye1, Dye2 and Dye3 at 50  $\mu\text{M}$  in methanol solution. All the dyes showed two absorption maxima, one in the range of 370-385 nm and the other in the range of 510-525 nm, corresponding spectrum to the  $\pi\text{-}\pi^*$  transition of the bipyridine ligand and the metal-to-ligand charge transfer (MLCT) transition, respectively [66,67]. The absorption bands of Dye3 appeared at slightly longer wavelengths compared to N3 and Dye2. The cause of this reason might be the amide group of Dye3 which is electron withdrawing group stronger than carboxylic group and amide group of Dye2. For Dye1, eventhough, the bands of MLCT and  $\pi\text{-}\pi^*$  transition are the most red shift, the absorbance is the lowest. Among four dyes, N3 gave the highest molar extinction coefficient of around  $1 \times 10^4 \text{ M}^{-1}\text{cm}^{-1}$  (Table 3.1). The electronic absorption spectra of the dyes anchored on semiconductor  $\text{TiO}_2$  were also recorded. In solid state, the dyes also showed two broad absorption bands similar to the solution spectra (Figure 3.7b). The absorption spectrum of N3 still exhibited the highest absorbance. The absorbance of Dye2 and Dye3 were close to each other and the absorbance of Dye1 was the lowest. According to the absorbance in dye coated on  $\text{TiO}_2$  surface and the molar extinction coefficient, the relative surface coverage was calculated and put in Table 4. The surface coverage is the relative value of the number of dye molecule on  $\text{TiO}_2$  surface compare to N3. Therefore, the surface coverage of N3 is 1. As the results, the surface coverage Dye1 was only 0.3, it indicated that the small amount of Dye1 can adsorb on  $\text{TiO}_2$  surface because there isn't carboxylic group in the structure. The surface coverage of Dye2 and Dye3 were close to 1, it indicated that the numbers of dye molecules (N3, Dye2 and Dye3) on  $\text{TiO}_2$  surface were quite the same and the dye layer should be monolayer for the good electron transfer process.

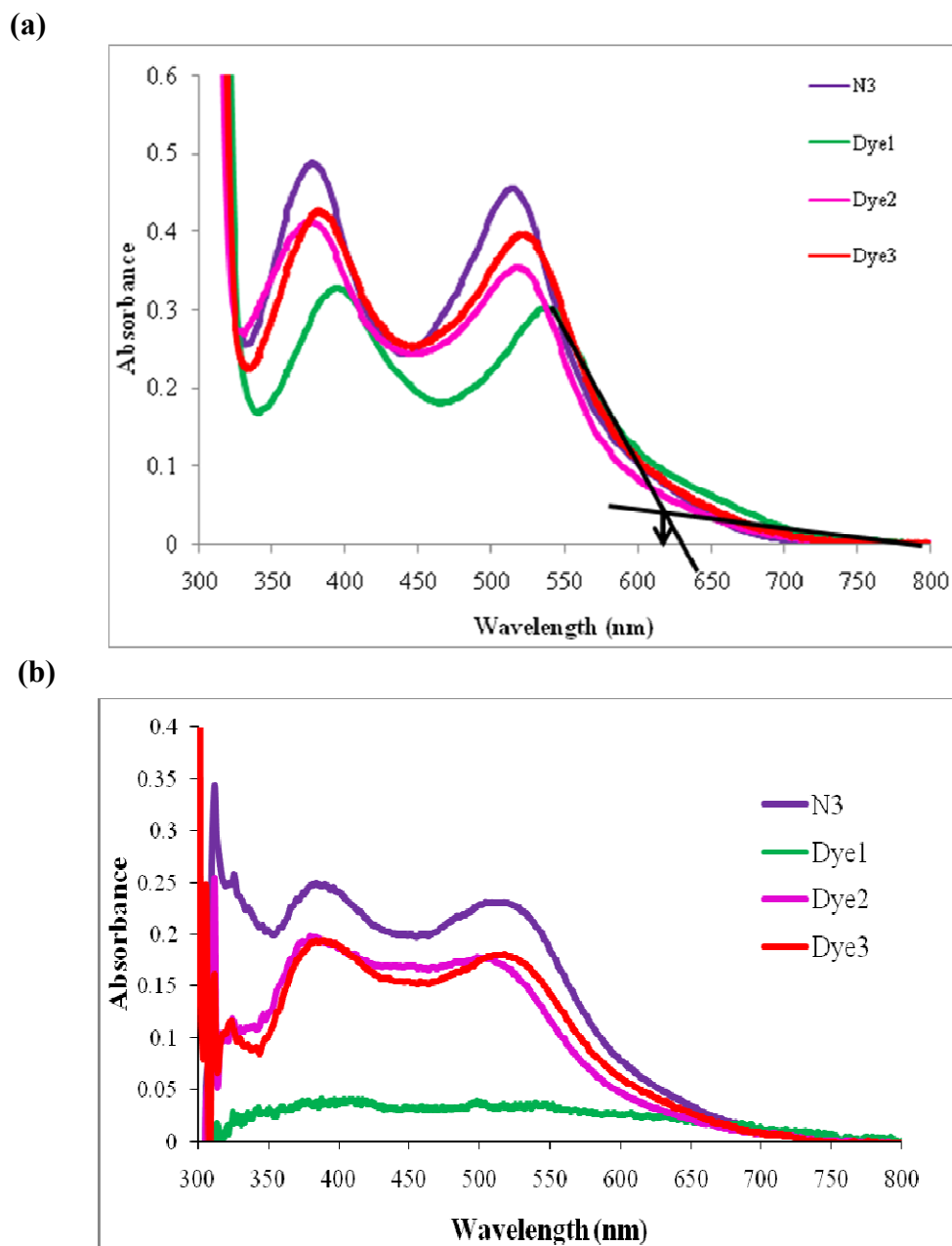


**Figure 3.7** The absorption spectra of (a) N3, Dye1, Dye2 and Dye3 at 50  $\mu\text{M}$  in DMSO for Dye1 and MeOH for N3, Dye2 and Dye3. (b) N3, Dye1, Dye2 and Dye3 anchored on 19  $\mu\text{m}$  nanocrystalline  $\text{TiO}_2$

**Table 3.1** Absorption and emission properties of N3, Dye1, Dye2 and Dye3 0.05 mM in DMSO for Dye1 and methanol for N3, Dye2 and Dye3.

Dye	$\pi-\pi^*$ (nm)	MLCT (nm)	$\epsilon \pi-\pi^*$ ( $M^{-1}cm^{-1}$ )	$\epsilon$ MLCT ( $M^{-1}cm^{-1}$ )	$\lambda_{emiss}$ (nm)
N3	378	514	10,100	9,436	753
Dye1	394	537	6,012	5,656	769
Dye2	375	518	7,768	6,644	772
Dye3	381	519	8,596	7,968	775

**Table 3.2** Absorption properties of N3, Dye1, Dye2 and Dye3 coated on 19  $\mu m$   $TiO_2$  thickness

Dye	$\pi-\pi^*$ (nm)	MLCT (nm)	Absorbance at $\pi-\pi^*$ transition	Relative surface coverage
N3	384	518	0.249	1.0
Dye1	404	517	0.040	0.3
Dye2	380	504	0.198	1.0
Dye3	384	518	0.194	0.9

The normalized absorption spectra and emission spectra of all the ruthenium complexes at 50  $\mu M$  in methanol and DMSO solution are shown in Figure 3.8. The emission spectra were obtained by using excitation wavelength at MLCT wavelength in each dye. All dyes showed relatively weak emission with only one emission maximum ( $\lambda_{em}$ ) in the range of 750-775 nm. Since the excitation wavelength is in the  $\pi-\pi^*$  transition band, this emission band corresponds to the  $\pi^*-\pi$  radiative decay.

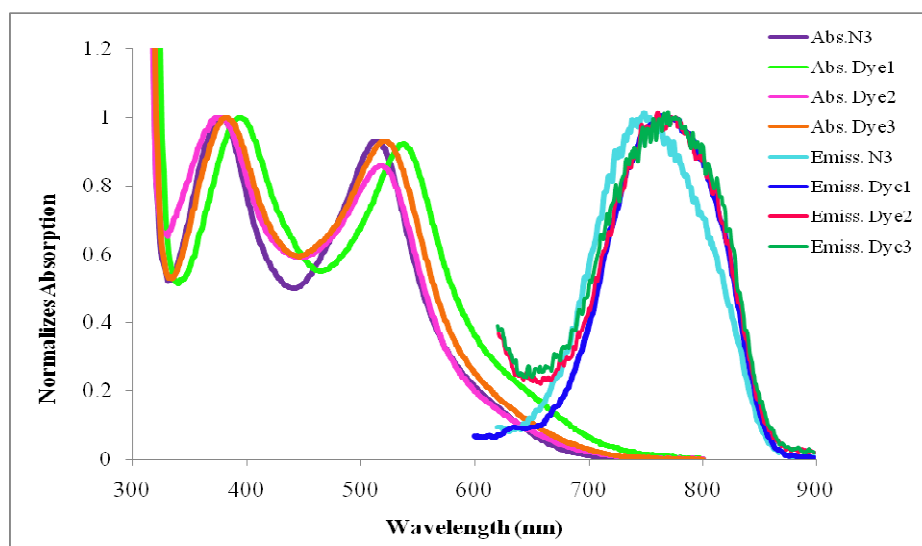


**Figure 3.8** The normalized absorption and emission spectra of N3, Dye1, Dye2 and Dye3 at 50  $\mu\text{M}$  in DMSO for Dye1 and MeOH for N3, Dye2 and Dye3.

### 3.6 Electrochemical data

The electrochemical behaviors of N3, Dye1, Dye2 and Dye3 were obtained using glassy carbon working electrode and Ag/AgCl reference electrode in DMSO for Dye1 and methanol for the rest of the dyes with 0.1 M tetra-*n*-butylammonium hexafluorophosphate as a supporting electrolyte. The electrolyte solution was degassed by nitrogen bubbling. The cyclic voltammograms are shown in Figure 3.10 and the redox potentials of the dyes at a scan rate of 100 mV/s. The electrochemical stability of all compounds was tested by four subsequent redox cycles. N3, Dye2 and Dye3 were electrochemically stable (Figure 3.9). From the cyclic voltammogram, the first oxidation is assigned to the Ru<sup>II</sup>/Ru<sup>III</sup> couple [68-72]. It is quasireversible. The first oxidation of N3, Dye1, Dye2 and Dye3 displayed at 0.85, 0.85, 0.73 and 0.82 V, respectively. The first oxidation of Dye2 is shifted cathodically by 0.12 V compared to N3 due to the donor influence of *N,N'*-(2,2'-bipyridine-4,4'-diyl)diacetamide) ligand to ruthenium metal [68].

The HOMO energy levels were calculated from the onset of oxidation potential ( $E_{\text{onset}}$ ) according to equation 1.  $E_{\text{onset}}$  in equation 1 is obtained from the cyclic voltammogram and 4.44 constant number is used when Ag/AgCl is applied as the reference [73-75].  $E_{\text{onset}}$  is the potential where the oxidative current starts to rise (the example of  $E_{\text{onset}}$  of Dye1 was shown in Figure 3.9 b).  $E_g$  in equation 3 is the lowest absorption energy obtained from the absorption edge of the absorption spectrum (the

example of wavelength from the absorption edge of Dye1 was shown in Figure 3.7 a). The wavelengths from the absorption edge of N3, Dye1, Dye2 and Dye3 which will be used in equation 3 are 622, 614, 589 and 621 nm, respectively. The LUMO energy level was calculated by adding the HOMO energy level with the energy band gap ( $E_g$ ). The results are shown in Table 3.3.

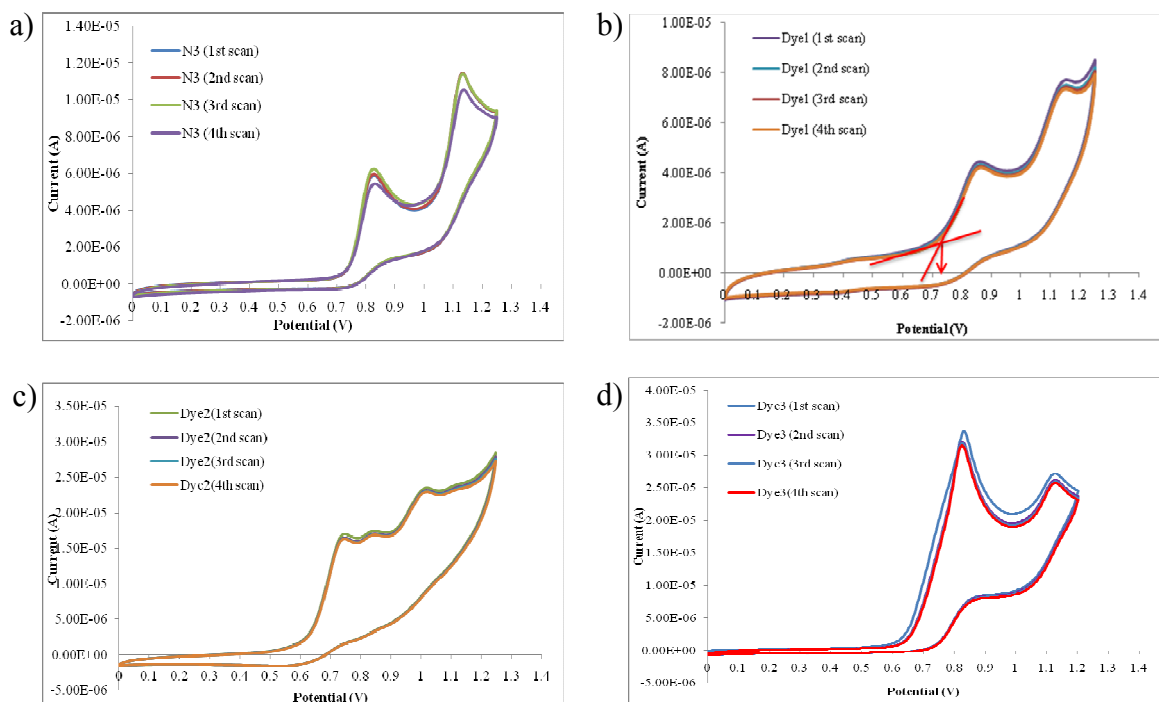


**Figure 3.9** Cyclic voltammograms of (a) N3, (b) Dye 1, (c) Dye 2 and (d) Dye3

$$E_{\text{HOMO}} = -(4.44 + E_{\text{onset}}) \quad (1)$$

$$E_{\text{LUMO}} = \text{HOMO} + E_g \quad (2)$$

$$E_g = \frac{hc}{\lambda} \quad (3)$$

$$h = 1240$$

**Table 3.3** Electrochemical parameters of Ruthenium complex sensitizer.

Compound	HOMO (eV)	LUMO (eV)	E <sub>g</sub> (eV)	E <sub>onset</sub>
N3	-5.19	-3.19	2.00	0.75
Dye1	-5.15	-3.33	2.02	0.71
Dye2	-5.04	-2.93	2.11	0.60
Dye3	-5.11	-3.11	2.00	0.67

### 3.7 Preparation of dye sensitized photovoltaic cells.

The preparation of dye sensitized solar cell was shown in chapter II. There are about four steps for DSSC fabrication, the last step is measuring the photovoltaic data (Figure 3.11). And there are many factors effecting the photovoltaic performance of the solar cell. Dye molecule is one of the most important factor which should be considered in DSSCs. The molecular structure of the dye should consist of anchoring group (carboxylic group) for attaching on TiO<sub>2</sub> surface otherwise, only small amount of dye molecule can adsorb on TiO<sub>2</sub> surface. Therefore the surface coverage value is low like Dye1 in table 3.2, for this reason the photovoltaic data will give the low value. The dye should also exhibit high extinction coefficient and wide absorption range. And the dye should adsorb on TiO<sub>2</sub> surface as a monolayer for the electron transfer process can efficiently occur. In addition, the LUMO level of the dye should be higher than the conduction band of TiO<sub>2</sub> for the thermodynamically driving force of the electron injection process. Figure 3.10 shows that the LUMO level of N3, Dye 1, Dye2 and Dye3, dyes are higher than the conduction band of TiO<sub>2</sub> [76,77]. So the electron injection from the excited dye to TiO<sub>2</sub> electrode is possible.

In this work, we studied the electronic effect of the substituents on the bipyridine ligand. The bipyridine ligand of N3 is 2,2'-bipyridine-4,4'-dicarboxylic acid in which the carboxyl group is an electron withdrawing group. Dye 1 consists of two identical bipyridine ligand with weaker electron withdrawing groups, 2,2'-bipyridine-4,4'-dicarboxamide. Dye2 consists of *N,N'*-(2,2'-bipyridine-4,4'-diyl)diacetamide, a bipyridine ligand with electron donating groups, and 2,2'-bipyridine-4,4'-dicarboxylic acid, a bipyridine ligand with electron withdrawing groups. Dye3 consists of 2,2'-bipyridine-4,4'-dicarboxamide, a bipyridine ligand with weak electron withdrawing group and 2,2'-bipyridine-4,4'-dicarboxylic acid, a bipyridine ligand with stronger

electron withdrawing groups. We assumed that the dye containing electron withdrawing group will exhibit higher efficiency like N3.

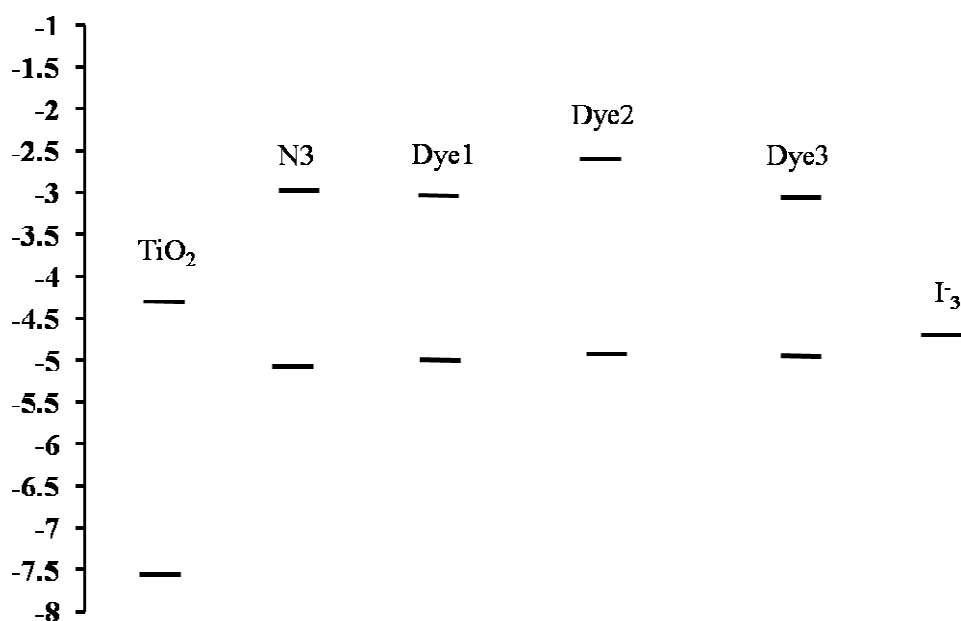


**Figure 3.10** Energy level diagram of N3, Dye1, Dye2 and Dye3 compare to TiO<sub>2</sub>.

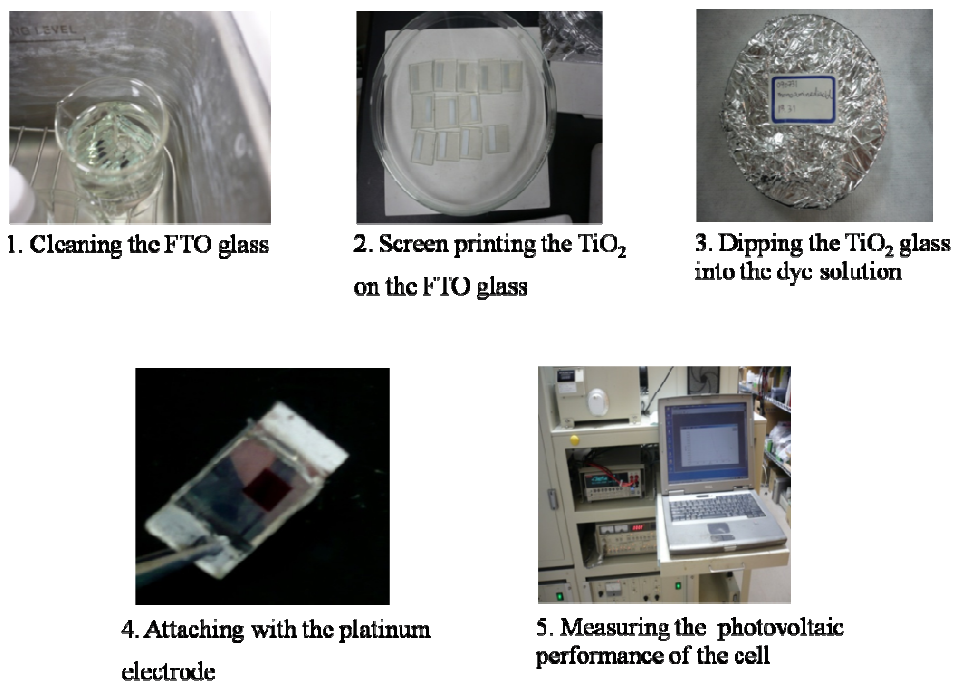


**Figure 3.11** The process of dye sensitized solar cell fabrication.

### 3.8 Photovoltaic performance

The photovoltaic performances of the photovoltaic cells fabricated with the ruthenium dyes as a sensitizer on nanocrystalline TiO<sub>2</sub> electrode were investigated using an electrolyte consisting of 0.6 M ethylmethylimidazolium dicyanamide, 0.05 M iodine, 0.5 M LiI, and 0.58 M 4-tert-butylpyridine in acetonitrile. The representative I-V curve of the cell under illumination with simulated AM 1.5 solar light are shown in Figure 3.12. The photovoltaic data obtained from the average of three cells for each dye showed that the cells using Dye1, Dye2 and Dye3 as the sensitizers exhibited significantly lower overall conversion efficiency (Table 3.4). While the open circuit voltage ( $V_{oc}$ ) were only slightly lower, the photocurrent density ( $J_{sc}$ ) of Dye1, Dye2 and Dye3 is significantly lower compared to N3 which should be the main contributor to the low conversion efficiency. Since the photophysical properties of these dyes were quite similar to N3, the low photocurrent density is likely caused by poor electron injection from the ruthenium dye to the TiO<sub>2</sub> electrode upon photoexcitation of Dye1, Dye2 and Dye3 are lower than N3. And the photovoltaic device with Dye1 as sensitizer showed the lowest efficiency due to the lowest molar extinction coefficient and there isn't carboxylic group to anchor on TiO<sub>2</sub> layer, therefore the small amount of Dye1 can absorb on the semiconductor surface and its photovoltaic data were poor.

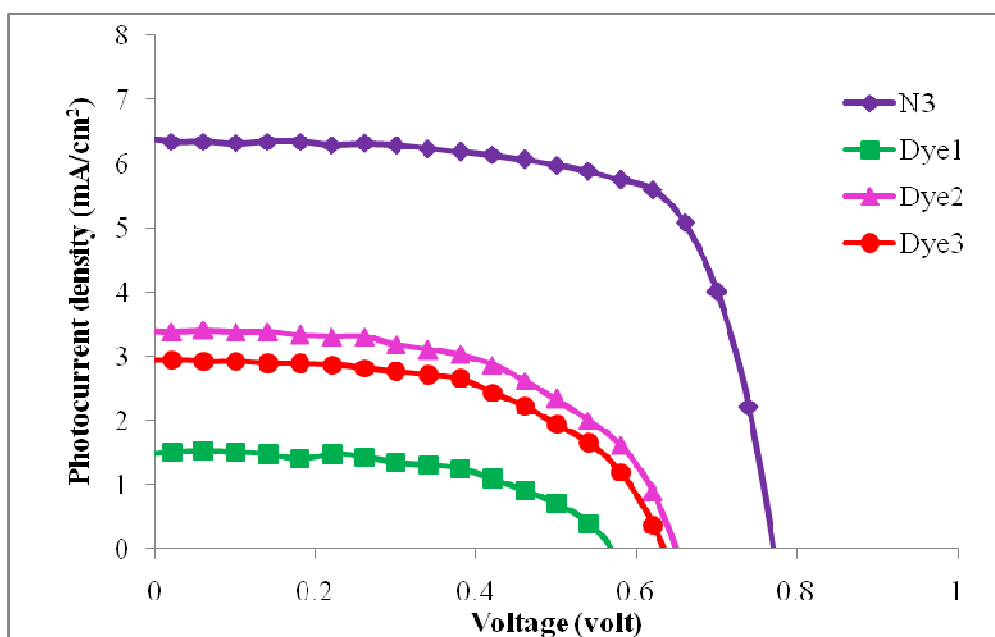


**Figure 3.12** I-V curve of N3, Dye1, Dye2 and Dye 3



**Table 3.4** Comparison of Photocurrent density ( $J_{sc}$ ), Open circuit voltage ( $V_{oc}$ ), Fill factor, and the Efficiency ( $\eta$ ) obtained using N3, Dye1, Dye2 and Dye3 on 19  $\mu\text{m}$  thick  $\text{TiO}_2$  electrodes under AM 1.5 Sun

Complex	Current density ( $\text{mA}/\text{cm}^2$ )	Open circuit voltage (V)	Fill factor	Efficiency, $\eta$ (%)
N3	6.38	0.77	0.71	3.47
Dye1	1.51	0.54	0.59	0.48
Dye2	3.42	0.65	0.55	1.21
Dye3	2.94	0.64	0.55	1.03

### 3.9 Preparation of dye sensitized photovoltaic cells by using polydiacetylene.

Blue polydiacetylene, (poly(pentacosadiynoic acid) or P(PCDA)), have UV-vis absorption peaks at 586 and 635 nm corresponding to its vibronic coupled  $\pi$ - $\pi^*$  transition. These absorption bands were expected to compliment with the ruthenium dye absorption peaked at 586 and 635 nm which may in turn increase the conversion efficiency of the DSSC. The DSSC fabricated from N3 and Dye2 with an extra layer of polydiacetylene vesicle were evaluated. The photovoltaic performance of the cells fabricated with polydiacetylene is shown in Table 3.5. As the result, the efficiency of the cells using an extra layer of P(PCDA) displayed lower efficiency comparing to the cells without P(PCDA). The lower efficiencies observed were due mainly to the ruthenium dye removal from the  $\text{TiO}_2$  upon immersion into the P(PCDA) aqueous solution (Figure 3.13). N3 which consist of carboxyl groups on both bipyridine ligands was removed from the nanocrystalline  $\text{TiO}_2$  surface in greater extent than Dye2 which consist of carboxyl groups on only one bipyridine ligand and the efficiency of solar cell using N3/P(PCDA) is lower than the other.

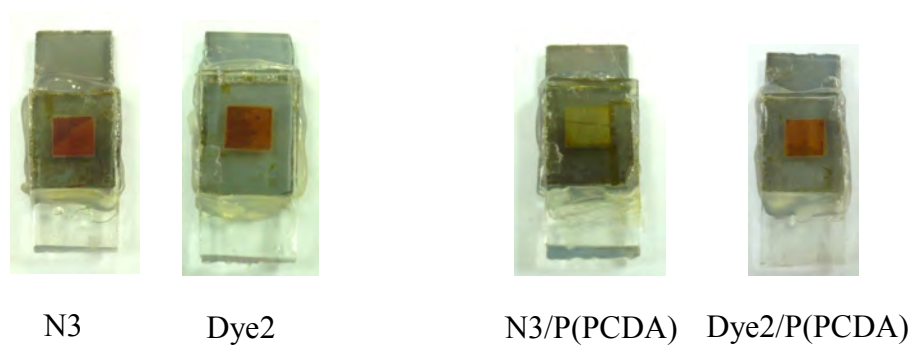


**Figure 3.13** Dye sensitized solar cells using a) N3 and Dye2 as sensitizers and b) using N3, Dye2 and P(PCDA) vesicle as sensitizers.

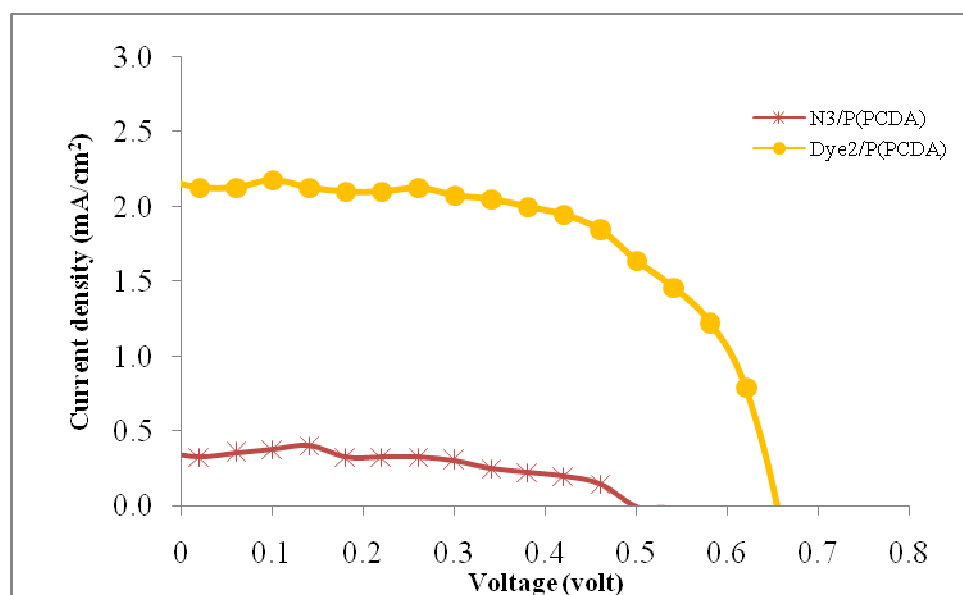


**Figure 3.14** I-V curve of N3/P(PCDA) and Dye2/P(PCDA).

**Table 3.5** Comparison of Photocurrent density ( $J_{sc}$ ), Open circuit voltage ( $V_{oc}$ ), Fill factor, and the Efficiency ( $\eta$ ) obtained using N3, Dye2 with polydiacetylene.

Complex	Current density (mA/cm <sup>2</sup> )	Open circuit voltage (V)	Fill factor	Efficiency, $\eta$ (%)
N3/ P(PCDA)	0.34	0.45	0.59	0.09
Dye2/ (PCDA)	2.13	0.65	0.62	0.85

## CHAPTER IV

### CONCLUSION

#### 4.1 Conclusion

Three new ruthenium complexes containing amide groups (Dye1, Dye2 and Dye3) were synthesized and studied as sensitizing dyes in dye-sensitized solar cells (DSSC) in comparison to N3 dye. Dye1 is a Ru complex consisting of two identical bipyridine ligands, 2,2'-bipyridine-4,4'-dicarboxamide, and two thiocyanate groups. Dye2 and Dye3 consist of two different bipyridine ligands and two thiocyanate groups coordinating to Ru center. The bipyridine ligands of Dye2 are *N,N'*-(2,2'-bipyridine-4,4'-diyl)diacetamide and 4,4'-dicarboxy-2,2'-bipyridine while those of Dye 3 are 2,2'-bipyridine-4,4'-dicarboxamide and 4,4'-dicarboxy-2,2'-bipyridine. The performances of the photovoltaic cells fabricated with the ruthenium dyes as a sensitizer on nanocrystalline TiO<sub>2</sub> electrode were investigated using an electrolyte consisting of I<sup>-</sup>/I<sub>3</sub><sup>-</sup>. The photovoltaic data showed that the cells using Dye1, Dye2 and Dye3 as the sensitizers exhibited overall conversion efficiencies in the range of 0.48-1.21% significantly lower than the value 3.47% obtained from the cell fabricated from N3. While the open circuit voltage ( $V_{oc}$ ) of Dye2 and Dye3 were only slightly lower, the photocurrent density ( $J_{sc}$ ) is significantly lower compared to N3 which should be the main contributor to the low conversion efficiency. Since the photophysical and electrochemical properties of Dye1, Dye2 and Dye3 are quite similar to N3. The low photocurrent density maybe caused by either low surface coverage of the Dye1 on TiO<sub>2</sub> electrode or poor electron injection from the dye to the TiO<sub>2</sub> electrode upon photoexcitation. For Dye1 which showed the lowest conversion efficiency, the surface coverage was found to be about 0.3% of that of N3 indicating that the primary amide is a poorer anchoring group comparing with the carboxylic group. Therefore, the low conversion efficiency of the photovoltaic cell fabricated from Dye1 is probably contributed by both low surface coverage of the dye and poor electron injection. As the surface coverage of Dye2 and Dye3 on TiO<sub>2</sub> electrode were determined to be relatively the same as N3, the lower conversion efficiency should derive mainly from the poor electron injection.

#### **4.2 Suggestion for the future work**

Further research should involve variation of the substituent on the 2,2'-bipyridine with various electronic properties such as alkyl, amino, nitro or  $\pi$ -conjugated chain. It is however necessary to incorporate at least one 2,2'-bipyridine ligand containing carboxylic groups to maintain the high surface coverage on the TiO<sub>2</sub> electrode. In addition, increase of absorption spectrum range by using mixture of dyes, a dye cocktail, is also interesting.

## REFERENCES

- [1] O' Regan, B.; Gratzel, M. A low cost, high-efficiency solar cell based on dye-sensitized colloidal TiO<sub>2</sub> film. *Nature*. 353 (1991): 737-740.
- [2] Quan, V. A. *Degradation of the solar cell dye sensitizer N719 preliminary building of dye-sensitized solar cell*. Master's Thesis, Department of Life Science and Chemistry. Roskild University, 2006.
- [3] Gratzel, M.; Kalyanasundaram, K. Applications of functionalized transition metal complexes in photonic and optoelectronic devices. *Coor. Chem. Rev.* 177 (1998): 347-414.
- [4] Hagfeldt, A.; Gratzel, M. Molecular Photonics. *Acc. Chem. Rev.* 33 (2000) : 269-277.
- [5] Hara, K.; et al. Influence of electrolyte on the photovoltaic performance of a dye sensitized TiO<sub>2</sub> solar cell base on a Ru(II)terpyridyl complex photosensitizer. *Solar Energy Materials and Solar cells*. 85 (2005): 21-30.
- [6] Nakashima, T.; Satoh, N.; Albrecht, K.; Yamamoto, K. Interface modification on TiO<sub>2</sub> electrode using dendrimers in dye sensitized solar cells. *Chem. Mater.* 20 (2008): 2538-2543.
- [7] Song, L. Q.; et al. Photoinduced intra molecular electron transfer in aniline containing Ru(II)polypyridine complexes. *J. Photochem. Photobiol. A-chem.* 165 (2004): 137-142.
- [8] Nazeeruddin, M. K.; Klein, C.; Gratzel, M. Synthesis of novel ruthenium sensitizers and their application in dye sensitized solar cells. *Coor. Chem. Rev.* 249 (2005): 1460-1467.
- [9] Nazeeruddin, M. K.; et al. Conversion of light to electricity by cis-x<sub>2</sub>bis(2,2'-bipyridyl-4,4'-dicarboxylate)ruthenium(II)charge-transfer sensitizers (X = Cl<sup>-</sup>, Br<sup>-</sup>, I<sup>-</sup>, CN<sup>-</sup> and SCN<sup>-</sup>) on nanocrystalline titanium dioxide electrodes. *J. Am. Chem. Soc.* 115 (1993): 6382-6390.
- [10] Gratzel, M. Dye sensitized solar cells. *J. Photochem. Photobiol. C-Rev.* 4 (2003): 145-153.
- [11] Nazeeruddin, M. K.; et al. Engineering of efficient panchromatic sensitizers for nanocrystalline TiO<sub>2</sub> based solar cells. *J. Am. Chem. Soc.* 123 (2001): 1613-1624.

- [12] Hagberg, D. P.; et al. Molecular engineering of organic sensitizers for dye sensitized solar cell applications. *J. Am. Chem. Soc.* 130 (2008): 6259-6266.
- [13] Bessho, T.; et al. New paradigm in molecular engineering of sensitizers for solar cell applications. *J. Am. Chem. Soc.* 31 (2009): 5930-5943.
- [14] Gratzel, M. Solar energy conversion by dye sensitized photovoltaic cells. *Inorg. Chem.* 44 (2005): 6841-6851.
- [15] Zhao, D.; et al. Enhanced photocatalytic degradation of dye pollutants under visible irradiation on Al(III) modified TiO<sub>2</sub>: Structure, Interaction and interfacial electron transfer. *Environ. Sci. Technol.* 42 (2008): 308-314.
- [16] Shi, D.; et al. New efficiency records for stable dye sensitized solar cells with low volatility and ionic liquid electrolyte. *J. Phy. Chem. C.* 112 (2008): 17046-17050.
- [17] Shi, D.; et al. New organic sensitizers for stable dye sensitized solar cells with solvent free ionic liquid electrolyte. *J. Phy. Chem. C.* 112 (2008): 17478-17485.
- [18] Cao, Y.; et al. Dye sensitized solar cells with solvent free ionic liquid electrolytes. *J. Phy. Chem. C.* 112 (2008): 13775-13781.
- [19] Wang, P.; Zakeeruddin, S.M.; Moser, J. E.; Nazeeruddin, M. K.; Sekiguchi, T.; Gratzel, M. A stable quasi solid state dye sensitized solar cell with an amphiphilic ruthenium sensitizer and polymer gel electrolyte. *Nature. Mat.* 2 (2003): 402-407. 20.
- [20] Perzhdo, O. V.; Duncan, W. R.; Prezhdo, V. V.; Dynamics of the photoexcited electron at the chromophore-semiconductor interface. *Acc. Chem. Res.* 41 (2008): 339-348.
- [21] Bredas, J. L.; Norton, J. E.; Cornil, J.; Coropceanu, V. Molecular understanding of organic solar cell. *Acc. Chem. Rev.* 42 (2009): 1619-1699.
- [22] Halme, J. *Dye-sensitized nanostructured and organic photovoltaic cells: technical review and preliminary tests*. Master's Thesis, Department of Engineering Physics and Mathematics. Helsinki University of Technology, 2002.

- [23] Shankar, K.; et al. Highly efficient solar cells using TiO<sub>2</sub> nanotube arrays sensitized with a donor antenna dye. *Nano. Lett.* 8 (2008): 1645-1659.
- [24] Si, W.; Qijin, Z.; Christoph, B. Solvent effect on structure, morphology and photophysical properties of an Azo chromophore-functionalized polydiacetylene. *Macromolecules.* 43 (2010): 6142-6151.
- [25] Zhong, L.; Zhu, X.; Duan, P.; Liu, M. Photopolymerization and formation of a stable purple Langmuir-Blodgett film based on the Gemini-type amphiphilic diacetylene derivatives. *J. Phys. Chem. B.* 114 (2010): 8871-8878.
- [26] Li, F.; et al. Photopolymerization of self-assembled monolayers of diacetylenic alkylphosphonic acid on group-III nitride substrates. *Langmuir.* 26 (2010) : 10725-10730.
- [27] Okada, S.; Peng, S.; Spevak, W.; Charych, D. Color and chromism of polydiacetylene vesicle. Color and chromism of polydiacetylene vesicle. *Acc. Chem. Rev.* 31 (1998): 229-239.
- [28] Skoog, D. A.; Principle of instrumental analysis, Third Edition, p.684-688.
- [29] Nazeeruddin, M. K.; et al. Investigation of sensitizer absorption and the influence of protons on current and voltage of a dye-sensitized nanocrystalline TiO<sub>2</sub> solar cell. *J. Phys. Chem.* 107 (2003): 8981-8987.
- [30] Wang, P.; et al. Stable new sensitizer with improved light harvesting for nanocrystalline dye sensitized solar cell. *Adv. Mater.* 16 (2004): 1806-1811.
- [31] Klein, C.; Nazeeruddin, M. K.; Censo, D. D.; Liska, P.; Gratzel, M. Amphiphilic ruthenium sensitizers in dye sensitized solar cells. *Inorg. Chem.* 43 (2004): 4216-4226.
- [32] Lagref, J. J.; Nazeeruddin, M. K.; Gratzel, M. Artificial photosynthesis based on dye sensitized nanocrystalline TiO<sub>2</sub> solar cells. *Inorg Chim Acta.* 361 (2008): 735-745.
- [33] Wang, P.; et al. Amphiphilic ruthenium sensitizer with 4,4'-diphosphonic acid-2,2'-bipyridine as anchoring ligand for nanocrystalline dye sensitized solar cells. *J. Phys. Chem. B.* 108 (2004): 17553-17559.

- [34] Schmidt-Mende, L.; Kroeze, J. E.; Durrant, J. R.; Nazeeruddin, M. K.; Gratzel, M. Effect of hydrocarbon chain length of amphiphilic ruthenium dyes on solia-state dye sensitized photovoltaics. *Nano. Lett.* 5 (2005): 1315-1320.
- [35] Kroeze, J. E.; et al. Alkyl chain barriers for kinetic optimization in dye sensitized solar cells. *J. Am. Chem. Soc.* 128 (2006): 16376-16383.
- [36] Klein, C.; et al. Engineering of a novel ruthenium sensitizer and its application in dye sensitized solar cell for conversion of sunlight into electricity. *Inorg. Chem.* 44 (2005): 178-180.
- [37] Jang, S. R.; et al. Oligophenylenevinylene functionalized Ru(II)bipyridine sensitizers for efficient dye sensitized nanocrystalline TiO<sub>2</sub> solar cells. *Chem. Mater.* 18 (2006): 5604-5608.
- [38] Jung, I.; Choi, H.; Lee, J. K.; Song, K. H.; Kang, S. O.; Ko, J. New ruthenium sensitizers containing styryl and antenna fragments. *Inorg. Chimi. Acta.* 360 (2007): 3518-3524.
- [39] Nazeeruddin, M. K.; et al. A high molar extinction coefficient charge transfer sensitizer and its application in dye sensitized solar cell. *J. Photochem. Photobiol. A-chem.* 185 (2007): 331 -337.
- [40] Kuang, D.; et al. High-efficiency and stable mesoscopic dye sensitized solar cells base on a high molar extinction coefficient ruthenium sensitizer and nonvolatile electrolyte. *Adv. Mater.* 19 (2007): 1133-1137.
- [41] Cao, Y.; et al. Dye sensitized solar cells with a high absorbtivity ruthenium sensitizer featuring a 2-(hexylthio)thiophene conjugated bipyridine. *J. Phys. Chem C.* 113 (2009): 6290-6297.
- [42] Gao, F.; et al. Conjugation of selenophene with bipyridine for a high molar extinction coefficient sensitizer in dye sensitized solar cell. *Inorg. Chem.* 48 (2009): 2664-2669.
- [43] Liu, K. Y.; Hsu, C. L.; Hsing, S.; Chen, J. G.; Ho, K. C.; Lin, K. F. Synthesis and characterization of cross-linkable ruthenium complex dye and it application on dye sensitized solar cell. *J. Polymer. Science. Part A, Polymer Chem.* 48 (2010): 366-372.
- [44] Kissarwan, H.; Ghaddar, T. H. Enhancement of photovoltaic performance of a novel dye "T18" with ketene thioacetal groups as electron donors for high



- efficiency dye sensitized solar cells. *Inorg. Chim. Acta.* 363 (2010): 2409-2415.
- [45] Lee, K. E.; Gomez, M. A.; Elouatik, S.; Demopoulos, G. P. Further understanding of adsorption mechanism of N719 on anatase TiO<sub>2</sub> films for DSSC applications using vibrational spectroscopy and confocal Raman imaging. *Langmuir.* 26(2010): 9575-9583.
- [46] Wenkert, D.; Woodward, R. B. Studies of 2,2'-Bipyridine-*N,N'*-Dioxide. *J. Org. Chem.* 48(1983): 283-289.
- [47] Zhang, D.; Telo, J. P.; Liao, C.; Hightower, S. E.; Clennan, E. L. Experimental and computational studies of nuclear substituted 1,1'-dimethyl-2,2'-bipyridinium tetrafluoroborates. *J. Phys. Chem A.* 111(2007): 13567-13574.
- [48] Kavnagh, P.; Leech, D. Improved synthesis of 4,4'-diamino-2,2'-bipyridine from 4,4'-dinitro-2,2'-bipyridine-*N,N'*-dioxide. *Tetrahedron Lett.*, 45(2004): 121-123.
- [49] Kuboki, T.; Araki, K.; Yamada, M.; Shiraishi, S. Mesophase structure of higher alkanoyl derivative of 6,6'-diamino-2,2'-bipyridine and their metal complexes. *Bull. Chem Soc. Jpn.* 67(1994): 948-955.
- [50] Garelli, N.; Vierling, P. Synthesis of new amphiphilic perfluoroalkylated bipyridines. *J. Org. Chem.* 57(1992): 3046-3051.
- [51] Maerker, G.; Case, F. H. The synthesis of some 4,4'-disubstituted-2,2'-bipyridines. *J. Am. Chem. Soc.* 80(1958): 2745-2748.
- [52] Nazeeruddin, M. K.; et al. Acid-base equilibria of (2,2'-bipyridyl-4,4'-dicarboxylic acid)ruthenium(II) complexes and the effect of protonation on charge-transfer sensitization of nanocrystalline titania. *Inorg. Chem.* 38(1999): 6298-6305.
- [53] Adam, C. J.; Bowen, L. E.; Humphrey, M. G.; Morrall, J. P. L.; Samoc, M.; Yellowlees, L. J. Ruthenium bipyridyl compounds with two terminal alkynyl ligands. *Dalton Trans.* (2004): 4130-4138.
- [54] Devadoss, C.; Bharathi, P.; Moore, J. S. Energy transfer in dendritic macromolecules : molecular size effect and the role of an energy gradient. *J. Am. Chem.Soc* 118 (1996): 9635-9644.

- [55] Pesak, D.; Moore, J. S. Synthesis and characterization of water soluble dendritic macromolecules with a stiff hydrocarbon interior. *Macromolecules*. 30 (1997): 6467-6482.
- [56] Nantalaksakul, A.; dasari, R. R.; Ahn, T. S.; Al-kaysi, R.; Bardeen, C.;J.; Thayumanavan, S. Dendrimer analogues of linear molecules to evaluate energy and charge transfer properties. *Org. Lett* 8 (2006): 2981-2984.
- [57] Zhang, X.; Ren, X.; Xu, Q. H.; Loh, K. P.; Chen, Z. K. One and two photon turn-on fluorescent probe for cysteine and homocysteine with large emission shift. *Org. Lett.* 11 (2009): 1257-1260.
- [58] Dhungel, S.; Park, J. G. Optimization of paste formulation for TiO<sub>2</sub> nanoparticles with wide range of size distribution for its application in dye sensitized solar cells. *Renew. Energy*. 35 (2010): 2776-2780.
- [59] Nazeeruddin, M. K ; et al. Combined experimental and DFT-TDDFT computational study of photoelectrochemical cell ruthenium sensitizers. *J. Am. Chem. Soc.* 127(2005): 16835-16847.
- [60] Buscaino, R.; Baiocchi, C.; Barolo, C.; Gratzel, M.; Nazeeruddin, M. K.; Viscardi. G. A mass spectrometric analysis of sensitizer solution used for dye sensitized solar cell. *Inorg. Chimi. Acta.* 361(2008): 798-805.
- [61] Marino, J. P.; Nguyen, H. N. Bulky trialkylsilyl acetylenes in the Cadiot-Chodkiewicz ceoss coupling reaction. *J. Org. Chem.* 67 (2002): 6841-6844.
- [62] Montalbetti, C.; Faique, V. Amide bond formayion and peptide coupling. *Tetrahedron*. 61 (2005): 10827-10852.
- [63] Song, J.; Cheng, Q.; Kopta, S.; Steven, R. C. Modulating artificial membrane morphology: pH-induced chromatic transition and nanostructural transformation of a bolaamphiphilic conjugated polymer from blue helical ribbons to red nanofibers. *J. Am. Chem. Soc.* 123 (2001): 3205-3213.
- [64] Li, P.; Xu, J. C. The X-ray structures of HOBt based immonium type coupling reagents and the rearrangement of benzotriazolyl esters of *N*-vs. *O*-substituted forms. *J. Chem. Soc. Perkin trans. 2* (2001): 113-120.
- [65] Hayashi, Y.; et al. Analisis of amide bond formation with an  $\alpha$ -hydroxy- $\beta$ -aminoacid derivative, 3-amino-2hydroxy-4-phenylbutanoic acid, as an

- acyl component: Byproduction of homobislactone. *J. Org. Chem.* 66 (2001): 5537-5544.
- [66] Pope, S. J. A.; Coe, B. J.; Faulkner, S.; Laye, R. H. Metal to ligand charge transfer sensitization of near infrared emitting lanthanides in trimetallic arrays  $M_2Ln$  ( $M = Ru, Re, \text{ or } Os$ ;  $Ln = Nd, Er \text{ or } Yb$ ). *Dalton Trans.* (2005): 1482-1490.
- [67] Karki, L.; Hupp, J. T. Electroabsorption studies of metal to ligand charge transfer in  $Ru(\text{phenanthroline})_3^{2+}$ : Evidence for intrinsic charge localization in the initially formed excited state. *Inorg. Chem.* 36 (1997): 3318-3321.
- [68] Rawling, T.; Austin, C.; Buchholz, F.; Colbran, S. B.; McDonagh, A. M. Ruthenium phthalocyanine bipyridyl dyads as sensitizers for dye sensitized solar cells : dye coverage versus molecular efficiency. *Inorg. Chem.* 48 (2009): 3215-3227.
- [69] Wolfbauer, G.; Bond, A. M.; Deacon, G. B.; Macfarlane, D. R.; Spiccia, L. Experimental and theoretical investigations of the effect of deprotonation on electronic spectra and reversible potentials of photovoltaic sensitizer : Deprotonation of  $cis-L_2RuX_2$  ( $L = 2,2'$ -bipyridine-4,4'-dicarboxylic acid;  $X = CN^-, NCS^-$ ) by electrochemical reduction at platinum electrodes. *J. Am. Chem. Soc.* 122 (2000): 130-142.
- [70] Bond, A. M.; Deacon, G.B.; Howitt, J.; Macfarlane, D. R.; Spiccia, L.; Wolfbauer, G. J. Voltammetric determination of the reversible redox potential for the oxidation of the highly surface active polypyridyl ruthenium photovoltaic sensitizer  $cis-Ru(II)(dcbpy)_2(NCS)_2$ . *J. Electrochem. Soc.* 146 (1999): 648-656
- [71] Cecchet, F.; et al. Solvent effects on the oxidative electrochemical behavior of  $cis$ -Bis (isothiocyanato) ruthenium (II) –bis-2,2'-bipyridine-4,4'-dicarboxylic acid. *J. Phy. Chem. B.* 106 (2002): 3926-3932.
- [72] Stein, E.; Oki, S. Y.; Vichi, E. J. S. Synthesis and electrochemical characterization of bimetallic ruthenium complexes with bridging  $\eta^2$  ( $\sigma, \sigma$ )-1,3-butadiyne-1,4-diyl ligand. *J. Braz. Chem. Soc.* 11 (2000): 252-256.

- [73] Chen, Z. K.; Huang, W. A family of electroluminescent silyl substituted poly(phenylenevinylene)s: synthesis, characterization and structure-property relationships. *Macromolecule*. 33 (2000): 9015-9025.
- [74] Kaya, I.; Baycan, F. Synthesis, characterization, conductivity, band gap and thermal analysis of poly-2-[(4-mercaptophenyl) imino methyl] phenol and some of its polymer metal complexes. *Synthetic. Metal*. 157 (2007): 659-669.
- [75] Xu, X.; Chen, H.; Cai, X. R.; Li, Y.; Jiang, Q. Synthesis and properties of polyfluorene copolymers bearing thiophene and porphyrin. *Chinese Chemical Letters*. 18 (2007): 879-882.
- [76] Gratzel, M. Photoelectrochemical cells. *Nature*. 414 (2001): 338-344.
- [77] Durr, M.; Rosselli, S.; Yasuda, A.; Nelles, G. Band gap engineering of metal oxides for dye sensitized solar cells. *J. Phy. Chem.B*. 110 (2006): 21899-21902.

**APPENDICES**

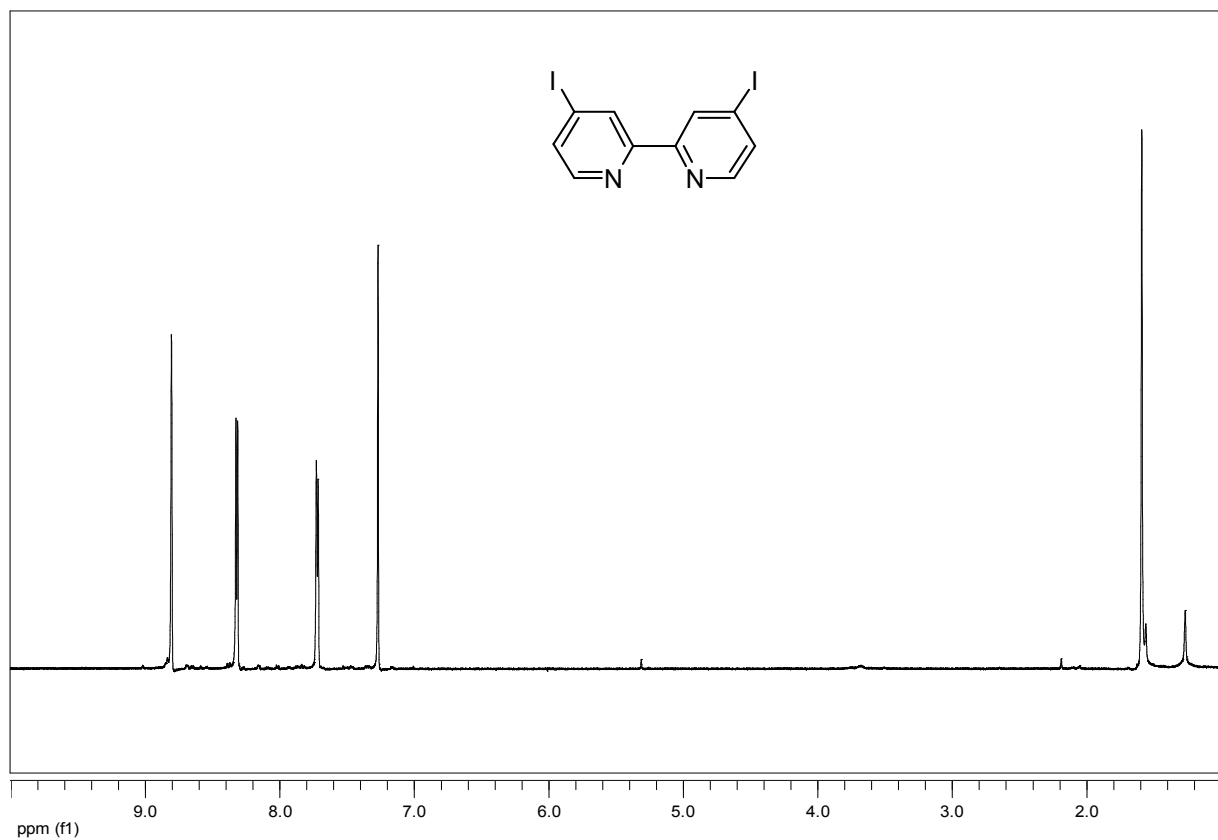


**Figure A1** <sup>1</sup>H NMR spectrum of 4,4'-diiodo-2,2'-bipyridine.

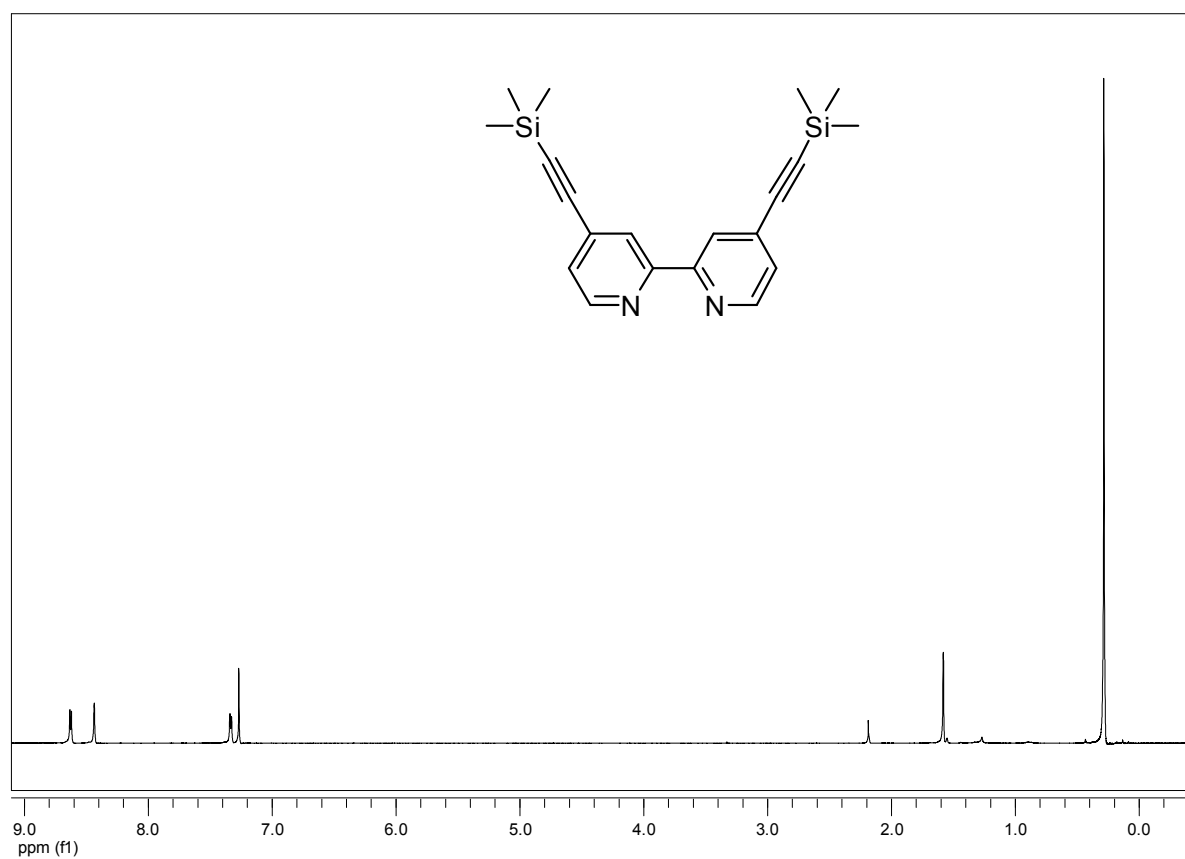


**Figure A2** <sup>1</sup>H NMR spectrum of 4,4'-bis((trimethylsilyl)ethynyl)-2,2'-bipyridine.

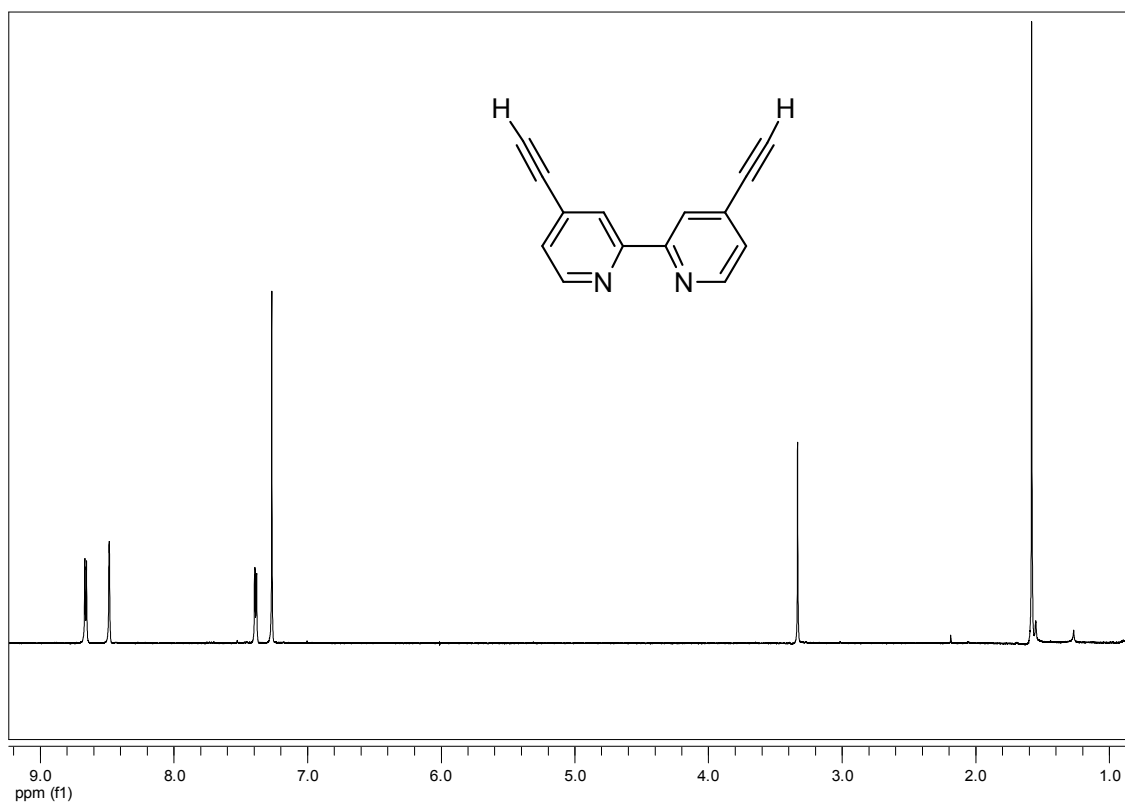


**Figure A3** <sup>1</sup>H NMR spectrum of 4,4'-diethynyl-2,2'-bipyridine.

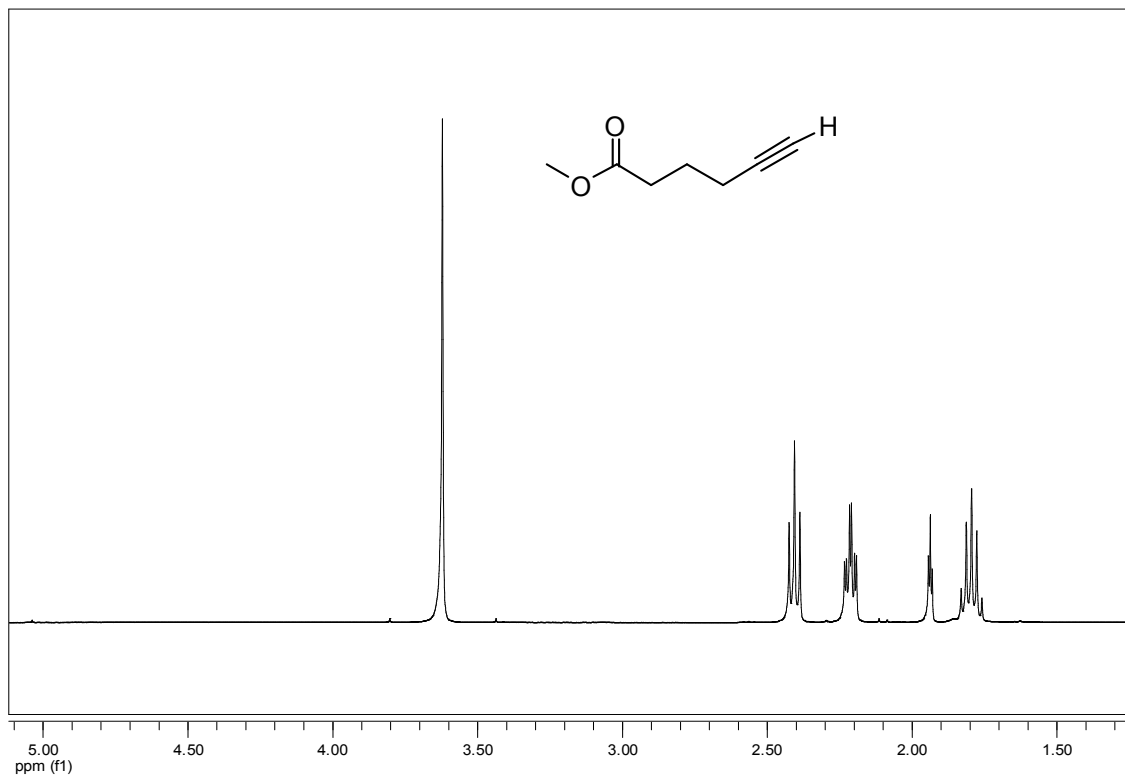


**Figure A4** <sup>1</sup>H NMR spectrum of methyl hexynoate.

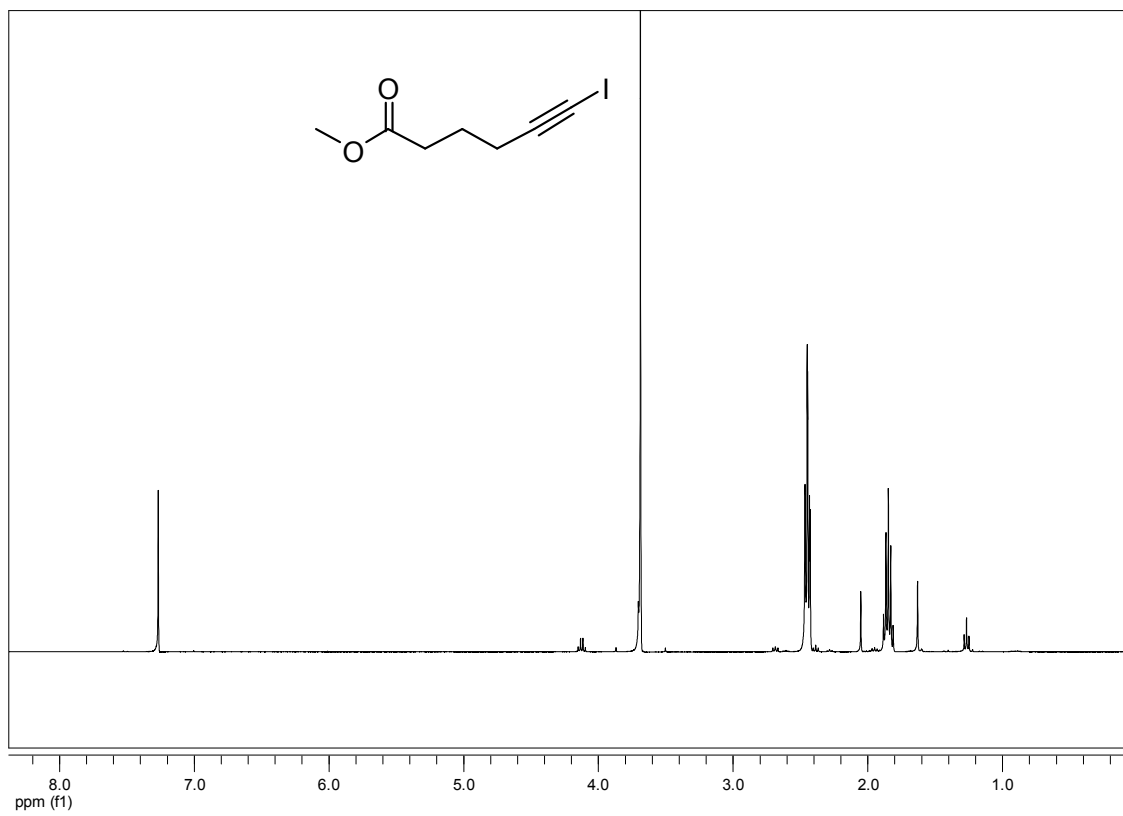


**Figure A5**  $^1\text{H}$  NMR spectrum of iodo methyl hexynoate.



## VITAE

Pagasukon Mekrattanachai was born on March 2<sup>nd</sup> , 1984 in Lampang, Thailand. She graduated a Bachelor degree from Department of Chemistry, Faculty of Science, Chulalongkorn University in 2007. After that she further studied the master degree majoring in organic chemistry, Faculty of Science, Chulalongkorn University and completed the program in 2010. His address is 145 Phaholyothin Road, Ban Pong, Ngao, Lampang, Thailand, 52110.